EQUILIBRIUM AND DIFFUSION IN MOLECULAR SIEVES

A THESIS IN CHEMICAL ENGINEERING

Presented to the faculty of the American University of Sharjah
College of Engineering
in partial fulfillment of
the requirements for the degree

MASTER OF SCIENCE

by

QASSIM H. DIRAR

B.S. 2009

Sharjah, UAE

July 2011

We approve the thesis of Qassim Hassan Mohammed Ahmed Dirar

Date of signature

Dr. Kevin Loughlin Professor Department of Chemical Engineering Thesis advisor	
Dr. Naif Darwish Professor Department of Chemical Engineering Graduate Committee	
Dr. Dana Abouelnasr Associate Professor Department of Chemical Engineering Graduate Committee	
Dr. Yehya Amin El Sayed Assistant Professor Department of Chemistry Graduate Committee	
Dr. Dana Abouelnasr Department Head Department of Chemical Engineering	
Dr. Hany El Kadi Associate Dean College of Engineering	
Dr. Yousef Al-Assaf Dean College of Engineering	
Dr. Gautam Sen Vice Provost Research and Graduate Studies	

EQUILIBRIUM AND DIFFUSION IN MOLECULAR SIEVES

Qassim Hassan Mohammed Ahmed Dirar, Candidate for the Master of Science Degree

American University of Sharjah, 2011

ABSTRACT

Two topics in equilibrium and one in diffusion in zeolites are examined. The sorption of CO_2 in 5A and 13X zeolites is detailed. Thirteen studies from the literature and one unreported study are examined for saturation loading, q_{max}, Henry's constants, K_H, isosteric heat of adsorption, $-\Delta H_q$, and isotherm model for the new data. The saturation loadings, q_{max}, are greater than those derived from theoretical calculations of density based on the Modified Rackett equation combined with the relevant crystallographic data for the zeolite when the reduced temperature is greater than 0.9. This implies that the molar volume of the adsorbate is less than that in the equivalent liquid phase. Henry's constant, K_H, values for both zeolites are calculated. The isosteric heat of adsorption on 13X zeolite is less than the calorimetric value; a hypothesis is advanced for this phenomenon.

Fits of the multisite Langmuir isotherm of n-alkanes on 5A zeolite are examined. The values of q_{max} and hence θ are predetermined using a recent paper. Some of the new fits were successful but many were not. Best fits were achieved for C_2 and C_4.

The study of nonisothermal sorption of water on 5A zeolite that has been measured on an Intelligent Gravimetric Analyzer (IGA) is modeled. This data shows that for a partial pressure step change of zero to 1 mbar at 20°C, a temperature rise of 17°C arises causing the adsorption to be nonisothermal. This rise in temperature raises the diffusion coefficient causing the mass uptake to be a two resistance model rather than a one resistance model. The mass uptake and temperature are modeled.

CONTENTS

LIST OF TABLES

LIST OF FIGURES

NOMENCLATURE

a	cell width (pm) (Chapter 2)
a	external area per unit particle (3/R) (cm^{-1})
A_i	virial coefficients (cm^3/mol, 100 g Z/g, 1/kPa)
b	Langmuir parameter/adsorption affinity parameter (cm^3/mol, 1/kPa)
b_0	Langmuir parameter at reference temperature /adsorption affinity parameter (cm^3/mol, 1/kPa)
Bi	Biot number for mass transfer
b_i	Langmuir parameter/adsorption affinity parameter at initial temperature (cm^3/mol, 1/kPa)
c	fluid phase concentration (mole/cm^3, g/g)
C^*	equilibrium gas phase concentration at gas-solid interface (mole/cm^3, g/g)
c_b	bulk equilibrium saturation concentration (mole/cm^3, g/g)
c_i	initial fluid phase concentration (mole/cm^3, g/g)
c_o	initial/reference fluid phase concentration (mole/cm^3, g/g)
C_p	heat capacity (J/mol.K)
C_s	heat capacity solid (J/mol.K)
D, D_c	crystal diffusivity (m^2/s, cm^2/s)
D_e	effective particle diffusivity
D_m	molecular diffusivity (m^2/sec)
D_p	pore diffusivity (cm^2/s)
D_{p0}	pore diffusivity at reference temperature (cm^2/s)
D_s	surface diffusivity (cm^2/s)

D_{s0}	surface diffusivity at reference temperature (cm^2/s)
E_q	activation energy (J/mol)
F	fractional uptake
f_i	fractional size of site i.
h	heat transfer coefficient ($W/cm^2.K$)
H	Henry's constant (g/100 g Z kPa)(Chapter 3)
k	boltzmann's constant (Chapter 3)
K	equilibrium parameter (Chapter 4)
k(t)	rate of movement of shock front
K_0	pre-exponential Henry's constant (g/100 g Z kPa) (Chapter 2)
K_0	pre-exponential Henry's constant (kPa^{-1}) (Chapter 3)
K_{eq}	Henry's constant (kPa^{-1}) (Chapter 3)
k_f	fluid film resistance (cm/s)
K_H	Henry's constant (g/100 g Z kPa) (Chapter 2)
k_m	mass transfer coefficient (cm/s)
k_s	pore mouth resistance (cm/s)
l	bed depth
L	mobility constant (mol/cm.s.atm)
LeBi	Lewis Biot number for heat transfer
M	molecular weight of zeolite (Chapter 2)
m_∞	mass adsorbed at infinite time (μg)
m_t	mass adsorbed in time t (μg)
MW,MW_{H2O}	molecular weight, water

n	number of carbon units in molecule (Chapter 3)
N_0	Avogadro's number
N_p	flux in the pore volume, (mol/cm^2.s)
N_q	flux in the adsorbed phase, (mol/cm^2.s)
N_r	mass flux in r direction, (mol/cm^2.s)
p,P	partial pressure of adsorbate, (kpa)
P_C	critical pressure (kPa)
P_F	freezing point pressure (kPa)
p_n	roots of the transcendental equation
P_T	triple point pressure (kPa)
q	adsorbed phase concentration (g/100 g Z, mol/cm^3)
q_∞	saturated adsorbed phase concentration (g/100 g Z, mol/cm^3)
q^*	equilibrium adsorbed phase concentration at gas-solid interface (g/g Z, mole/cm^3)
q^*_{max}	saturated adsorbed phase concentration based on adsorbent (g/100 g ads)
q_i	initial adsorbed phase concentration (g/100 g Z, mol/cm^3) (Chapter 5)
q_{max}	saturated adsorbed phase concentration based on zeolite crystal (g/100 g Z, mol/cm^3)
q_o	initial adsorbed phase concentration (g/100 g Z, mol/cm^3) (Chapter 4)
q_s	adsorbed phase concentration, in equilibrium with c_o (g/100 g Z, mol/cm^3)

$q_{sat\ crystal}$	saturated adsorbed phase concentration for pure 5A crystal (g/100 g Z, mol/cm^3)
q_{sat}	saturated adsorbed phase concentration (g/100 g Z, mol/cm^3)
$\bar{q}$	average adsorbed phase concentration (g/g Z, mole/cm^3)
r	crystallite radial coordinate (cm, m)
R	gas constant ((atm.cm^3/mol.K), (J/mol.K)) (Chapter 2)
R	mean particle radius (cm) (Chapter 4 and 5)
r_c	crystallite radial coordinate (cm, m)
R_f	shock front radius (m)
R_g	gas constant ((atm.cm^3/mol.K), (J/mol.K)) (Chapter 5)
R_P	pellet radius (cm, m)
T	temperature (K)
t	time (s)
t	Toth heterogeneity parameter, dimensionless. (Chapter 2)
T_0	reference temperature (K)
T_b	bulk gas temperature (K)
T_B	normal boiling point temperature (K)
T_c	critical temperature (K)
T_{car}	critical adsorbate reduced temperature
T_F	freezing point temperature (K)
T_r	reduced temperature
T_T	triple point temperature (K)
u	molecular interaction energy (J/K)

V_c	critical volume (m^3/kmol)
V_{cell}	volume of pseudo unit cell of 5A, 1870 $Å^3$
V_{sat}	saturated density for liquids (cm^3/g)
V_α	volume of α cage $Å^3$
V_β or v	volume of β cage $Å^3$
y	dimensionless gas phase concentration
$y_{i,exp}$	experimental data point
$y_{i,th}$	theoretical data point
Z	formula unit of the cell (Chapter 2)
Z	zeolite
Z_c	critical compressibility
Z_{RA}	Rackett parameter

Greek Symbols

$(-\Delta H)$	heat of adsorption (J/mol)
$(-\Delta H_0)$	heat of adsorption at zero loading. (J/mol)
$(-\Delta H_q)$	isosteric heat of adsorption (J/mol)
$(-\Delta H_{ads})$	heat of adsorption (Chapter 5) (J/mol)
Δu	differential molecular interaction energy (J)
ϵ	external void fraction of adsorbent bed
ϵ_c	void fraction of the crystallite
ϵ_p	void fraction of the particle
ϵ_z	external void fraction for zeolite crystal
θ	fractional loading/coverage

μ	chemical potential (J/mol)
μ_G	chemical potential for ideal gases (J/mol)
ϱ	density (g/cm^3, kg/m^3)
ϱ	framework density (g/cm^3, kg/m^3) (Chapter 2)
ϱ_{sat}	saturation density of adsorbate (g/cm^3)
ϱ_Z	density of zeolite crystal (g/cm^3, kg/m^3)

ACKNOWLEDGEMENTS

I'd like to start with the name of Allah the most gracious the most merciful and second with thanking Allah for all he gave me and for the blessing of completing this work. Prophet Mohammed, Peace be Upon Him, said: "He who does not thank people, does not thank Allah" .So I'd like to seize this chance and thank all who helped me reach this point. I thank my lovely and sacrificing mother for her unconditional love and support. She is the only person in this world who believes that I can do almost anything and continuously pushing me to become a better me. I thank my father for his big heart and for the great belief he has in me. I also like to thank my brother Mohammed and my sister Wijdan for their love and support.

After that, I want to thank my thesis advisor Dr. Kevin Loughlin. I'd like to thank him, for he always made me feel that I'm capable of achieving great things. He always showed a great concern about my development as a graduate student. He was very patient with me when I was a newbie in the field of adsorption. His continuous and sincere advises are precious gifts that I'll continue to cherish and remember. I thank him for I never felt lost during the course of preparing this thesis. He made things clear and simple from day one and this continued until the end of this thesis. I'd also like to thank the Department of Chemical Engineering at the American University of Sharjah for giving me the chance to do my master degree. I thank them as they gave me the chance to discover the joy of teaching and research. With this a word of thanks to the entire Chemical Engineering faculty as they were the ones who explained concepts I use on a daily basis. I'd also like to thank Dr. Nabil Abdel Jabbar for his continuous support from my days as an undergraduate student to my last days as a graduate student. I'd also like to thank Dr. Rachid Chebbi for his admirable care and sincere advises. I thank my best friend Osamah, for his continuous support and for helping me developing the nomenclature of this thesis. I thank my dear friends Amjad and Abdul Monem, for continuously believing that I can do special things and pushing me to pursue my PhD. I also thank people with whom I shared classes and never hesitated to give me a hand when I needed to: Ahmad Al Nabulsi, a Mechatronics graduate student, Amin Al Shareef, a Mechanical Engineering graduate student who is in Canada now to pursue his PhD, and my colleagues in the Chemical Engineering graduate program: Wassen, Rabee, Omar, Alaa for giving me the digitizer in particular, Emad, Naif, and Fahd.

PREFACE

I'm sure that a lot of people who will come across this thesis will ask the question: Why Adsorption? My answer to this question is that this phenomenon will always surprise you. There's always something that needs to be discovered and studied. I find the physics of this phenomenon very interesting. Also, it happens that Adsorption research is carried out by an excellent faculty and the topic is interesting, so Why not?!!!.The purpose of this research is to study equilibrium and kinetics of adsorption of different adsorbate-adsorbent systems. The adsorption of CO_2 on 5A and 13X zeolites is discussed in Chapter 2. The chapter presents a complete equilibrium analysis along with a proposed model to estimate the saturation concentration of CO_2 on 5A and 13X. The content of this chapter is submitted to the Journal of Chemical Engineering and Data and will be presented at an AICHE conference. In Chapter 3 parameters of the MSL model are reevaluated. The importance of this work lies in the use of this model in predicting breakthrough curves in adsorption column. In Chapter 4 and Chapter 5 study of adsorption kinetics is discussed. Available kinetic data is available and modeled. Mathematical derivations are explained in detail along with the application of numerical techniques to solve the model. I tried my best to make this thesis a future reference for AUS students in particular and adsorption researchers in general. I ask Allah to bless this work and make it a beneficial work.

DEDICATION

Dedicated to my Mother

CHAPTER 1. OVERVIEW

1.1 Adsorption

The separation of gases and liquids using solids is an ancient practice. This practice or process is called adsorption, which is nothing more than the preferential partitioning of substances from the gaseous or liquid phase onto the surface of a solid substrate. In simpler words, it is the tendency of molecules to stick to surfaces. Starting with the use of bone char in decolorization, the subsequent use of activated carbon to remove nerve gas from the battlefield, to several modern applications, adsorption phenomena is a useful and efficient tool for separation and purification. The process of adsorption involves separation of a substance from one phase accompanied by its accumulation or concentration at the surface of another. The adsorbing phase is the adsorbent, and the material concentrated or adsorbed at the surface of that phase is the adsorbate. Adsorption is thus different from absorption, a process in which material transferred from one phase to another (e.g. liquid) interpenetrates the second phase to form a "solution". The term sorption is a general expression encompassing both processes. Physical adsorption is caused mainly by van der Waals forces and electrostatic forces between adsorbate molecules and the atoms which compose the adsorbent surface. Thus adsorbents are characterized first by surface properties such as surface area and polarity. A large specific surface area is preferable for providing large adsorption capacity, but the creation of a large internal surface area in a limited volume inevitably gives rise to large numbers of small sized pores between adsorption surfaces. The size of the micropores determines the accessibility of adsorbate molecules to the internal adsorption surface, so the pore size distribution of micropores is another important property for characterizing adsorptivity of adsorbents. Especially materials such as zeolite and carbon molecular sieves can be specifically engineered with precise pore size distributions and hence tuned for a particular separation. Surface polarity corresponds to affinity with polar substances such as water or alcohols. Polar adsorbents are thus called "hydrophillic" and aluminosilicates such as zeolites, porous alumina, silica gel or silica-alumina are examples of adsorbents of this type. On the other hand, nonpolar adsorbents are generally "hydrophobic". Carbonaceous adsorbents, polymer adsorbents and silicalite are typical nonpolar adsorbents. These adsorbents have more affinity with oil or hydrocarbons than water. The use of the adsorbent is decided by the application. A list of applications is provided below [1].

Table 1: List of applications of adsorbents in gas bulk separation

Gas Bulk Separations (b)	
Separation (a)	Adsorbent
Normal paraffins, isoparafins, aromatics	Zeolite
N_2/O_2	Zeolite
O_2/N_2	Carbon molecular sieve
CO, CH_4, CO_2, N_2, A, NH_3/H_2	Zeolite, activated carbon
Acetone/vent streams	Activated carbon
C_2H_4/vent streams	Activated carbon
H_2O/ethanol	Zeolite

Table 2: List of applications of adsorbents in gas purification

Gas Purifications (c)	
Separation (a)	Adsorbent
H_2O/olefin-containing cracked gas, natural gas, air, synthesis gas, etc	Silica, alumina, zeolite
CO_2/C_2H_4, natural gas, etc.	Zeolite
Organics/vent streams	Activated carbon, others
Sulfur compounds/natural gas, hydrogen, liquified petroleum gas (LPG), etc.	Zeolite
Solvents/air	Activated carbon
Odors/air	Activated carbon
NO_x/N_2	Zeolite
SO_2/vent streams	Zeolite
Hg/chlor-alkali cell gas effluent	Zeolite

a : Adsorbates listed first

b: Adsorbate concentrations of about 10 wt. % or higher in the feed

c : Adsorbate concentrations generally less than about 3 wt.% in the feed [1].

Since a general idea about adsorption is given, a general idea about the adsorbates used in this work is also useful. During the course of this thesis, adsorption on two adsorbents is studied. The two adsorbents are Zeolite 5A and Zeolite 13X.

1.2 Zeolites A

Since research involves zeolites, a general perspective about the structure of these materials is useful. The structure of zeolite A is shown schematically in Figure 1 [2].

Figure 1**:** Structure of Zeolite A.

The pseudo cell consists of eight β cages located at the corners of a cube and joined through four-membered oxygen rings (S4R). This arrangement forms a large polyhedral α cage of free diameter about 11.4 Å accessible through eight-membered oxygen windows. Stacking these units in a cubic lattice gives a three dimensional isotropic channel structure, constricted by eight-membered oxygen rings. Each pseudo cell contains 24 tetrahedral (AlO_2 or SiO_2) units and as the Si/Al ratio in zeolites A is always close to 1.0 there are 12 univalent exchange-able cations per cell. Three distinct cation sites have been identified; near the centers of the six-rings in the eight corners of the central cavity (type I), in the eight membered-rings (type II), and on the cage wall in close proximity to a four-ring (type III). With most cations the type I sites are preferentially occupied, followed by the type II sites, and the type III sites are filled only after all sites of types I and II have been occupied. In the sodium form (4A) there are 12 cations per cage. Eight are accommodated in the type I sites and three in the type II sites (the six eight-rings are each shared between two cages) with one cation in a type III site. All the windows are therefore partially obstructed by a sodium cation and the effective aperture of the sieve is therefore reduced from about 4.4 to 3.8 Å. If the Na^+ cations are exchanged for Ca^{+2} or Mg^{+2} the number of cations per cell decreases. At 67% exchange there are only eight cations per cell and these can be accommodated in the type I sites. Thus in Ca^{+2} or Mg^{+2} forms (5A) the effective aperture is increased and somewhat larger molecules can penetrate up to about 5 A° [3].

1.3 Zeolites X

The zeolite X structure is shown in Figure 2. The crystallographic unit cell consists of an array of eight cages containing a total of 192 AlO_2 and SiO_2 tetrahedral units. The framework may be thought of as a tetrahedral lattice of sodalite units connected through six-membered oxygen bridges, or equivalently as a tetrahedral arrangement of double six-ring units.

Figure 2: Structure of zeolite 13X.

The resulting channel structure is very open with each cage connected to four other cages through twelve-membered oxygen rings of free diameter ~7.4 Å. Quite large molecules such as neopentane and tertiary butyl amine can penetrate these pores. The X zeolite has an Si/Al ratio within the range 1-1.5. The number of exchangeable cations in this zeolite is about 10-12 per cage. The distribution of the cations between the various sites depends both on the nature and number of the cations and is affected by the presence of traces of moisture. There is even some evidence the equilibrium distribution may change when the sieve is loaded with adsorbent. The adsorptive properties of X sieves may therefore be greatly modified by ion exchange and improvements in selectivity can sometimes be obtained by using mixed cationic forms. While it is evident that the variation in adsorptive properties is probably related to redistribution of the cations among the possible sites, the precise relationship between the adsorptive properties and the cation distribution is still not fully understood [3].

1.4 Adsorbates

Adsorbates in this work are CO_2 on 5A and 13X, H_2O on 5A, and C_1 to C_{18} n-alkanes on 5A. The properties of CO_2 and H_2O are quoted from the website: www.cheric.org.

Table 3: CO_2 Basic Properties

Property	Value	Units
Molecular Weight	44.0098	
Normal Boiling Point Temp. (T_B)	194.7	K
Freezing Point Temp. (T_F)	216.58	K
Triple Point Temp. (T_T)	216.58	K
Triple Point Press. (P_T)	518.5	kPa
Critical Temperature. (T_C)	304.1400	K
Critical Pressure (P_C)	7375	kPa
Critical Volume (V_C)	0.0940	m^3/kg-mol
Critical Compressibility (Z_C)	0.2741	
Acentric Factor	0.2390	

Table 4: H2O Basic Properties

Property	Value	Units
Molecular Weight	18.0152	
Normal Boiling Point Temp. (T_B)	373.1500	K
Freezing Point Temp. (T_F)	273.1500	K
Triple Point Temp. (T_T)	273.1600	K
Triple Point Press. (P_T)	0.6117	kPa
Critical Temperature. (T_C)	647.1400	K
Critical Pressure (P_C)	22060.0000	kPa
Critical Volume (V_C)	0.0560	m^3/kg-mol
Critical Compressibility (Z_C)	0.2296	
Acentric Factor	0.3440	

In addition, the components from C_1 to C_{18} will be used and their properties can also be found on the same site.

1.5 Diffusion concepts

The concepts of diffusion in a pellet or in a crystal are developed in chapters four and five. The differential mass balance on a spherical shell element is derived from first principles. Then, the equations for one and two resistance models are derived from the primary differential mass balance presented in chapters four and five respectively. The one resistance models reviewed are: film model, micropore diffusion control, macropore diffusion control, pore mouth resistance and shrinking core model. The nonisothermal bed diffusion model is reviewed as a two resistance model consisting of a macropore diffusion combined with a surface heat transfer effect.

1.6 Objectives and Deliverables

The objectives of this MS Thesis include the following:

1. Present new data for the adsorption of CO_2 on 13X zeolite.
2. Model the saturation loading of CO_2, q_{max} (g/100 g Z), for both 5A and 13X zeolites using available literature data.
3. Determine the intrinsic Henry constants, K_H, for both 5A and 13X zeolites using multiple studies from the literature
4. Derive the isosteric heat of sorption of CO_2 on both 5A and 13X zeolites as a function of loading for multiple studies.
5. Model the new data for CO_2 on 13X zeolite using the Toth isotherm. The results of this modeling are compared with the intrinsic values of q_{max} and Henry constants calculated earlier.
6. Evaluate the MSL parameters taking into account recent knowledge of sorbate densities.
7. Explore different optimization techniques for the MSL model and develop successful ones.
8. Model the data of nonisothermal water adsorption on 5A.
9. Calculate diffusion and heat transfer coefficients.

Based on the objectives mentioned above the following are the deliverables:

1. Intrinsic properties of CO_2 adsorption on 5A/13X zeolite will be presented.
2. Revised MSL parameters for C_2 and C_4, will be provided.
3. Propose a model for the nonisothermal adsorption of water on zeolite 5A.
4. Report diffusion and heat transfer coefficients.
5. Plot of the nonisothermal adsorption model and the data to check the validity of the proposed model.
6. Analysis of the effect of various parameters on the nonisothermal adsorption of water on zeolite 5A.

CHAPTER 2. INTRINSIC ADSORPTION PROPERTIES OF CO_2 ON 5A AND 13X ZEOLITE

(This chapter was submitted to the Journal of Chemical Engineering & Data)

2.1 Introduction

Concern over climate warming and the need for sequestration of carbon dioxide has resulted in many studies of the adsorption of carbon dioxide on 5A and 13X zeolite. Recently Llano-Restrepo [4] comprehensively reviewed the literature for the adsorption of CO_2 on NaX zeolite, the basis of 13X zeolite. His primary purpose was to model the isotherms using a generalized statistical thermodynamic adsorption model (GTSA) and derive the isosteric heats of adsorption. For this, he used the data of Pulin et al. [5] as his source. He also provides structural interpretation of the adsorption of CO_2 on the NaX zeolite. His work can be criticized as the number of parameters required to model the GTSA isotherms is large, well over 6, more likely 12 when the pre-exponential factors and heats of adsorption are included. Secondly, he has only used one set of data for his modeling purposes although there are many sets of data available in the literature. Thirdly, the values of q_{max} used may be suspect. A similar comprehensive review of the adsorption of CO_2 on 5A zeolite is not available, particularly for high pressure adsorption data.

An intrinsic property is defined as a fundamental adsorbate-adsorbent interaction uninfluenced by a secondary variable. The traditional means of calculating parameters for an adsorption model result in an interaction between the Henry constant and the saturation loading, which tends to limit the intrinsic nature of the resulting parameters.

Untabulated data for CO_2 adsorption on NaX (13X) and CaA (5A) are extracted from literature papers by digitizing the appropriate figures. The focus was on both the high and low pressure end of the isotherms. The authors wanted to acquire as much high pressure loading data as possible. However, in general, high pressure loading data is rare when compared to studies at low to moderate pressure. Seven studies were analyzed for zeolite 13X in which two contained high pressure data. Similarly, five studies were analyzed for zeolite 5A in which only two contained high pressure data. The low pressure data is useful for extracting the Henry constants, and all the data is useful for extracting the isosteric heat of sorption.

2.2 Theory

The theoretical saturation loading in 13X and 5A zeolites may be calculated from first principles for zeolite crystals as:

$$q_{max}\left(\frac{g}{100\ g\ Z}\right) = 100\,\frac{\rho_{sat}\epsilon_Z}{\rho_Z} \qquad 2.1$$

where $\rho_{sat}$is the saturation density of the adsorbate in g/cm^3, ϵ_Z is the zeolite crystal porosity, and ρ_Z is the zeolite density in g/cm^3. For molecular sieves containing a fraction ω of crystals with a fraction (1-ω) of binder, a factor of ω must be used to relate the reported loading based on adsorbent $q^*_{max}\left(\frac{g}{100\ g\ ads}\right)$ to that based on crystals.

$$q_{max}\left(\frac{g}{100\ g\ Z}\right) = \left(\frac{1}{\omega}\right) q^*_{max}\left(\frac{g}{100\ g\ ads}\right) \qquad 2.2$$

In these equations, the saturation density for liquids below the critical point is calculated using the modified Rackett equation:

$$V_{sat}\ (\frac{cm^3}{g}) = \frac{1}{\rho_{sat}} = \left(\frac{RT_C}{P_C MW}\right) Z_{RA}^{\left[1+(1-T_r)^{\frac{2}{7}}\right]} \qquad 2.3$$

where R (atm cm^3/mol K) is the universal gas constant, T_c (K) is the critical temperature, P_c (atm) is the critical pressure, MW (g/mol) is the molecular weight, Z_{RA} is the Rackett parameter, and T_r is the reduced temperature.

Or the Rackett equation:

$$V_{sat}(\frac{cm^3}{g}) = \frac{1}{\rho_{sat}} = V_C Z_C^{(1-T_r)^{\frac{2}{7}}} \qquad 2.4$$

where V_C is the critical volume (cm^3/g), Z_C is the critical compressibility, and T_r is the reduced temperature. Substituting equation 2.3 in equation 2.1 gives:

$$q_{max}\left(\frac{g}{100\ gZ}\right) = 100\,\frac{\epsilon_Z}{\rho_Z}\left(\frac{P_C MW}{RT_C}\right) Z_{RA}^{-\left[1+(1-T_r)^{\frac{2}{7}}\right]} \qquad 2.5$$

The values of ε_Z and ϱ_Z may be found from Breck's text [6]. However, the author was unclear as to the specific meaning of the properties in his Tables [Table 2.18 and Table 2.63]; accordingly the parameters were recalculated from first principles.

The data in Table 5 is taken from Table 2.63 of Breck's text for zeolite X [6]. Only the data relevant to this work is included.

Table 5: Recalculation of Properties of Zeolite 13X from Breck's3 text

Chemical Composition	
Typical Unit Cell Contents	$Na_{86}[(AlO_2)_{86}(SiO_2)_{106}].264H_2O$
Variations	Si/Al = 1 to 1.5
Crystallographic Data	
Symmetry	cubic
Density	1.93 g/cc
Unit Cell Constants	a=25.02 -24.86 Å; X-Ray powder data
Unit Cell Volume	15,362 – 15,670 $Å^3$
Structural Properties	
Void Volume	0.50 cc/cc
Framework Density	1.31 g/cc
Free aperture	12-ring, 7.4 Å; 6-ring 2.2 Å
Largest Molecule admitted to 12 ring	$(C_4H_9)_3N$; kinetic Diameter, is 8.1 Å
Largest Molecule admitted to 6 ring (from page 636)	H_2O; kinetic Diameter, is 2.65 Å

*Data source is Table 2.63 in Breck's[3] text.

For the crystal unit cell of NaX given in Table 5, the basic building units of the crystal are itemized in Table 6; assuming covalent bonding, the atomic volume for each specie and for all species is calculated for both the dehydrated and hydrated crystal. The total solid volume and the volume of solid plus occluded water is also calculated.

Table 6: Basic Building Units for $Na_{86}[(AlO_2)_{86}(SiO_2)_{106}].264H_2O$ Zeolite

Specie	Atomic Mass	n	Covalent Radius(pm)	Atomic Volume (pm^3)	Atomic Volume (m^3)	Sigma Volume (m^3)
Dehydrated Crystal						
Si	28.086	106	111	5.73E+06	5.73E-30	6.07E-28
O	15.999	384	66	1.20E+06	1.20E-30	4.62E-28
Al	26.982	86	121	7.42E+06	7.42E-30	6.38E-28
Na	22.99	86	166	1.92E+07	1.92E-29	1.65E-27
Total Solid Volume (m^3)						3.36E-27
Hydrated Crystal						
H_2O	18.01	264	4754.788	2.99E+07	2.99E-29	7.89E-27
Total Volume (Solid + Occluded Water) (m^3)						1.136E-26

The derived properties for the crystal are presented in Table 7.

Table 7: Derived Properties from the Basic Building Units for 13X & 5A Zeolites

Property	13X	5A
Unit Cell Volume, a^3 (m^3)	1.56E-26	1.87E-27
Fraction Solids puc	0.215	0.223
Fraction Water puc	0.505	0.432
Fraction Excluded Volume puc	0.280	0.345
Volume (large or α cage) puc (m^3)	1.21E-27	1.51E-28
Fractional Volume β cage puc	0.077	0.081
Fractional Volume large cage	0.708	0.696
Fractional Void Volume (β+large or α cage)	0.785	0.777
Fractional Void Volume (Occluded) total cell	0.505	0.432
Fractional Void Volume (Occluded) (large or α cage) cage	0.455	0.387
Framework Density (g/cm^3)	1.43	1.48
Moles in 1 cc (=ϱ/MW(MW=cell atomic mass))	1.07E-04	8.86E-04
Cells in 1 cc (=moles*N_0)	6.42E+19	5.34E+20
Conversion Factor (molecule puc)/(mmole/g)	13.42	N/A
Conversion Factor for 1/8th of cell	1.68	1.67*

*Note the value typically used in the literature is 1.78.

**Data source for 5A data is Table 2.18 in Breck's[3] text.

The unit cell volume is calculated using 25 Å as the X-ray crystallographic width [6]. The fraction solids, fraction water, and the excluded volume are then calculated. As water is occluded in both the β and large cages, the excluded fractional volume of 0.28 is the volume unavailable to water due to the repulsion forces between the crystal lattice and the occluded water. The fractional volume of the β cage (≡ 8*151 Å (volume of sodalite cage in Breck's[3] text)) is 0.077. Therefore the fractional occluded volume of the large cage is the fractional volume of water minus 0.077 and is 0.428. The fractional occluded volume of both cages is taken equivalent to water (≡0.505). This is in agreement with the void volume of 0.500 given in Breck's[3] text [6]. The framework density for the dehydrated zeolite is calculated using the equation 2.6:

$$\rho\left(\frac{g}{cm^3}\right) = \frac{Z*M}{a^3 N_0 10^{-30}} \qquad 2.6$$

where Z is the formula unit (=1 puc), M is the atomic mass unit of the cell, a (pm) is the cell width and N_0 is Avogadro's number ($6.023*10^{23}$). The framework density is found to be 1.43 g/cm^3, similar to that calculated by Dubinin and coworkers [7] but different from the value of 1.31 g/cm^3given in Breck's book [6]. Finally the conversion factor from molecules puc to mmol/g may be calculated from the inverse of the expression:

$$conversion\ factor\ \left(\frac{molecule/cell}{mmol/g}\right) = \frac{\rho\ N_0}{\#cells * 1000} \qquad 2.7$$

and is presented in the last two lines of Table 7. The calculations for the 5A cell are also given in Table 7 using a similar analysis. The excluded volume of 34.5 % for 5A is higher than the 28 % excluded volume for the 13X zeolite. This is a reflection of the smaller large cavity in the 5A type zeolite. The occlusion volume is 43.2 % for the unit cell of 5A for water and ammonia, but is only 38.7 % for all other sorbates as they are unable to access the β cage in the 5A zeolite. The occlusion volume and framework density are 0.432 and 1.48 g/cm^3 different from Breck's[3] values of 0.47 and 1.27 g/cm^3 (Table 2.18) [6]. Steric effects may increase the size of the excluded volumes for other sorbates.

To interpret the intrinsic Henry constant, K_H, from experimental data, it is desirable that data be measured in the low concentration region where the fractional coverage, $\theta=q/q_{max}$ is less than 0.5. However this is very seldom achieved particularly at temperatures below a reduced temperature of 0.8 as the isotherms tend to be highly rectangular under these conditions. To take into account all the available data, it is desirable to use a model isotherm applicable over a wide span of concentrations. Most models have two or more parameters including the Henry constant, K_H (g/100 g kPa), and fractional coverage, $\theta=q/q_{max}$, among their parameter list. However, frequently an interaction is observed to occur between the derived values of K_H (g/100 g kPa) and θ, reducing the level of confidence in each parameter, and possibly invalidating the intrinsic result. An isotherm that does not have this inherent problem is the virial adsorption isotherm:

$$P = \frac{q}{K_H} exp(A_1 q + A_2 q^2 + \cdots) \qquad 2.8$$

as there is no term involving θ included. On rearrangement, the plot of this isotherm becomes a straight line at low concentrations, by just retaining the first term of the series:

$$ln\left(\frac{p}{q}\right) = -lnK_H + A_1 q \qquad 2.9$$

A plot of ln((p (kPa))/q (g/100 g Z)) versus q (g/100 g Z) is a straight line of slope A_1 and intercept –ln(K_H (g/100 g Z kPa)). According to Barrer [8], the coefficient A_1 is slightly temperature dependent. The coefficient K_H, Henry's constant, may be expressed by the van't Hoff equation:

$$K_H = K_0 exp\left(\frac{-\Delta H_0}{RT}\right) \qquad 2.10$$

where K_0 (g/100 g Z kPa) is the pre-exponential factor and ($-\Delta H_0$) is the heat of adsorption at zero loading.

The Toth isotherm model, for energetic heterogeneous surfaces, is fitted to the new data as follows:

$$q = \frac{q_{max} P}{(b+P^t)^{1/t}} \quad 2.11$$

For Toth isotherm, K_H (g/100 g Z kPa) is defined as:

$$K_H = q_{max} b^{-1/t} \quad 2.12$$

The variation of the isosteric heat with loading may be found using the relationship presented by Shen and Bulow [9]:

$$(-\Delta H)_q = -R \left(\frac{\partial \ln P}{\partial \left(\frac{1}{T}\right)} \right)_q \quad 2.13$$

By plotting ln(p (kPa)) versus 1/T (K) at different fixed values of q (g/100 g Z), the variation of heat of adsorption with loading is determined.

2.3 Experimental

The apparatus and procedure used to produce the unpublished set of data is identical to that reported in the earlier work of Abdul-Rehman et al. [10].

2.4 Results and Discussion

The literature studies used for both zeolites are tabulated in Table 8.

Table 8: CO2 studies on 5A and 13X zeolite

5A				
Year	Authors	Adsorbent	Fraction Zeolite	Type
1990	Chen et al. [11]	5A Union Carbide Co.	0.80	Volumetric
2002	Pakseresht et al. [12]	5A Union Carbide Co.	0.80	Volumetric
1998	Mulloth and Finn [13]	5A AlliedSignal Inc.	unknown	Volumetric
1998	Wang et al. [14]	5A	1.0	Volumetric
2003	Brandani et al. [15]	CaA	1.0	ZLC
2008	Merel et al. [16]	5A Axens (IFP)	unknown	Packed Bed
2009	Wang and Levan [17]	5A Grace-Davison	0.80	Volumetric
2009	Tili et al. [18]	5A	unknown	Gravimetric
2010	Saha et al. [19]	5A SINOPEC, China	unknown	Volumetric
13X				
Year	Authors	Adsorbent	Fraction Zeolite	Type
1968	Avgul et al. [20]	NaX - $0.06H:0.94NaAlO_2:1.38SiO_2$	1.0	Volumetric
1982	Hyun and Danner [21]	Linde 13X pellets	0.8	Volumetric
1989	Burgess [22]	Linde 13X pellets	0.8	Volumetric
1997	Kyaw et al. [23]	13X Fuji-Davison	unknown	Volumetric
1998	Wang et al. [14]	13X	1.0	Volumetric
2001	Pulin et al. [5]	NaX	1.0	Gravimetric for < 100 kPa Volumetric for > 100 kPa
2001	Siriwardane et al. [24]	Su¨d Chemie Inc	unknown	Volumetric
2003	Cavenati et al. [25]	13X CECA (France)	0.83	Gravimetric
2003	Brandani et al. [15]	NaX	0.82	ZLC
2008	Merel et al. [16]	13X Axens (IFP)	unknown	Packed Bed
2009	Li et al. [26]	13X pellets	unknown	Gravimetric
2009	Wang and Levan [17]	13X Grace-Davison	0.80	Volumetric

Five columns are displayed, year of publication, authors, zeolite source, % binder, and apparatus type. Studies in which the % binder is unknown were not considered further (Mulloth and Finn [13], Merel et al. [16], Tlili et al. [18], Saha et al. [19], Kyaw et al. [23], Siriwardane et al. [24], and Li et al. [26]). As mentioned previously, unpublished data for

the adsorption of CO_2 on 13X zeolite [22], tabulated in Table 9, and digitized or tabular data from the literature are used in this study.

Table 9: Unpublished data for sorption of CO_2 on 13X

T=280 K		T=300 K		T=300 K		T=325 K		T=350 K	
P (kPa)	q (g/100 g Z)	P (kPa)	q (g/100 g Z)	P (kPa)	q (g/100 g Z)	P (kPa)	q (g/100 g Z)	P (kPa)	q (g/100 g Z)
0.004	1.140	0.016	1.861	0.016	1.861	0.016	0.449	0.050	0.625
0.007	2.226	0.030	2.508	0.030	2.508	0.038	1.214	0.124	1.250
0.013	3.111	0.088	4.391	0.088	4.391	0.078	1.998	0.198	1.729
0.022	4.013	0.200	6.112	0.200	6.112	0.138	3.014	0.274	2.240
0.038	4.932	0.410	7.889	0.410	7.889	0.216	3.766	0.476	3.128
0.058	5.777	0.768	9.623	0.768	9.623	0.384	4.708	0.752	4.039
0.114	7.339	1.328	11.427	1.328	11.427	0.540	5.575	1.088	4.884
0.206	8.888	1.708	12.267	1.708	12.267	0.924	6.855	1.556	5.716
0.450	11.216	2.024	13.006	2.024	13.006	1.446	8.096	2.366	6.802
0.946	13.644	3.444	14.560	3.444	14.560	2.138	9.227	3.156	7.625
2.074	16.078					3.274	10.608	4.486	8.703
5.230	18.458					5.270	12.184	7.352	10.309
						8.350	13.737	10.860	11.682
						10.460	14.815	10.860	11.682
						10.460	14.819	19.420	13.552
						16.200	16.196	30.986	15.127
						26.122	17.446	46.800	16.399
						38.600	18.326	64.508	17.305
						61.374	19.422	64.508	17.301

The data for zeolite 5A are plotted as ln(q (g/100 g Z)) versus ln(p (kPa)), in Figure 3, and as q (g/100 g Z), versus ln(p (kPa)), in Figure 4 and Figure 5.

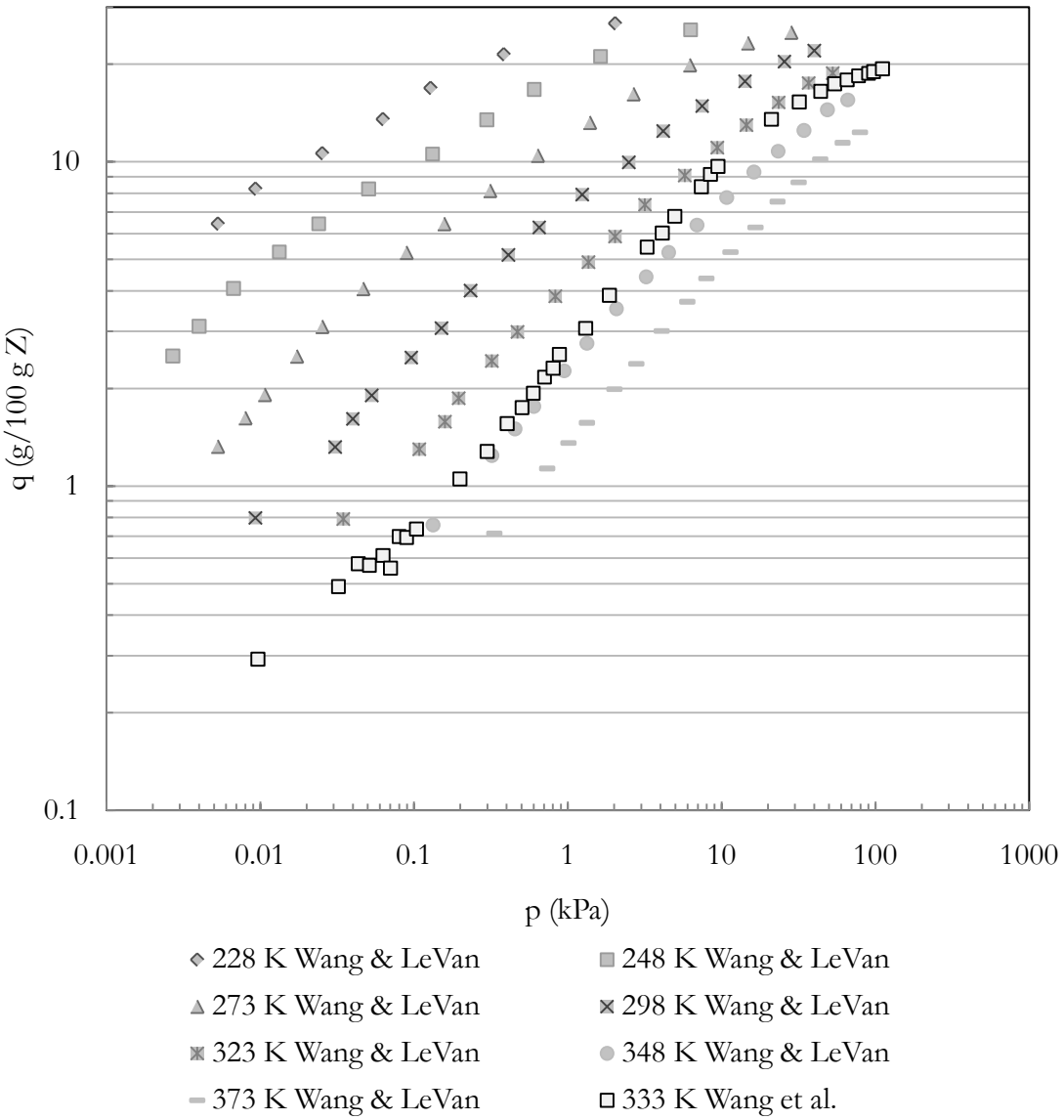

Figure 3: A log-log plot of CO_2 adsorption isotherms on zeolite 5A, showing the considered data for saturation loading estimation.

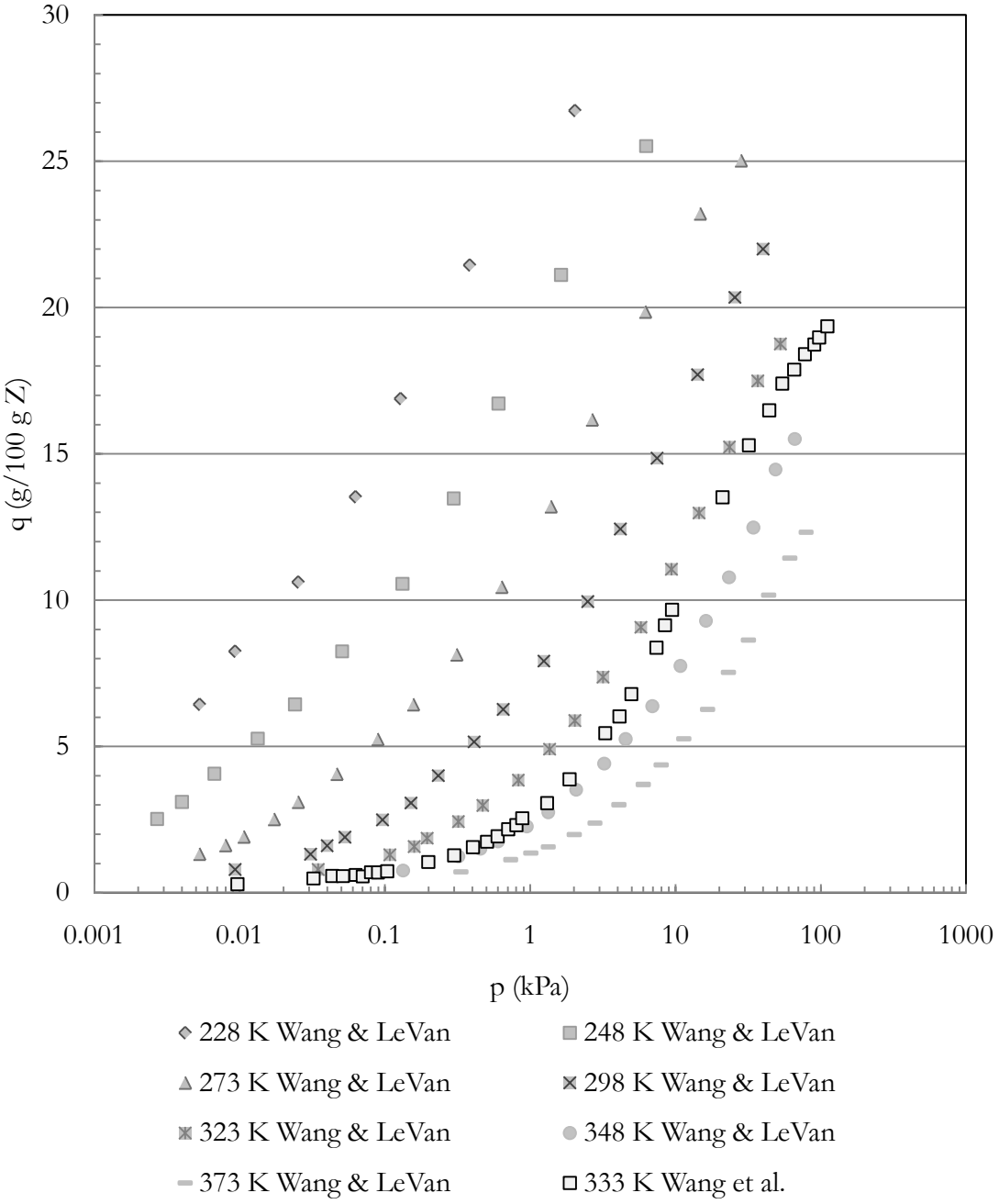

Figure 4: A semilog plot of CO_2 adsorption isotherms on zeolite 5A, showing the considered data for saturation loading estimation.

Plots of ln(q (g/100 g Z)) versus ln(p (kPa)) show the saturation limit while plots of q/(g/100 g Z) versus ln(p (kPa)) assist in verifying the consistency of studies, i.e. verifying whether isotherms are crossing or are in the incorrect location or have wrong shape. Figure 1b illustrates the adsorption isotherms of carbon dioxide on zeolite 5A plotted as adsorbent concentration, q (g/100 g Z) versus ln(p (kPa)) that are retained after careful analysis. Removed isotherms are shown in Figure 5.

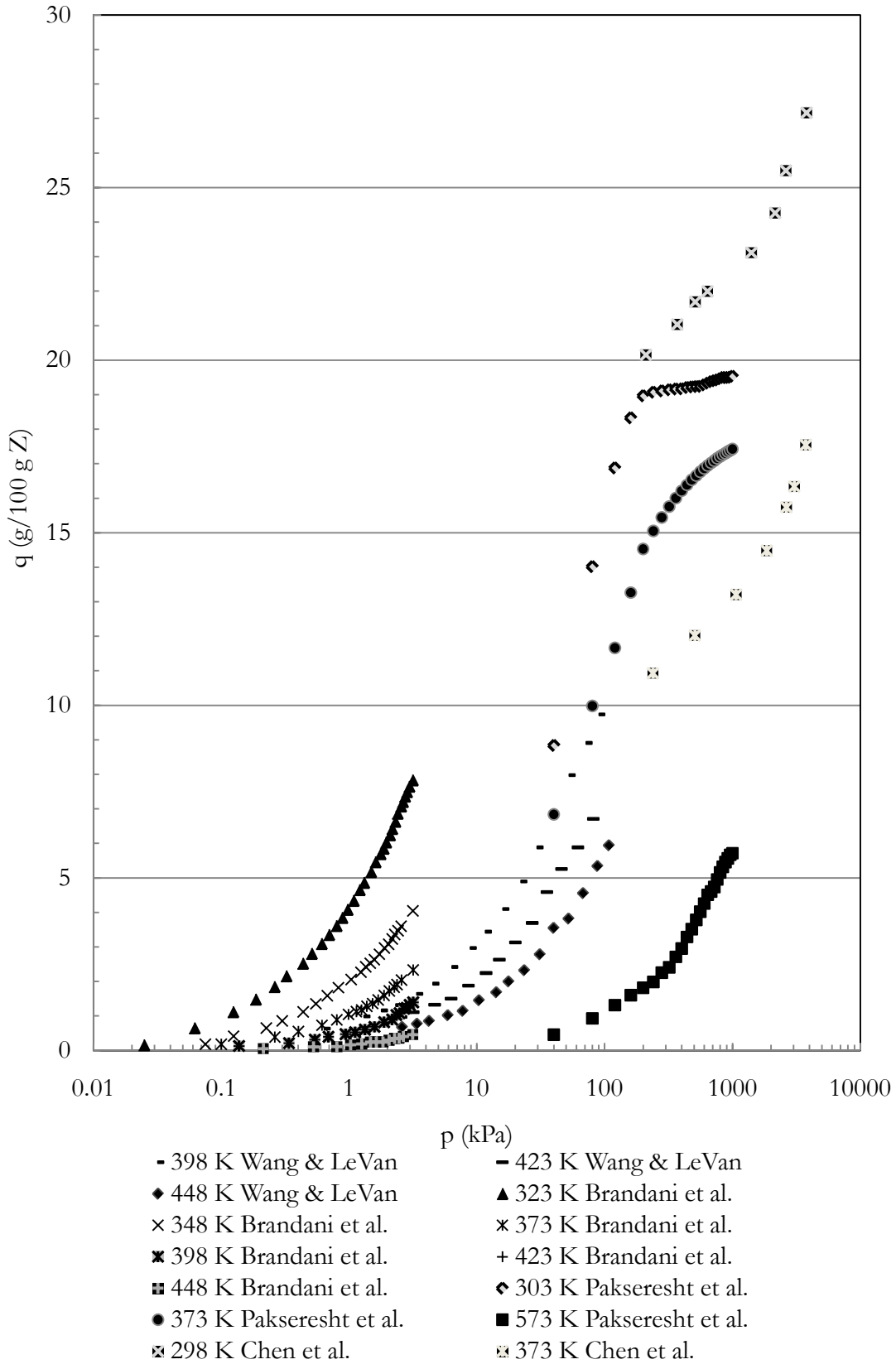

Figure 5: Eliminated studies from saturation loading estimation of the adsorption of CO_2 on zeolite 5A.

The isotherms of Pakseresht et al. [12] and Chen et al. [11] have been rejected due to not conforming to the shape or position of the retained isotherms. For Pakseresht et al. [12], the isotherm at 303 K appears to level off incorrectly, the isotherm at 373 K is out of position and convexing upward at the top end, and the isotherm at 573 K does not appear to be far enough to the right in comparison to the other isotherms. For Chen et al. [11] the isotherm at 298 K is out of position, adjacent to 398 K isotherms, and the 373 K isotherm is convexing upwards. Both sets of isotherms were measured in a volumetric apparatus. Low concentration isotherms were not included in the estimation of saturation q_{max} (g/100 g Z) values as obviously they are far from saturation. Examples are the isotherms of Brandani et al. [15] and the 398 K, 423 K and 443 K isotherm of Wang and LeVan [17].

The data for the adsorption of carbon dioxide on 13X are plotted in Figure 6, Figure 7, and Figure 8. Similar to the analysis for 5A, studies for 13X are plotted in two ways, as ln(q (g/100 g Z)) vs. ln(p (kPa)) in Figure 6 and as q (g/100 g Z) vs. ln(p (kPa)) in Figure 7 and Figure 8, to show the saturation limit and check for consistency respectively. After careful analysis the data at low concentration which consequently didn't reach saturation (Brandani et al. [15], Wang and LeVan [17], and Avgul et al. [20]) are omitted from the analysis of the saturation loading, q_{max} (g/100 g Z). These are shown in Figure 8. Figure 6 and Figure 7 show the accepted data for the saturation loading study. Isotherms rejected for too low saturation concentration in Figure 8 are included in the estimation of the intrinsic Henry constants.

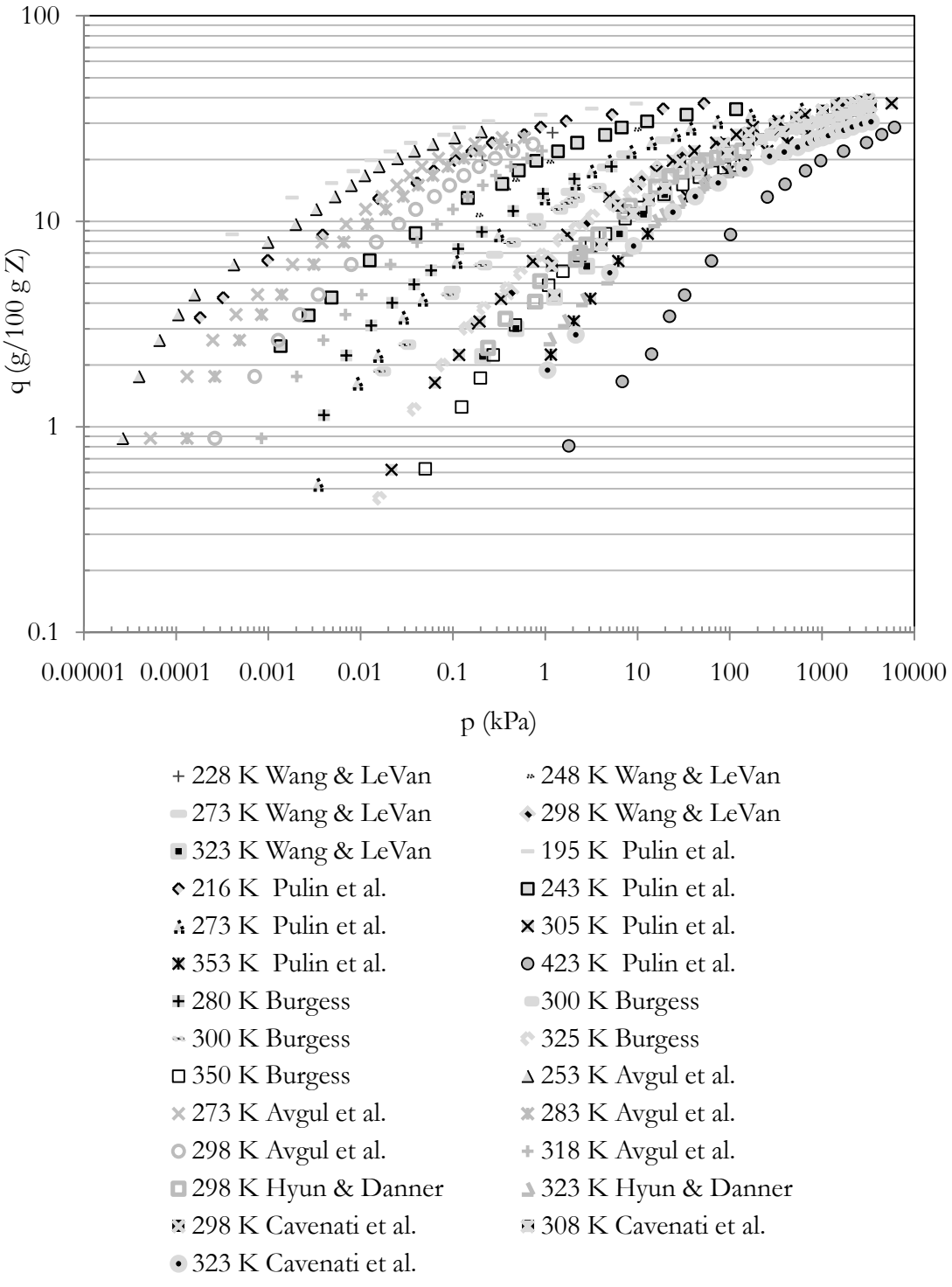

Figure 6: A log-log plot of CO_2 adsorption isotherms on zeolite 13X, showing the considered data for saturation loading estimation.

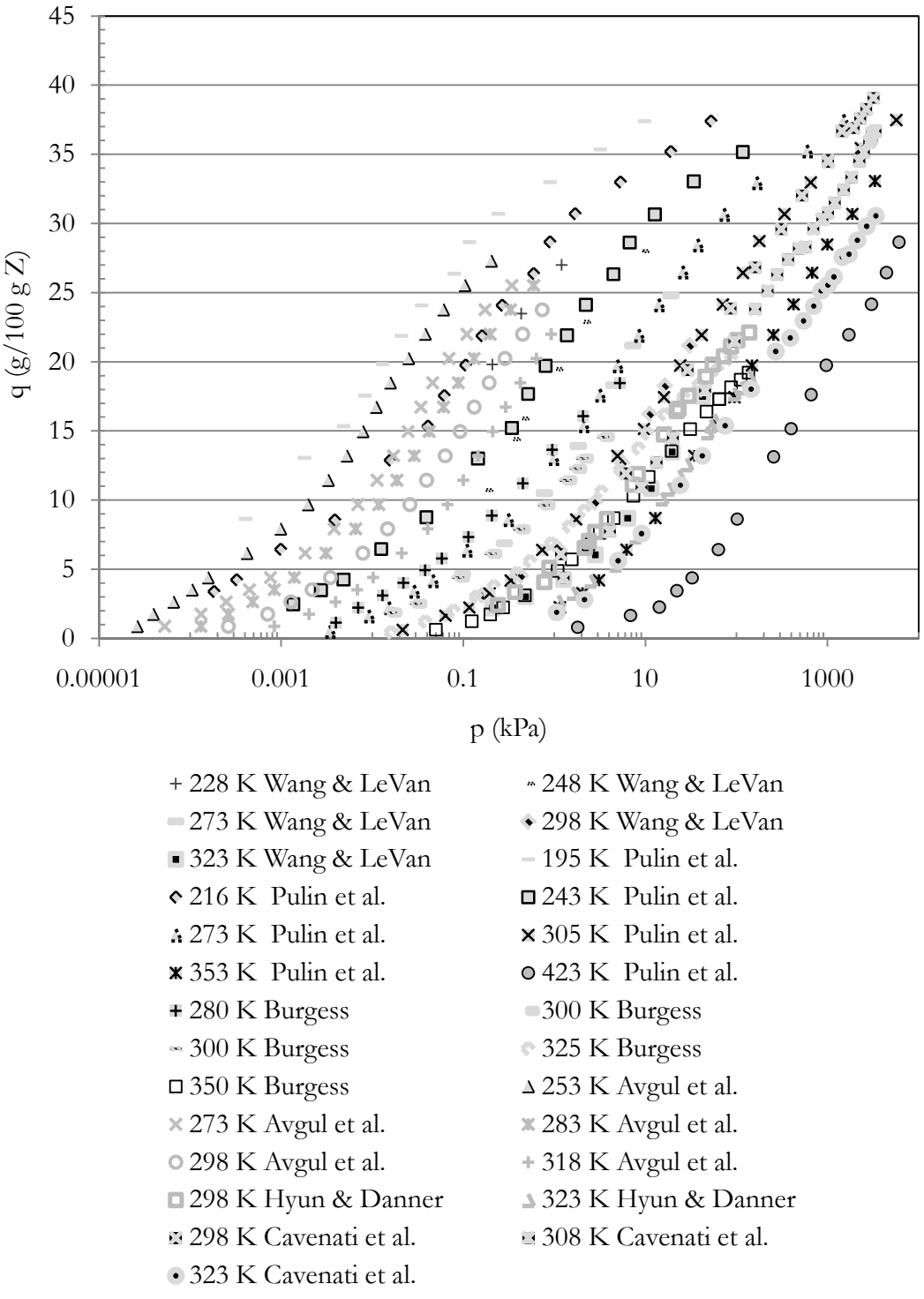

Figure 7: A semilog plot of CO_2 adsorption isotherms on zeolite 13X, showing the considered data for saturation loading estimation.

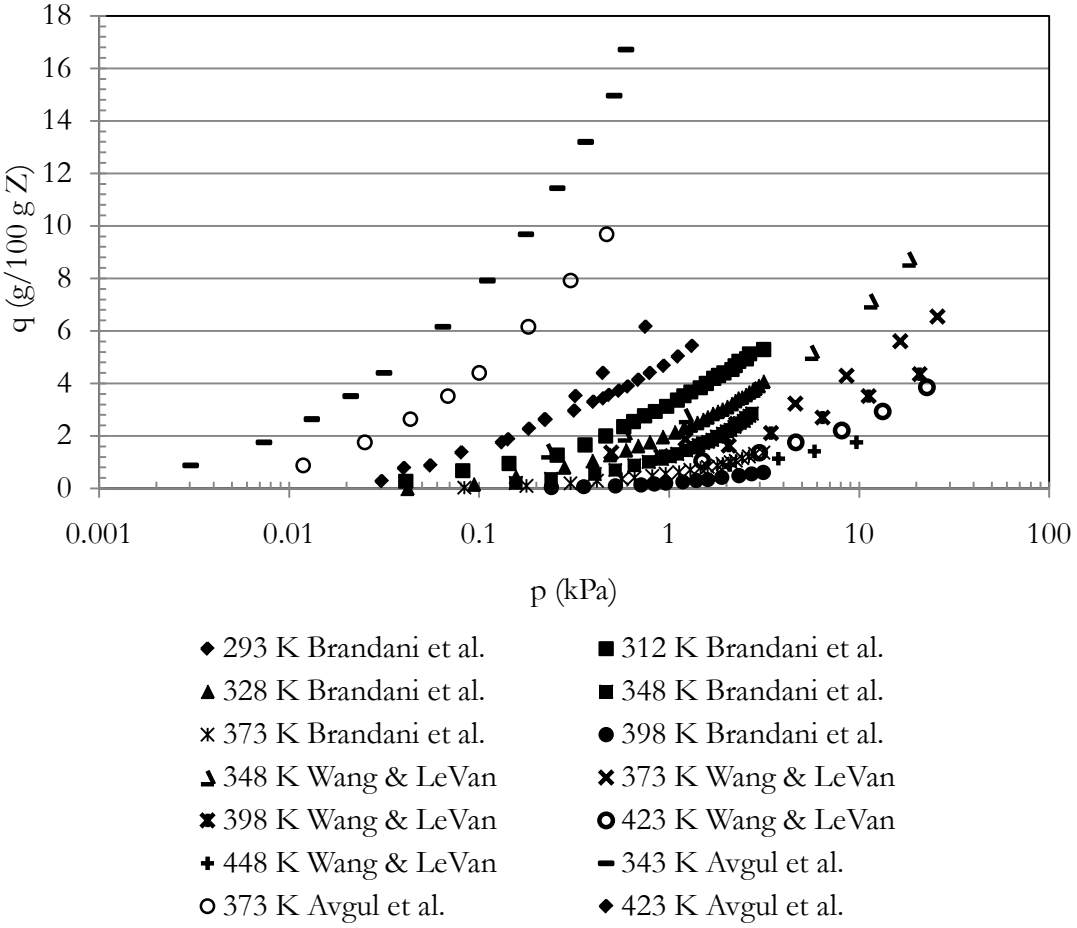

Figure 8: Eliminated studies from saturation loading estimation of the adsorption of CO_2 on zeolite 13X.

The saturation loading is taken as the value of q_{max} (g/100 g Z) for the isotherms deemed close to saturation as shown in Figure 3 and Figure 6. It is difficult to quantify the accuracy of this estimation as the approach to saturation is not clear in many cases. The estimated q_{max} (g/100 g Z) values are deemed to be accurate to ±3-5%. The q_{max} (g/100 g Z) values are plotted in Figure 9 and Figure 10 as q_{max} (g/100 g Z) versus T_r for 5A and 13X respectively.

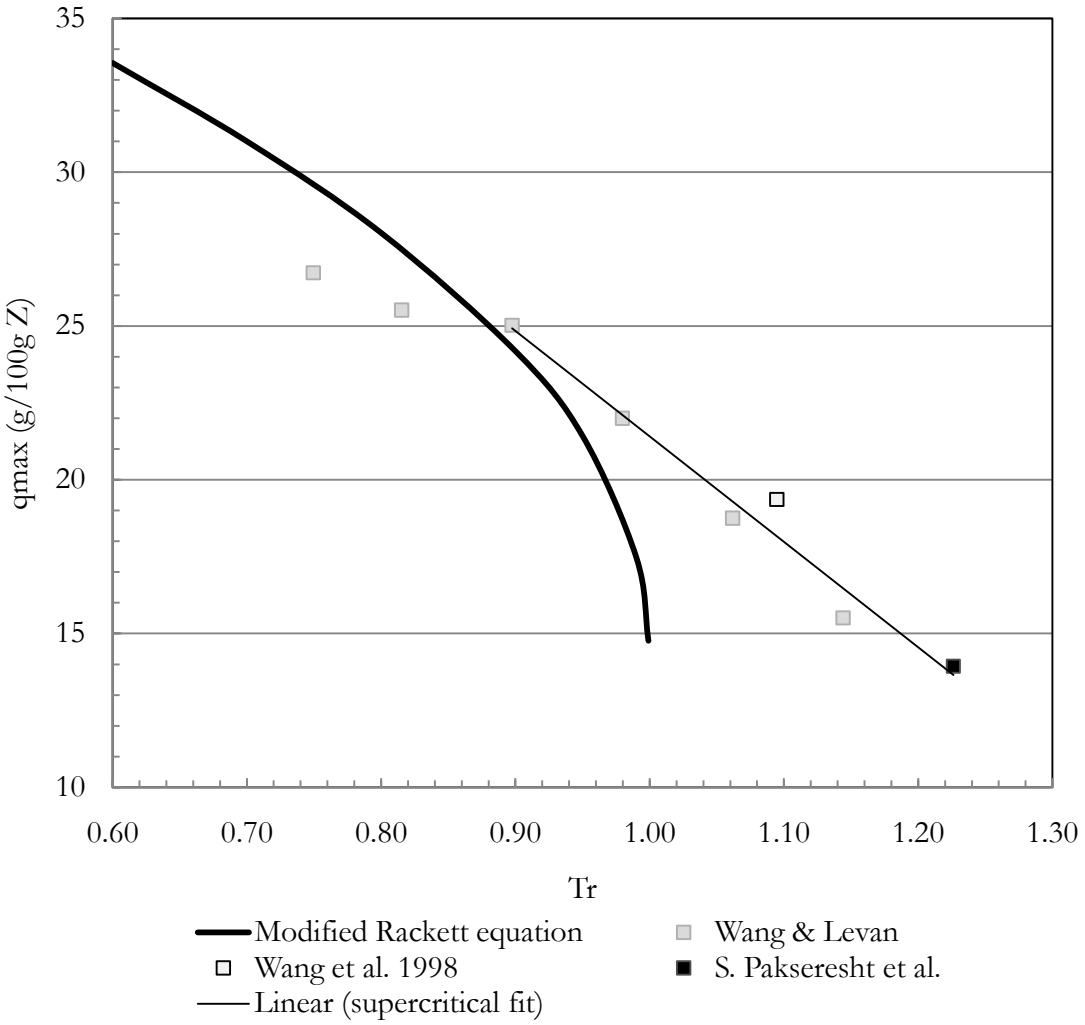

Figure 9: Estimation of the saturation loading of the adsorption of CO_2 on zeolite 5A from the Modified Rackett equation, q_{max} (g/100 g Z), and the corresponding experimental values.

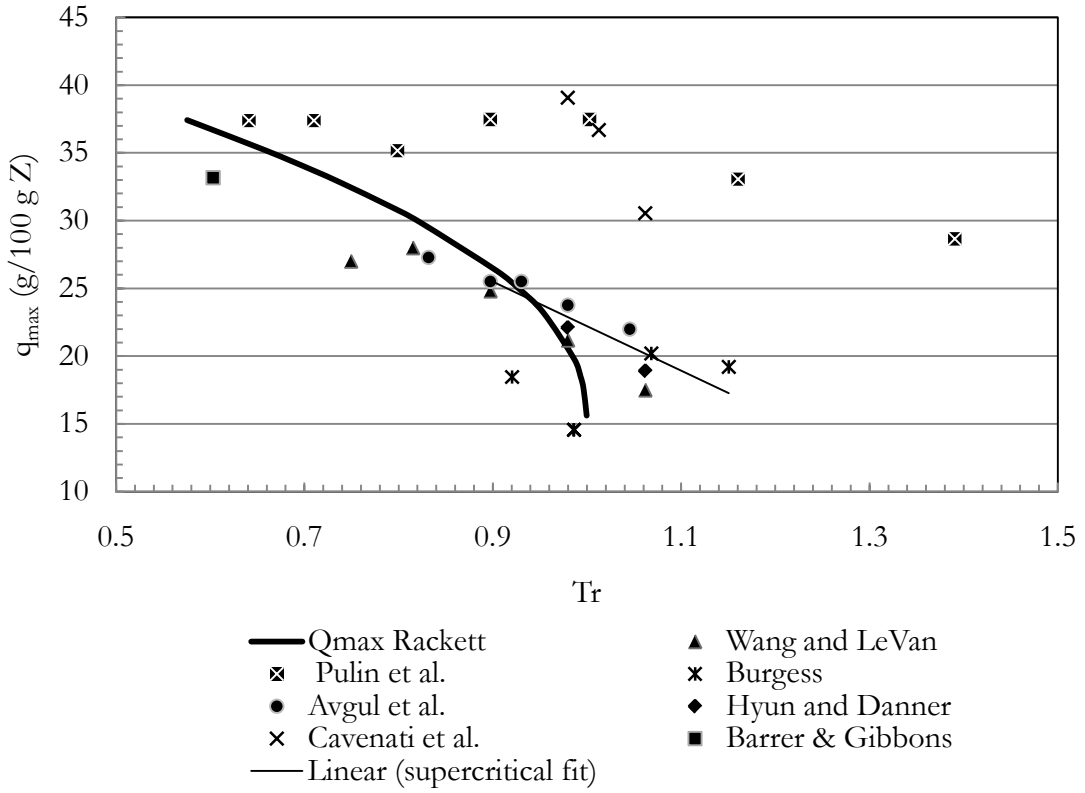

Figure 10: Estimation of the saturation loading of the adsorption of CO_2 on zeolite 13X from the Modified Rackett equation, q_{max} (g/100 g Z), and the corresponding experimental values.

Theoretical values derived from employing Modified Rackett's equation are calculated using equation 5 and are shown as dashed lines in Figure 9 and Figure 10. The value of εz and ϱ_z (g/cm3) are taken from Table 7 data and are 0.387 and 1.48 for 5A and 0.455 and 1.43 for 13X respectively. Figure 9 and Figure 10 demonstrate a good agreement between the Modified Rackett equation and the experimental values at subcritical region below Tr = 0.9, but at values above this value and in the supercritical region the deviation increases with the increase of temperature. The data by Pulin et al. [5] for 13X in Figure 10 is significantly higher than other studies. None of the other studies considered for this work except for the work of Cavenati et al. [25] support the data by Pulin et al. [5]. However; it can be seen that the data by Pulin et al. [5] follows the same trend as other studies when increasing temperature while this conclusion cannot be made for the data of Cavenati et al. [25], as more data is needed. The reliability of the data of Pulin et al. [5] and Cavenati et al. [25] needs to be verified by another laboratory. The q_{max} (g/100 g Z) values are slightly above the theoretical value suggesting that the molar volumes of CO_2 are smaller in the zeolite than in the liquid phase [27]. Further

many of the values are above a T_r of 1 for which we have no prediction. The saturation loading appears to change linearly with temperature above a T_r of 0.9, and to test this observation the values above T_r of 0.9 are fitted through a straight line. Further many of the values are above a T_r of 1 for which we have no prediction. The saturation loading appears to change linearly with temperature above a T_r of 0.9, and to test this observation the values above T_r of 0.9 are fitted through a straight line.

$$For\ 5A\ zeolite \qquad q_{max} = -34.291 * T_r + 55.696 \qquad R = 0.983 \qquad 2.14$$

$$For\ 13X\ zeolite \qquad q_{max} = -32.866 * T_r + 55.078 \qquad R = 0.869 \qquad 2.15$$

A summary of saturation loading, experimental and calculated, is presented in Table 10. Values with "*" next to them are calculated using equation 2.14 and values with "**" next to them are calculated using equation 2.15.

Table 10: A summary of saturation loading values from the Modified Rackett equation, q_{max} (g/100 g Z), and the corresponding values from experimental data for 5A and 13X.

5A Zeolite			
Experimental Data			Modified Rackett Equation
T_r	Reference	q_{max} (g/100 g Z)	q_{max} (g/100 g Z)
0.75	Wang and Levan [17]	26.73	29.60
0.82	Wang and Levan [17]	25.52	27.52
0.90	Wang and Levan [17]	25.03	24.30
0.98	Wang and Levan [17]	22.00	18.91
1.06	Wang and Levan [17]	18.76	19.29*
1.14	Wang and Levan [17]	15.51	16.47*
1.09	Wang et al. [14]	19.36	18.16*
1.23	Pakseresht et al. [12]	13.94	13.65*
13X Zeolite			
Experimental Data			Modified Rackett Equation
T_r	Reference	q_{max} (g/100 g Z)	q_{max} (g/100 g Z)
0.60	Barrer & Gibbons [28]	33.18	33.49
0.64	Pulin et al. [5]	37.39	32.55
0.71	Pulin et al. [5]	37.39	30.73
0.75	Wang and Levan [17]	27.01	29.60
0.80	Pulin et al. [5]	35.16	28.07
0.82	Wang and Levan [17]	28.00	27.52
0.83	Avgul et al. [20]	27.28	26.95
0.90	Wang and Levan [17]	24.81	24.30
0.90	Pulin et al. [5]	37.46	24.30
0.90	Avgul et al. [20]	25.52	24.30
0.92	Burgess [22]	18.46	23.18
0.93	Avgul et al. [20]	25.52	22.64
0.98	Wang and Levan [17]	21.18	18.91
0.98	Avgul et al. [20]	23.76	18.91
0.98	Hyun and Danner [21]	22.11	18.91
0.98	Cavenati et al. [25]	39.08	18.91
0.99	Burgess [22]	14.56	18.08
0.99	Burgess [22]	14.56	18.08
1.00	Pulin et al. [5]	37.47	No Prediction
1.01	Cavenati et al. [25]	36.68	No Prediction
1.05	Avgul et al. [20]	22.00	20.72**
1.06	Wang and Levan [17]	17.49	20.18**
1.06	Hyun and Danner [21]	18.92	20.18**
1.06	Cavenati et al. [25]	30.55	No Prediction
1.07	Burgess [22]	20.20	19.96**
1.15	Burgess [22]	19.21	17.26**
1.16	Pulin et al. [5]	33.06	No Prediction
1.39	Pulin et al. [5]	28.65	No Prediction

The q_{max} (g/100 g Z) data in Figure 10 are the only data, compared to data for other sorbates, observed by authors to be greater than the q_{max} (g/100 g Z) value derived using the Rackett equation. In all other studies, the q_{max} (g/100 g Z) data is observed to be below the value estimated by the Rackett equation up to the critical adsorbate reduced temperature for both 5A and 13X zeolite (Abouelnasr and Loughlin [29] and Al Mousa [30]). From Figure 10, it is possible to estimate the critical adsorbate reduced temperature for the CO_2 molecule at 0.9. The higher q_{max} (g/100 g Z) experimental values indicate a smaller partial molar volume for the adsorbed CO_2 molecule than is observed in the saturated liquid phase [27]. The molar volumes of CO_2 are shown calculated for the saturated liquid phase and for the adsorbed phase in Table 11. Also shown is the molar volume at $T_r = 1.046$ in the bulk phase and in an ionic liquid for comparison purposes

Table 11: Molar Volumes of Carbon Dioxide in cm^3/mol

Adsorbate-Adsorbent system		
T_r	V_{sat} liquid	V adsorbed phase
0.8	40.92	40.92
0.85	43.56	38.28
0.9	47.52	40.92
0.95	53.68	43.868
1.0.	93.28	46.64
Bulk Phase and Ionic Liquid		
1.046 (at 318.15 K & 200 bar)	55	29

The molar volumes of the adsorbed phase are 5 to 25% less than for the saturated liquid. At the vapor liquid critical point, the adsorbed molar volume is one half that of the saturated critical phase. This latter value is similar to what is observed in ionic liquids as the value at $T_r = 1.046$ is half that of the equivalent value in the bulk phase. It is clear that the molar volumes of the adsorbed phase are less than that of an equivalent saturated liquid, and that this is similar to results observed in the carbon dioxide ionic liquid system. It is concluded that q_{max} (g/100 g Z) can satisfactorily be calculated using equation 2.5 up to a reduced temperature of 0.9 and using equation 2.14 and equation 2.15 above this T_r for the CO_2-5A and CO_2-13X systems. More experimental data is required above a T_r of 1.2.

To determine the intrinsic Henry constants, equation 2.9, is plotted in Figure 11 and Figure 12 as a plot of ln[(p (kPa)/(q (g/100 g Z)] vs. q (g/100 g Z) in the low loading region, where q (g/100 g Z) ≤ 7.

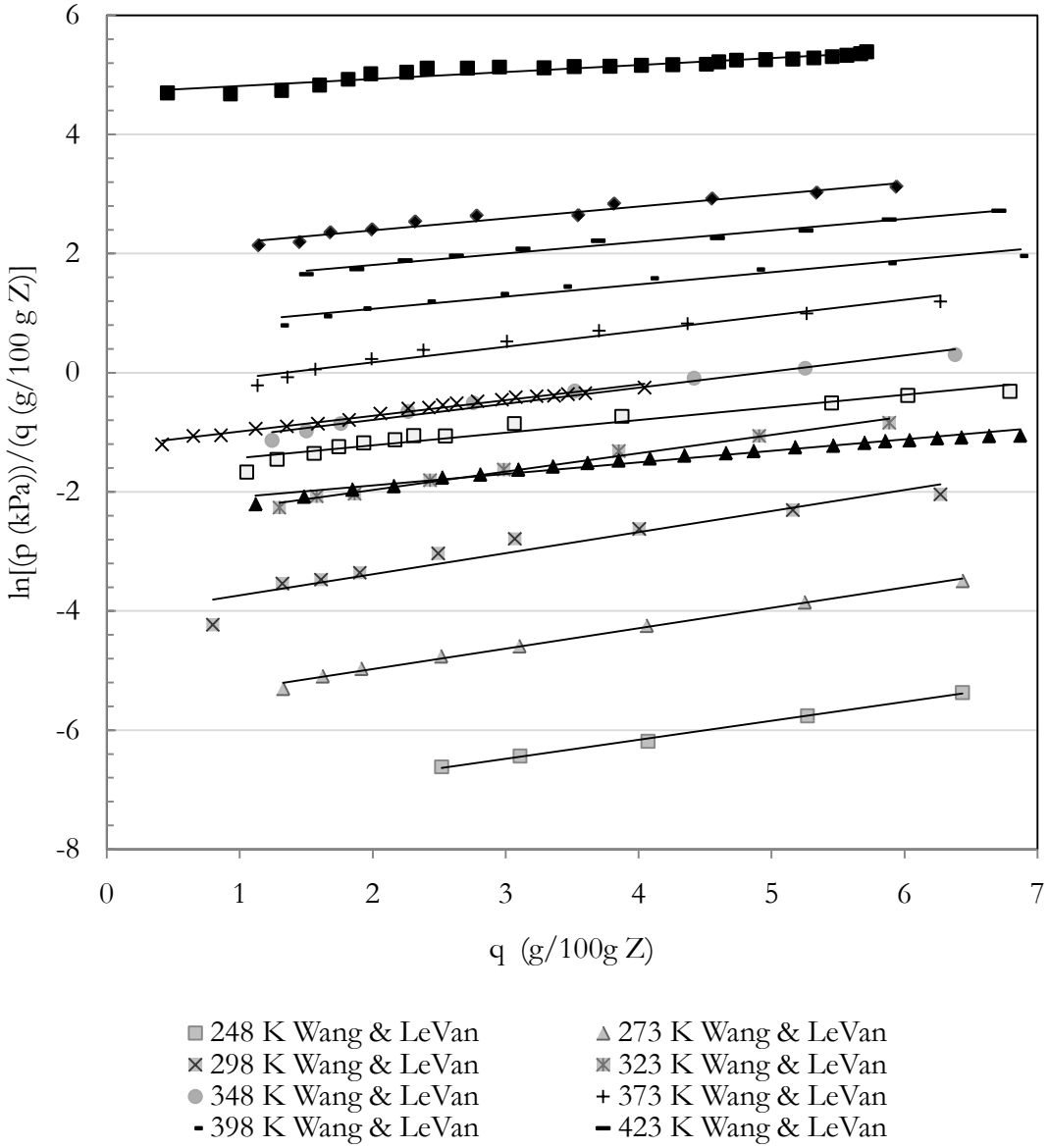

Figure 11: Virial fit for the adsorption of CO_2 on zeolite 5A studies without outliers at low loading region, i.e. q/(g/100 g Z)≤ 7.

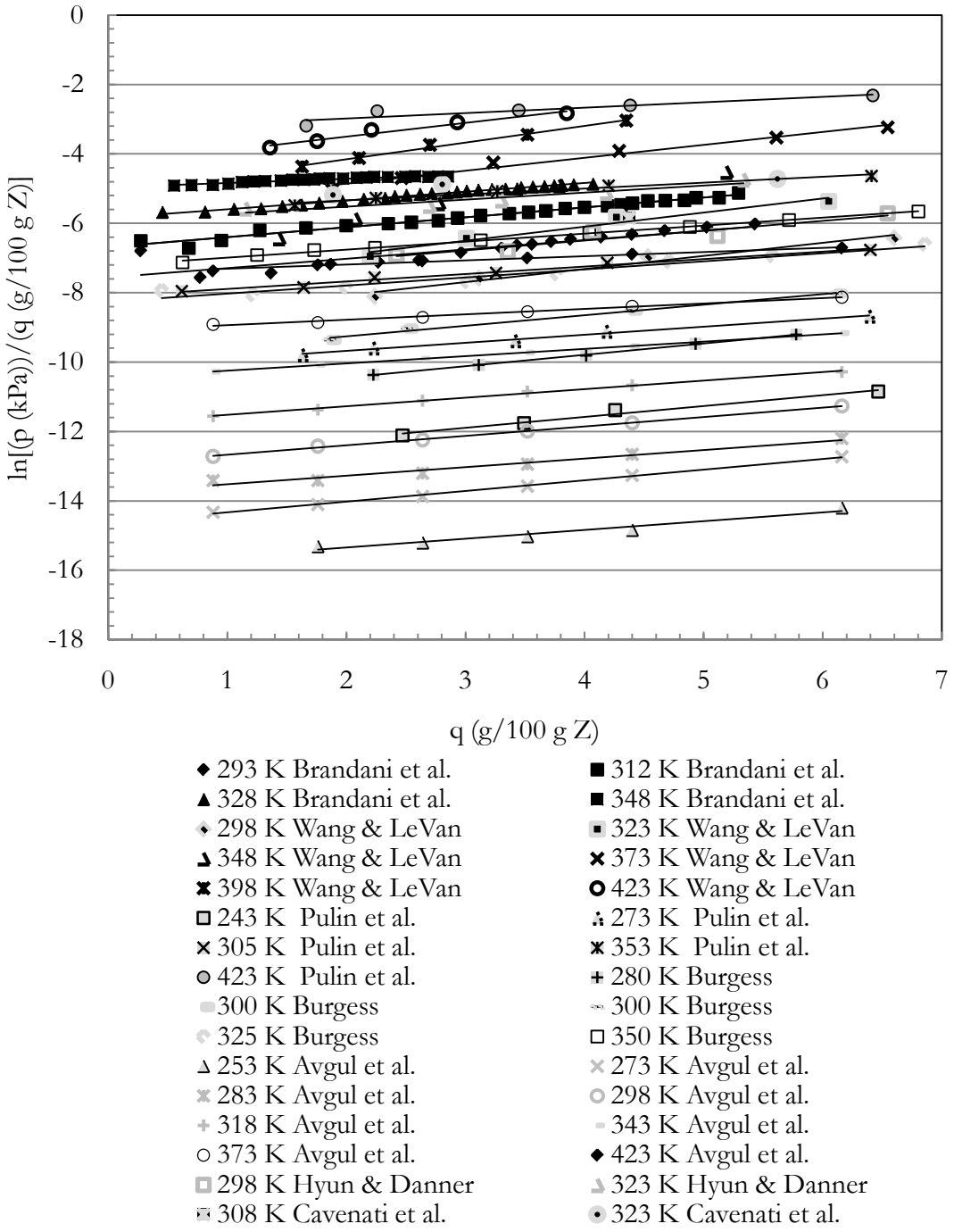

Figure 12: Virial fit for the adsorption of CO_2 on zeolite 13X studies without outliers at low loading region, i.e. q/(g/100 g Z)≤ 7.

This plot yields a straight line for each isotherm. Some outliers and isotherms with insufficient points in the low region were omitted. The Henry constant values are calculated from the intercept of the straight lines in Figure 11 and Figure 12, and are summarized in Table 12.

Table 12: Summary of Henry constants for CO_2 studies on 5A and 13X Zeolite

5A			13X		
Reference	T (K)	K_H (g/100 g Z kPa)	Reference	T (K)	K_H (g/100 g Z kPa)
Wang and Levan [17]	247	1094.00	Avgul et al. [20] **	253	7.69E+06
Wang and Levan [17]	273	286.40	Avgul et al. [20] **	273	2.28E+06
Wang and Levan [17]	298	48.72	Pulin et al. [5]	273	2.53E+04
Wang and Levan [17]	323	13.22	Burgess [22]	280	6.66E+04
Brandani et al. [15]	323	9.76	Avgul et al. [20] **	283	1.11E+06
Wang et al. [14]	333	5.17	Wang and Levan [17]	298	6807.34
Wang and Levan [17]	348	3.80	Hyun and Danner [21]	298	2068.27
Brandani et al. [15]	348	3.49	Avgul et al. [20] **	298	4.16E+05
Wang and Levan [17]	373	1.42	Burgess [22]	300	1.69E+04
Wang and Levan [17]	398	0.52	Burgess [22]	300	1.689E+04
Wang and Levan [17]	423	0.24	Pulin et al. [5]	305	3318.78
Wang and Levan [17]	448	0.14	Brandani et al. [15]	312	828.76
Pakseresht et al. [12]	573	0.0091	Avgul et al. [20] **	318	1.29E+05
			Wang and Levan [17]	323	2252.87
			Hyun and Danner [21]	323	373.76
			Burgess [22]	325	4484.21
			Brandani et al. [15]	328	346.61
			Avgul et al. [20] **	343	3.48E+04
			Brandani et al. [15]	348	148.11
			Wang and Levan [17]	348	790.09
			Burgess [22]	350	1364.02
			Pulin et al. [5]	353	384.33
			Brandani et al. [15]	373	71.79
			Wang and Levan [17]	373	271.96
			Avgul et al. [20] **	373	8291.94
			Wang and Levan[16]	398	167.51
			Brandani et al. [15]	398	20.25
			Wang and Levan [17]	423	66.09
			Pulin et al. [5]	423	26.84
			Avgul et al. [20] **	423	1693.62
			Wang and Levan [17]	448	93.53

The K_H (g/100 g Z kPa) values are plotted in a van't Hoff plot as shown in Figure 13 and Figure 14.

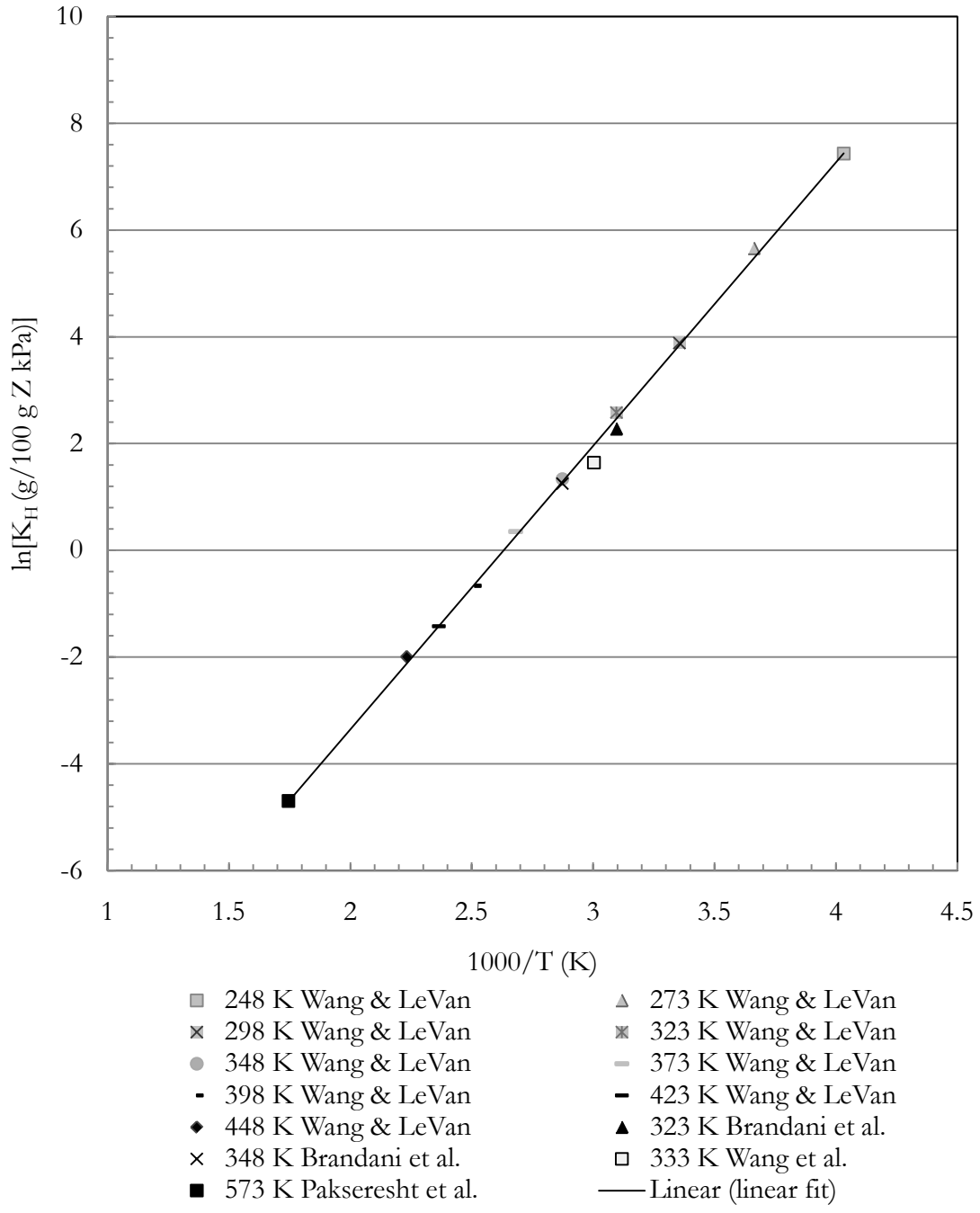

Figure 13: van't Hoff plot for the adsorption of CO_2 on zeolite 5A.

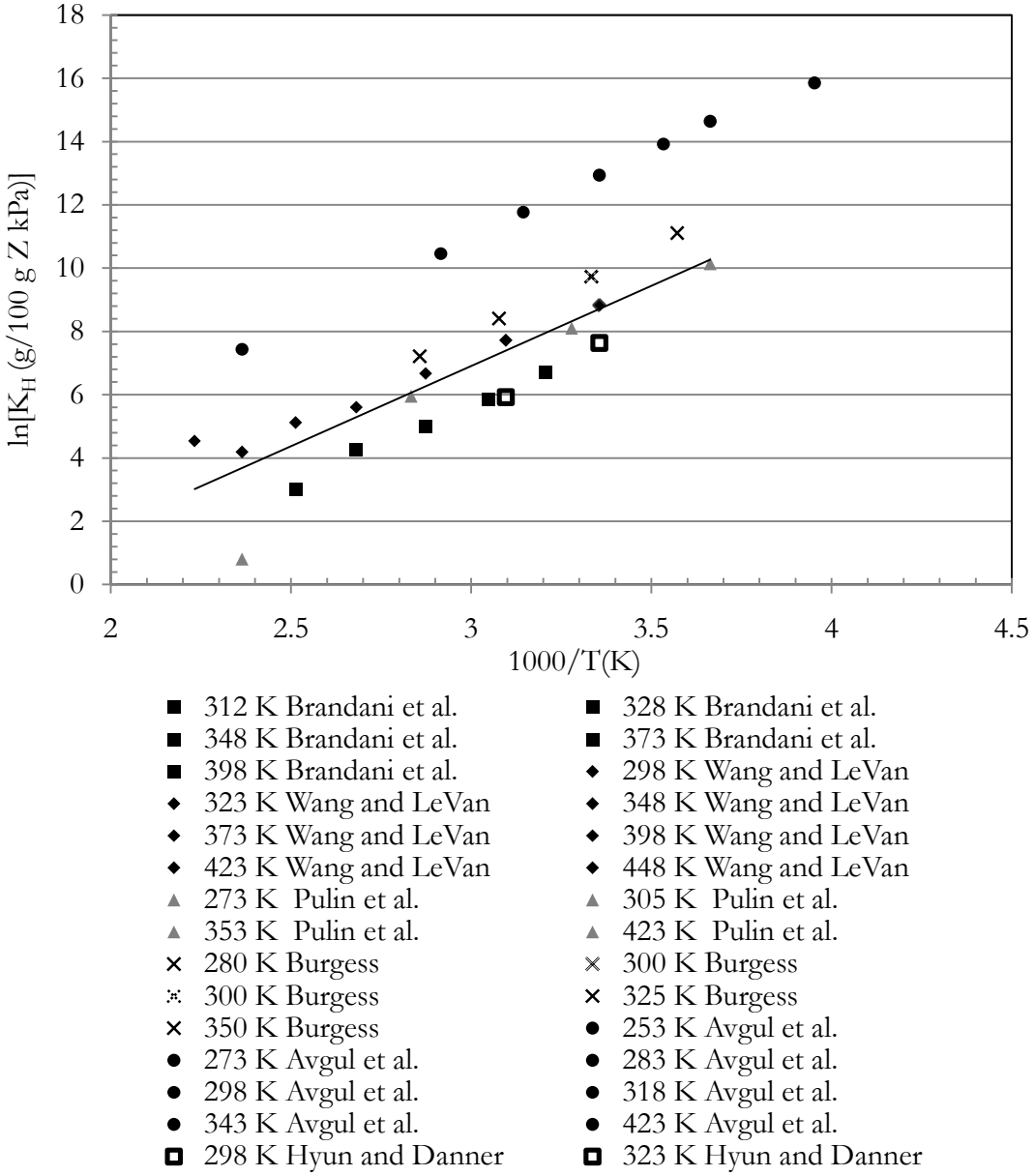

Figure 14: van't Hoff plot for the adsorption of CO_2 on zeolite 13X.

The slope of the straight line is the enthalpy of adsorption ($-\Delta H_0$) (kJ/mol). This was calculated to be 44.15 for the five studies used in the CO_2-5A system and 51.34 for the seven studies used in the CO_2-13X system. The correlation coefficient for the vant Hoff plots is 0.999 for the CO_2-5A system, and 0.899 for the CO_2-13X system. The correlation coefficient of 0.999 is a staggering number for studies from five different laboratories for the CO_2-5A system. The data of Avgul et al. [20] is shown plotted in Figure 12. However, it is not included in the calculation of the Henry constant or the heat of adsorption for the CO_2-13X system. The reason for this is that the NaX zeolite used by Avgul et al. [20] had the formula weight of $0.06H:0.94NaAlO_2:1.38SiO_2$. The inclusion of the hydrogen in the formula gave Henry constants two orders of magnitude

greater than for the normal NaX and accordingly was omitted from the calculation. The inclusion of hydrogen in the formula weight did not affect the saturation values, and that is why the data of Avgul et al. [20] was retained.

In calculating the Henry constants using the data in Figure 11 and Figure 12, the authors removed outliers. However, outliers became too consistent to retain the title of outliers. The removed outliers are shown in Figure 15 in a plot of ln[(p (kPa)/(q (g/100 g Z)] vs. q (g/100 g Z) at an extremely low loading, ≤ 1 for 13X.

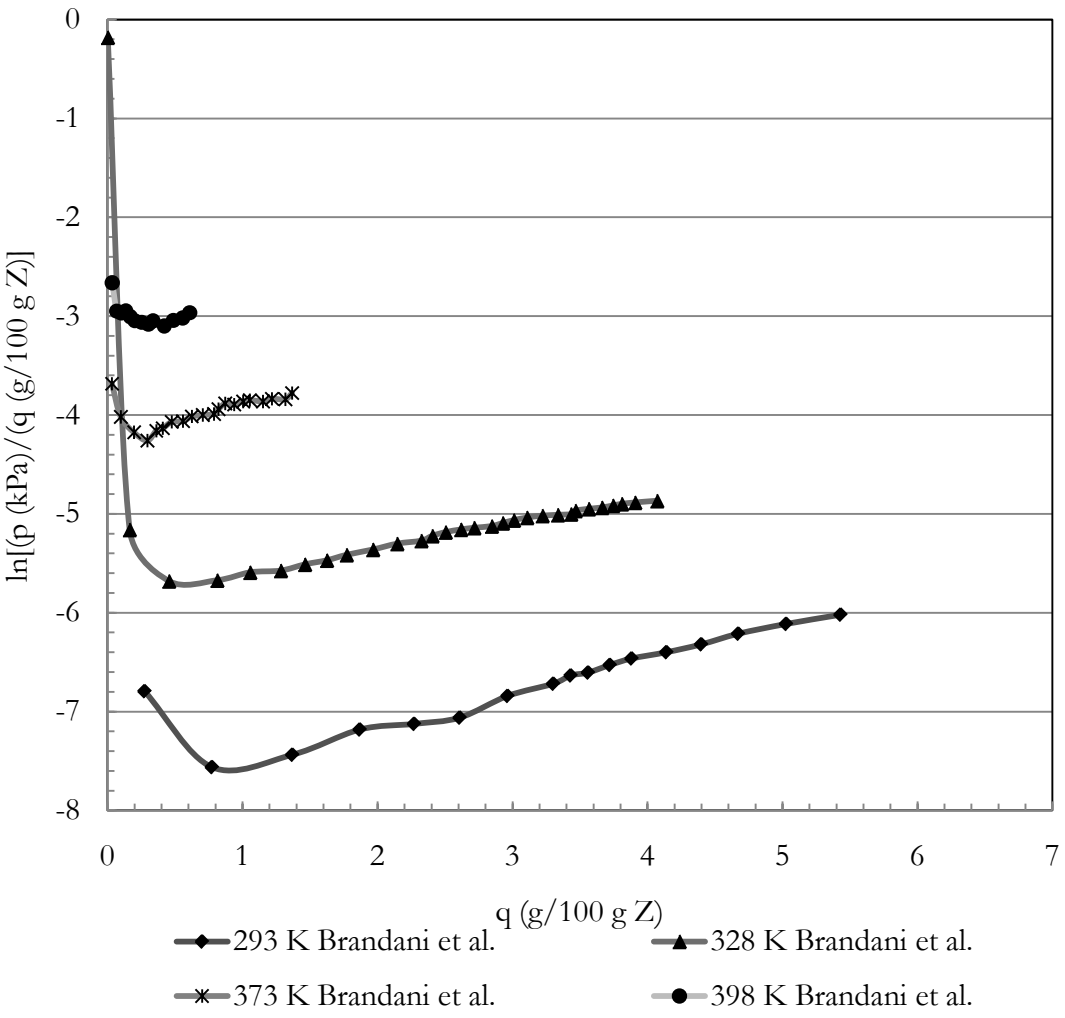

Figure 15: Virial fit for the adsorption of CO_2 on zeolite 13X showing isotherms with outliers.

It is clear that there is an unusual kink upwards at q (g/100 g Z) less than 0.5 indicating that an interesting effect has occurred. The reason for these outliers can be attributed to a differing kind of bonding for the initial single molecule of carbon dioxide adsorption. Llano-Restrepo [4] postulates that CO_2 molecules interacts with either one Na(2) ion to form a Na^+-CO_2 complex or with one Na(3) ion to form either a partially ionized or a

bidentate carbonate species. It is possible that either of these complexations could result in the initial unusual observed effect. Further, these complexations could cause the calorimetric measurement of the heat of adsorption to be larger initially as has been reported by Dunne et al. [31] and Shen et al. [32]. Also, since it only occurs at loadings of less than 0.5 g/100 g Z, it is quite possible that most of the non-calorimetric studies miss this effect as has been reported by Shen et al. [32].

The isosteric heats were calculated using equation 2.13 by plotting ln(p (kPa)) versus 1000/T (K) at constant loading as shown in Figure 16 and Figure 17 for 5A and 13X zeolites respectively.

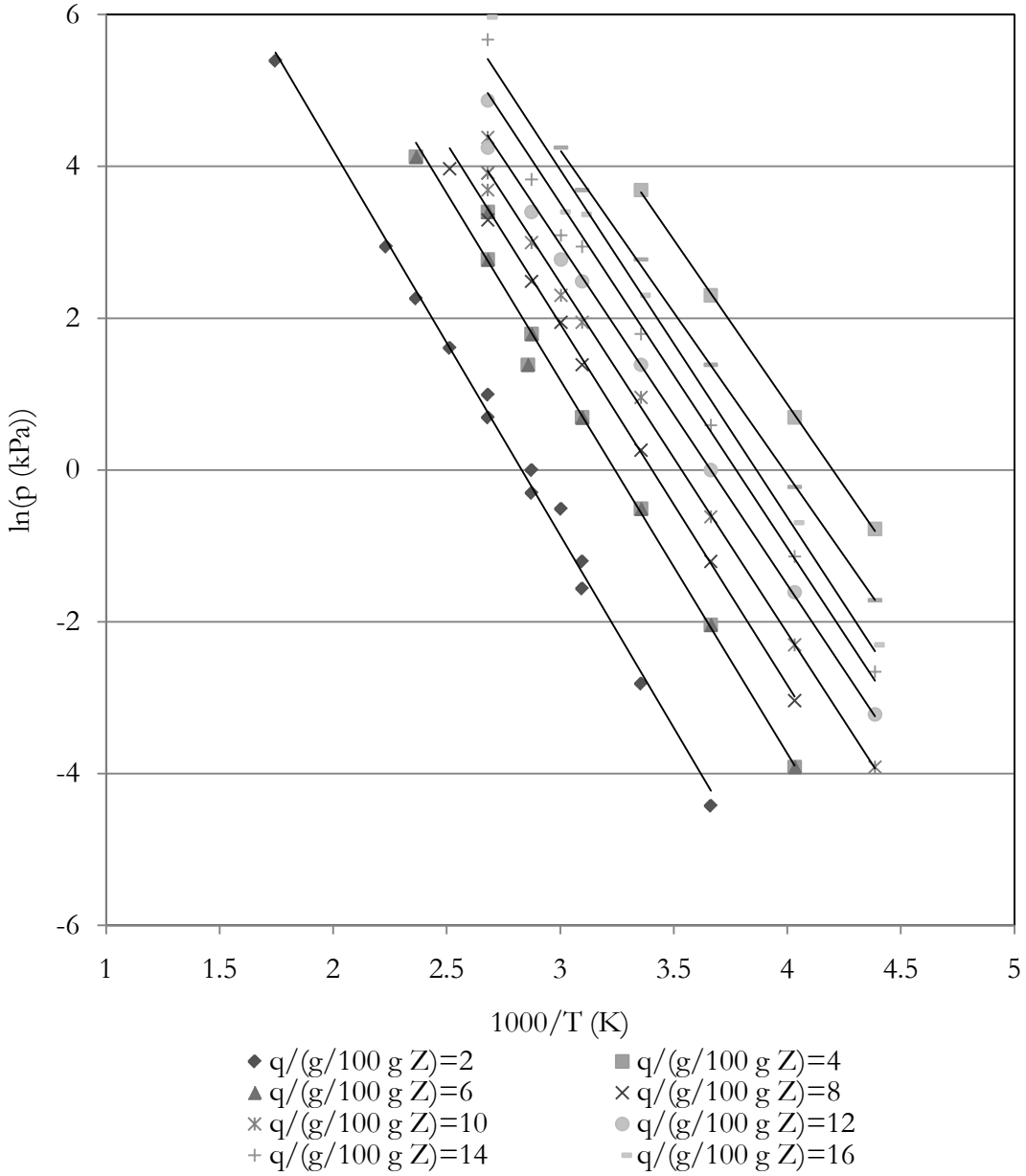

Figure 16: Sorption isosteres of CO_2 on zeolite 5A.

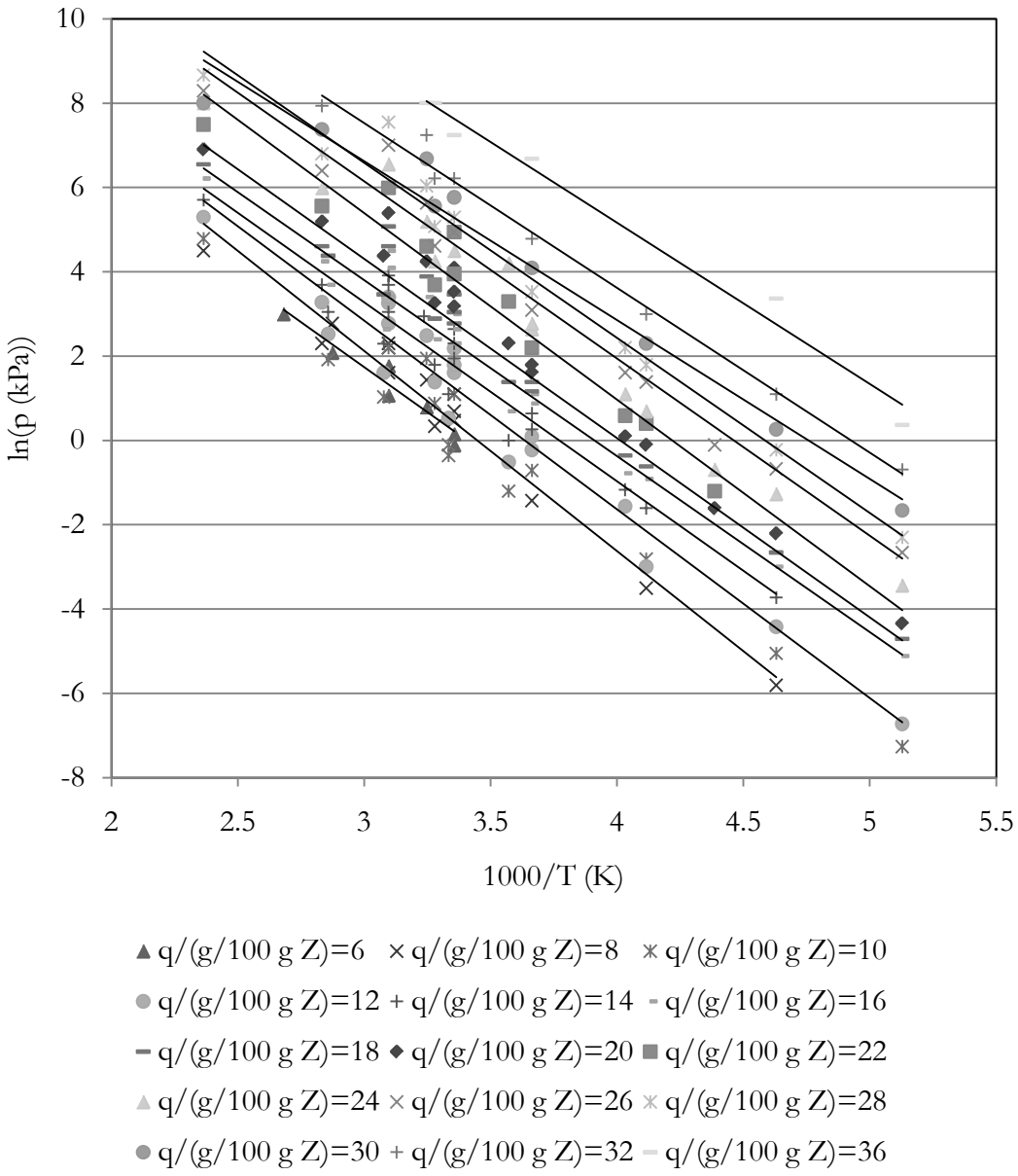

Figure 17: Sorption isosteres of CO_2 on zeolite 13X.

Five studies were used for the 5A calculations and seven studies were used for the 13X calculations. From equation 2.13, the slopes of the straight lines in Figure 16 and Figure 17 are the isosteric heats at the respective loading. The isosteric heats are compared in Figure 18 as functions of loading.

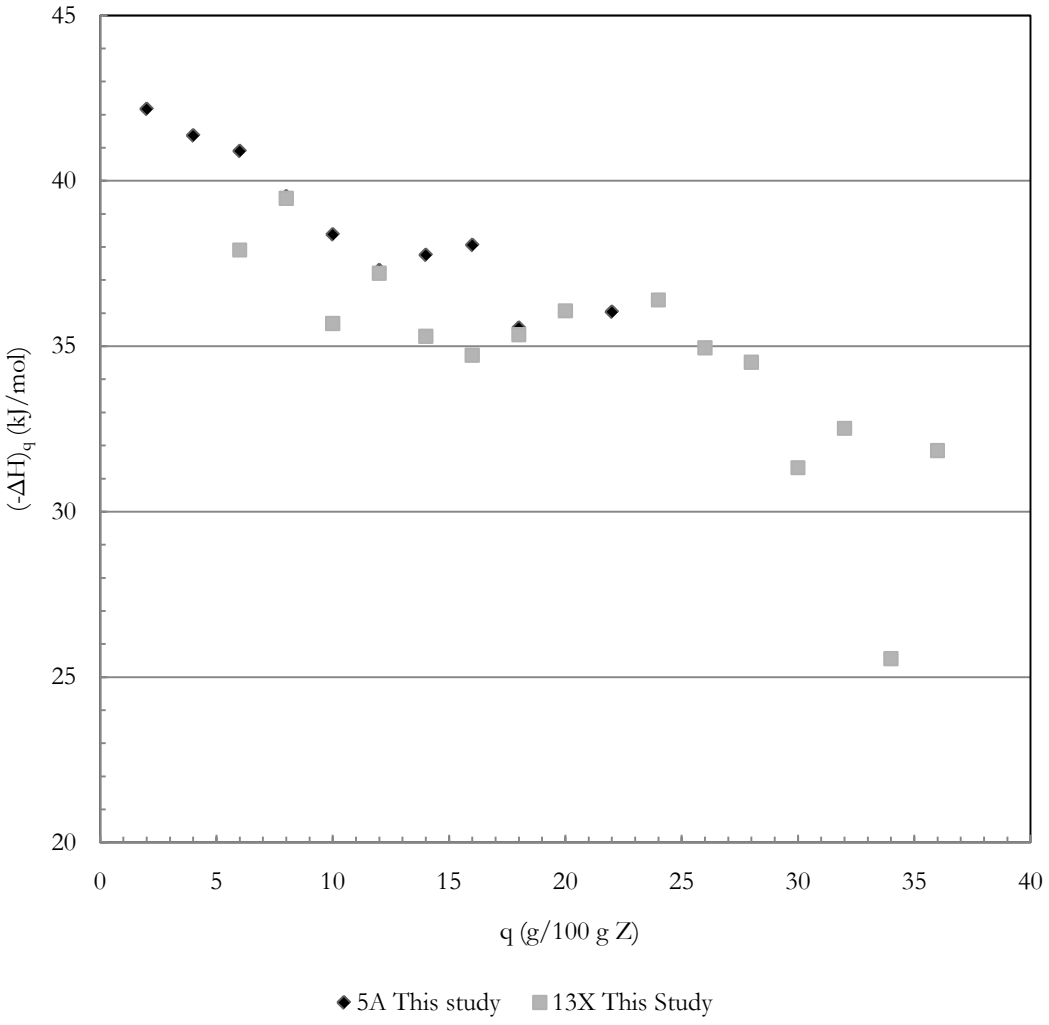

Figure 18: Isosteric heats as functions of loading for the adsorption of CO_2 on zeolites 5A and 13X.

The isosteric heat for 5A is slightly greater than that for 13X probably due the adsorption field in the more confined cavity. The isosteric heat decreases from approximately 45 kJ/mol at zero loading, decreasing linearly initially to approximately 35 kJ/mol, plateauing in the mid region at this value, and decreasing to 25.2 kJ/mol as saturation is approached. The heat of sublimation of carbon dioxide is 25.2 kJ/mol which is the lowest isosteric heat observed. The isosteric heats at different loadings for zeolite 5A and 13X are summarized in Table 13.

Table 13: Isosteric Heats $(-\Delta H)_q$ at different loadings q (g/100 g Z) for 5A and 13 X

5A		13X	
q (g/100 g Z)	$(-\Delta H)_q$ (kJ/mol)	q (g/100 g Z)	$(-\Delta H)_q$ (kJ/mol)
2	42.17	2	28.00
4	41.37	4	23.93
6	40.90	6	37.91
8	39.53	8	39.47
10	38.38	10	35.69
12	37.30	12	37.21
14	37.76	14	35.30
16	38.06	16	34.73
18	35.56	18	35.35
20	31.09	20	36.07
22	36.04	22	36.80
		24	36.40
		26	34.95
		28	34.52
		30	31.33
		32	32.52
		34	25.56
		36	31.85

The value of 45 kJ/mol is similar to the value of 44.1 kJ/mol obtained in the van't Hoff plot at zero loading for the Henry constant for 5A zeolite but is less than the value of 51.3 kJ/mol for 13X zeolite in a similar van't Hoff plot.

The data for 13X is again plotted in Figure 19 together with the study of Dunne et al. [31] and the two studies of Shen and Bulow [9], one adsorption isostere and one calorimetric measurement.

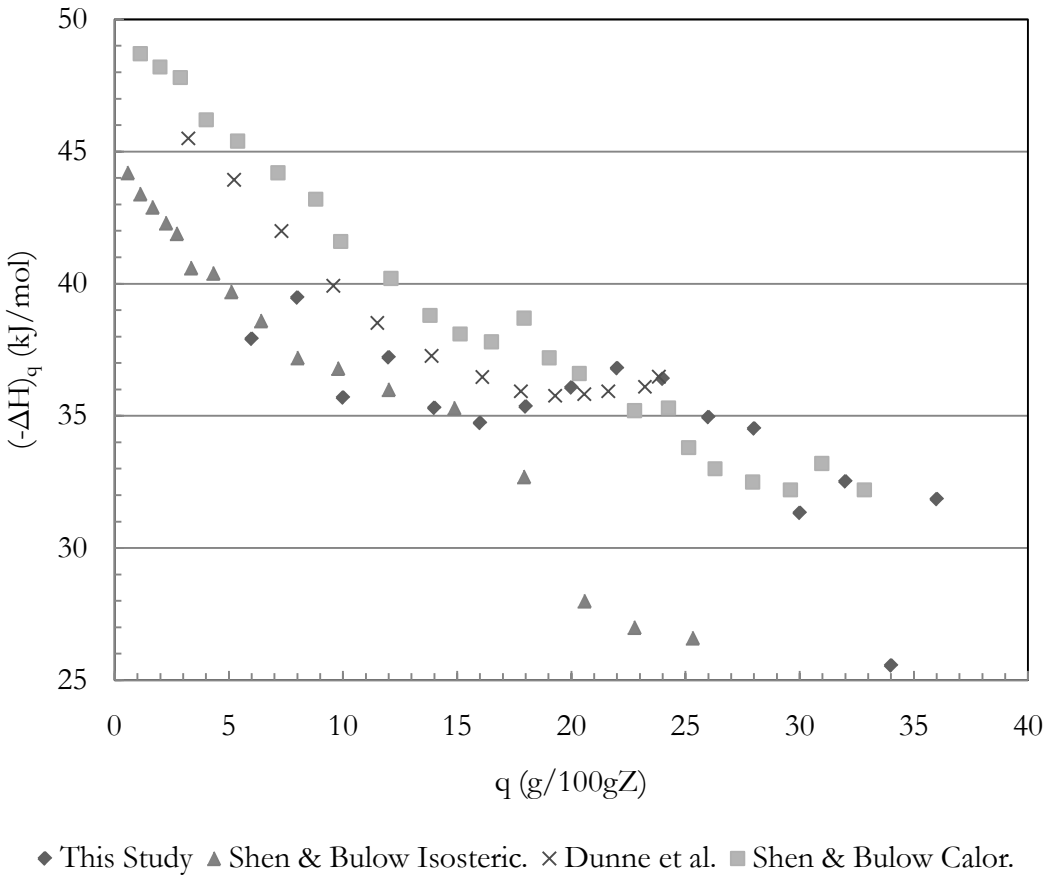

Figure 19: Isosteric heats, for different studies, as functions of loading for the adsorption of CO_2 on zeolite 13X.

Further studies are available in Figure 6 of Llano-Restrepo [4] but have not been included as the Figure becomes congested. The two calorimetric studies of Dunne et al. [31] and Shen and Bulow [9] have a zero loading value of approximately 50 kJ/mol, a gradually decreasing region to approximately 36 kJ/mol in the plateau region; Dunne et al.'s [31] study subsequently decreases as it starts to approach the heat of sublimation at higher loadings. The reported values in this study are lower than the calorimetric values in the decreasing region, similar in the plateau region, and in the approach to saturation region. The isosteric heat curve reported by Shen and Bulow [9] is the lowest of all the studies by approximately 3 to 5 kJ/mol. The zero calorimetric loading is consistent with the value of 51.3 kJ/mol obtained in the van't Hoff study of the Henry constant determination. The consistently lower values of the isosteric heat determination from the non calorimetric measurements reported in the literature may be attributed to the outlier region of less than 0.5 (g/100 g Z) reported in Figure 15 above. Finally, the sharp decrease from50 kJ/mol to the plateau region at 36 kJ/mol may be attributed to the interaction of the Na^+ ion with the quadrupole moment of CO_2; at high coverage the

high energy Na^+ ions become saturated and the gas-solid interaction energy is mainly dispersion [31].

Unpublished data for the adsorption of CO_2 on zeolite 13X by Burges [22] is presented in Table 9 and fitted to Toth isotherm, equation 2.11. The objective from this fitting is to compare the values of q_{max} (g/100 g Z) and K_H (g/100 g Z kPa) obtained from the model with the intrinsic values obtained from the previous analysis. The value of q_{max} (g/100 g Z) is obtained directly from the model or equation 2.15 and the Henry constant is obtained by equation 2.12. The Toth parameters are tabulated in Table 14 with the correlation coefficient for the Toth fit.

Table 14: Toth parameters for Burgess's Data

T_r	q_{max} (g/100 g Z)	q_{max} (Rackett)	R	b (1/kPa)	t	K_H (g/100 g Z kPa) (Toth)	K_H (g/100 g Z kPa) (Virial)
0.92	18.46	23.18	0.9989	0.2771	0.348	1141	6.66E+04
0.99	20.86	18.08	0.9998	0.4209	0.2640	1058	1.69E+04
0.99	22.29	18.08	0.9998	0.4197	0.421	1038	1.69E+04
1.07	23.31	19.96*	0.9985	0.7063	0.458	50	4.48E+03
1.15	23.85	17.26*	0.9999	1.0586	0.417	22	1364

* calculated using equation 2.15

The first observation about the results of the fit is the huge percentage difference at T_r=0.99. Another clear observation is the huge difference between the values of K_H (g/100 g Z kPa). The justification for the difference is that the fit is carried out over a small range and the value of K_H (g/100 g Z kPa) is impacted by the value of q_{max} (g/100 g Z), as they interact. The model's K_H (g/100 g Z kPa) values should not question the values obtained earlier and summarized in Table 12 because K_H (g/100 g Z kPa) is derived independently of q_{max} (g/100 g Z) and q_{max} (g/100 g Z) is dependent on the Modified Rackett equation and hence it is also independent of K_H (g/100 g Z kPa).

CHAPTER 3. REVISED N-ALKANE PARAMETERS FOR THE MULTI-SITE LANGMUIR (MSL) MODEL

3.1 Introduction

With various industries having adsorption at the heart of their process, it is absolutely critical to achieve optimum performance for the adsorption column. The MSL model is used frequently in predicting the break-through curves for adsorption columns. This shows the importance of estimating the correct values of parameters for this model. Correct values for the model parameters result in better prediction of the unit's operation. It will also help in revealing choices for improvement of productivity. Collecting a large number of studies and fit them using the MSL model and report the model parameters will be very valuable knowledge. A large number of studies gives confidence in results obtained. Previous work by Silva and Rodrigues [33] and Roma et al. [34] studied the adsorption of n-paraffins in 5A zeolite. Both works found that the MSL model can, in general, be used to fit experimental data. In this work, a set of data for a range of n-alkanes, C_1-C_{20}, is collected from literature and the intention is to fit the isotherms for these alkanes to the MSL model. The optimization for the MSL parameters is challenging as some parameters are very sensitive. As a result, not all alkanes gave satisfactory results when fitted to the MSL model. In this chapter, the successful fitting of C_2 and C_4 is presented along with optimized values for the model parameters. The Multisite Langmuir model used to model the adsorption of n-alkanes on 5A zeolite is:

$$K_{eq} exp\left(\frac{nu\theta}{kT}\right) = \frac{1}{p}\frac{\theta}{(1-\theta)^n} \quad 3.1$$

where the Henry's constant is defined as $K_{eq}=K_0\exp(-\Delta H_{ads}/RT)$ in (kPa^{-1}), u is the interaction energy between adsorbed molecules (positive for attraction and negative for repulsion) in (J/K), $\theta=q/q_{max}$ is the fractional coverage, n is the number of carbon atoms, p is the partial pressure of the adsorbate, and k is the Boltzmann's constant with the value $1.381*10^{-23}$ (J/K). The parameters required for the adsorption of n-alkanes on 5A zeolite for the multi site Langmuir model are the Henry's constant, K_{eq}, the saturated loading, q_{max}, and the interaction energy between adsorbed molecules, u. Loughlin and Abouelnasr [29] and Roma et al. [34] have successfully modeled the saturated sorbate loadings of C_1 to C_{18} n-alkanes on zeolite 5A. Hence, one of the three parameters in the MSL model, q_{sat}, may be determined a priori. The least squares fitting method will be used to determine the parameters of the MSL model. The sum of the square difference

between the experimental p and the calculated p will be minimized by varying the parameters K_{eq} and Δu [34], [33].

3.2 Optimization Techniques

Amid efforts to fit the MSL model, Roma et al. [34] have found the parameter, u, to be very sensitive during optimization. Accordingly, it is recommended starting the fitting by subdividing u in the following form:

$$u = \Delta u + kT \tag{3.2}$$

Then, Equation 3.2 becomes after taking the natural log of both sides:

$$\ln K_{eq} + \frac{n\Delta u\theta}{kT} + n\theta = -\ln p + ln\frac{\theta}{(1-\theta)^n} \tag{3.3}$$

First Technique

Using Equation 3.3, we can optimize the equation for the values of Δu and K_{eq} by minimizing the square difference between the experimental and theoretical values of the partial pressure, p. This procedure will result in multiple values of Δu's, one for each isotherm. The MSL equation will be:

$$p = \frac{1}{K_{eq}}\frac{\theta}{(1-\theta)^n} exp\left(-n\theta - \frac{n\Delta u\theta}{kT}\right) \tag{3.4}$$

Second Technique

An alternative fitting procedure is by using the following Equation:

$$K_{eq} = K_0 exp\left(\frac{-\Delta H}{RT}\right) \tag{3.5}$$

Substitute Equation 3.5 in Equation 3.3 to get:

$$\ln p = -n\theta - lnK_0 + \frac{\Delta H}{RT} - \frac{n\Delta u\theta}{kT} + \ln\frac{\theta}{(1-\theta)^n} \tag{3.6}$$

Take the exponential of Equation 3.6 to gives:

$$p = \frac{1}{K_0}\frac{\theta}{(1-\theta)^n} exp\left(\frac{\Delta H}{RT} - n\theta - \frac{n\Delta u\theta}{kT}\right) \tag{3.7}$$

For Equation 3.7 the only two unknowns are K_o and Δu. The equation must be written for all isotherms and then optimize for the two parameters simultaneously. This will give one value for K_0 and most importantly one value for Δu as well, which make this method, in theory, a more favorable one to implement.

Third Technique

The last fitting procedure is done by obtaining the value of K intrinsically using the Virial isotherm where possible. This leaves Δu as the only variable to be calculated in the MSL model. But this will only be valid for n-alkanes having a significant amount of low concentration data. A comparison of the K values derived in both models will be very valuable.

3.3 Analysis

To perform the optimization of the model's parameter, it is important to know how to obtain the values of other variables in the model. As mentioned earlier, the saturation concentration, q_{max}, is calculated using the model of [29], which states that the sorbate densities can be calculated using the modified Racket equation for estimating the density:

$$q_{max}\left(\frac{g}{100\ g\ z}\right) = 100\frac{\epsilon_z}{\rho_z}\left(\frac{P_c.MW}{RT_c}\right)Z_{RA}^{-\{1+(1-T_r)^{0.2857}\}} \quad 3.8$$

where P_c is the critical pressure (atm), T_c is the critical temperature (K), ε_z is the crystallographic 5A zeolite void volume, 0.47 cm^3/cm^3 of zeolite 5A [6], ϱ_z is the 5A zeolite density, MW is the molecular weight, T_r is the reduced temperature and Z_{RA} is a particular constant for the modified Racket equation, for which values are given in the paper by Spencer and Danner [35]. This equation is valid to estimate the q_{max} below the critical adsorbate reduced temperatures which are:

methane	T_{CAR}=0.83
ethane	T_{CAR}=0.96
all other n-alkanes	T_{CAR}=0.975

Above the critical adsorbate reduced temperatures, the recommended equation to use is:

$$q_{max} = 8.0 \pm 1.0\ \frac{g}{100\ g\ Z} \quad 3.9$$

Since the temperature of the system will be known, the reduced temperature can be calculated and from the value of T_r and hence calculating q_{max} will be straightforward following equation 3.8 or 3.9. Then, the value of θ can be calculated for each isotherm. The values of $-\Delta H_{ads}$ are obtained from [36]. The Henry constants can be calculated using the equation:

$$H = q_{max}K_{eq} \quad 3.10$$

3.4 Results and Discussion

In this section, the results of applying the first and second methods are discussed. The data for C_1-C_5 were fitted, and surprisingly only C_2 and C_4 gave acceptable results when applying the first method. The second method proved to be troublesome to apply as the set of data is large. This complicates the optimization even more since all isotherms should be optimized simultaneously. A Table of data optimized and optimized parameters are provided for C_2 and C_4. The optimization is carried out using "Solver" in Microsoft Excel. In addition to that, plots of the experimental data and fittings are

provided. For each set of data, p is calculated according to the first optimization techniques:

$$p = \frac{1}{K_{eq}} \frac{\theta}{(1-\theta)^n} exp\left(-n\theta - \frac{n\Delta u\theta}{kT}\right) \quad 3.4$$

where $\theta = q/q_{max}$ and q_{max} is calculated according to equation 3.8 and equation 3.9:

$$q_{max}\left(\frac{g}{100\ g\ Z}\right) = 100\frac{\epsilon_z}{\rho_z}\left(\frac{P_c.MW}{RT_c}\right)Z_{RA}^{-\{1+(1-T_r)^{0.2857}\}} \quad 3.8$$

$$q_{max} = 8.0 \pm 1.0\ \frac{g}{100\ g\ Z} \quad 3.9$$

3.4.1 C_2 Results

A set of available data of adsorption of C_2 on zeolite 5A is collected from literature. C_2 adsorption studies on 5A zeolite, the optimized parameters' values, and the respective coefficient of determination, R^2, are summarized in Table 15.

Table 15: Summary of C_2 adsorption studies on 5A zeolite, optimized parameters, and coefficient of determination

Reference	Isotherm Temperature (K)	q_{max} (g/100 g Z)	K_{eq} (kPa^{-1})	$\Delta u*10^{23}$ (J)	R^2
Loughlin [37]	230	11.361	28.567	-658.017	0.986
Loughlin [37]	273	9.463	0.550	-263.217	0.982
Richards	194.5	12.547	8.390	-1424.475	0.882
Richards	218	11.786	1232.857	-790.320	0.976
Richards	233	11.250	16.868	-295.846	0.910
Richards	253	10.444	0.898	-67.617	0.974
Richards	273	9.463	0.209	36.631	0.994
Richards	288	8.484	0.115	-14.675	0.939
Veyssiere	243	10.863	0.357	-35.846	0.908
Veyssiere	273	9.463	0.160	129.219	0.941
Veyssiere	293	8.055	0.069	1557.784	0.976
Veyssiere	298	9.000	3.690E-04	-98.924	0.392
Veyssiere	313	8.055	0.056	-658.017	0.980

During the execution of optimization, the small value of Δu made it difficult to obtain the desired results. To get around this problem, the optimization is run for the value of $\Delta u*10^{23}$ and then use the factor of 10^{-23} inside the same equation, equation 3.4, when calculating pressure, p. This solved the problem completely.

Using the values of parameters in Table 15, isotherms are plotted and compared to their experimental counterparts. From the coefficient of determination for the isotherm of Veyssiere at 298 K it can be seen that the MSL fit for this isotherm is not satisfactory. In addition, the first point of the isotherm of Veyssiere at 243 K is found to be an outlier and is subsequently removed. For the rest of isotherms, the fit is excellent confirming the validity of the optimization technique used and the value of parameters obtained.

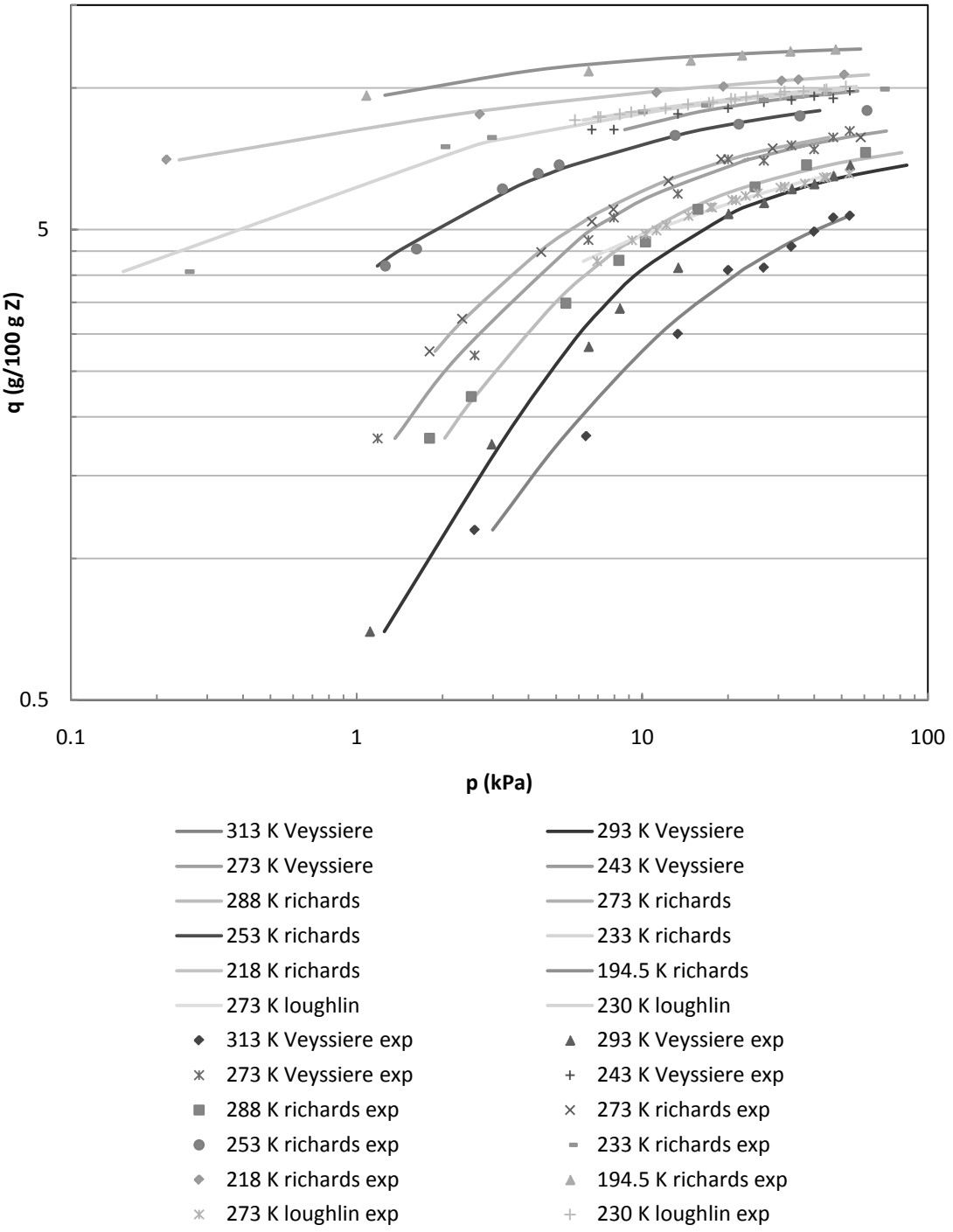

Figure 20: Fitting results for C_2 adsorption isotherms on zeolite 5A.

The value of the coefficient of determination, R^2, is calculated using the following relation:

$$R^2 = 1 - \frac{\sum_{i=1}^{m}(y_{exp} - y_i)^2}{\sum_{i=1}^{m}(y_{exp} - \bar{y})^2} \qquad 3.11$$

where y is the variable being optimized, y_{exp} is the experimental value of the variable y, y_i is the predicted value of the variable using the model, $\bar{y}$ is the arithmetic average of predicted values, i is the index referring to the number of predicted value, and m is the total number of predicted values.

3.4.2 C_4 Results

Results for C_4 are obtained in the same way as C_2. A summary of the results applying the first optimization technique is shown in Table 16.

Table 16: Summary of C_4 adsorption studies on 5A zeolite, optimized parameters, and coefficient of determination

Reference	Isotherm Temperature (K)	q_{max} (g/100 g Z)	K_{eq} (kPa^{-1})	$\Delta u*10^{23}$	R^2
Loughlin [37]	323	12.810	4.958	55.035	0.997
Loughlin [37]	358	11.619	0.004	956.306	0.900
Loughlin [37]	398	9.755	4.981E-04	1395.556	0.733
Loughlin [37]	423	7.180	-	-	-
Moller	371.4	11.083	0.118	465.522	0.643
Moller	371.8	11.066	0.003	1341.859	0.878
Moller	423.7	6.959	-	-	-
Moller	425.7	9.000	0.002	2067.184	0.390
Moller	480.6	9.000	0.021	339.574	0.992
Moller	480.7	9.000	0.017	369.691	0.963
Veyssiere	238	15.076	-	-	-
Veyssiere	273	14.212	2.621E04	-25.537	0.356
Veyssiere	303	13.399	0.001	1172.806	0.572
Veyssiere	323	12.806	1.057	188.006	0.835
Veyssiere	353	11.801	0.052	644.601	0.912

It is seen from Table 16 that the MSL model gives a satisfactory fit only for studies of Loughlin 323 K, Loughlin 358 K, Moller 480.6 K, Moller 480.6 K, Veyssiere 323 K, and Veyssiere 353K. For the rest of studies, the R^2 value is poor and the fit is unsatisfactory. Studies with good fit results are plotted in Figure 21 and Figure 22. Studies with no reported results are studies in which the MSL did not fit the data at all.

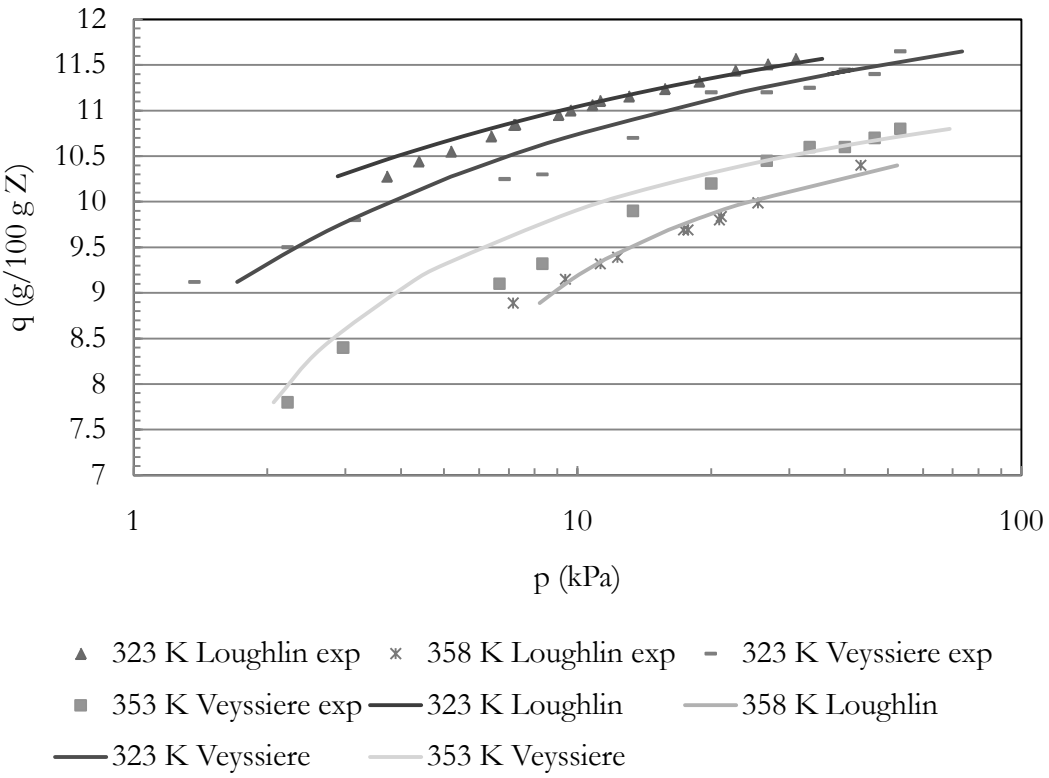

Figure 21: Fitting results for C_4 adsorption isotherms on zeolite 5A.

For the sake of clarity, Moller isotherms are plotted in separate figure.

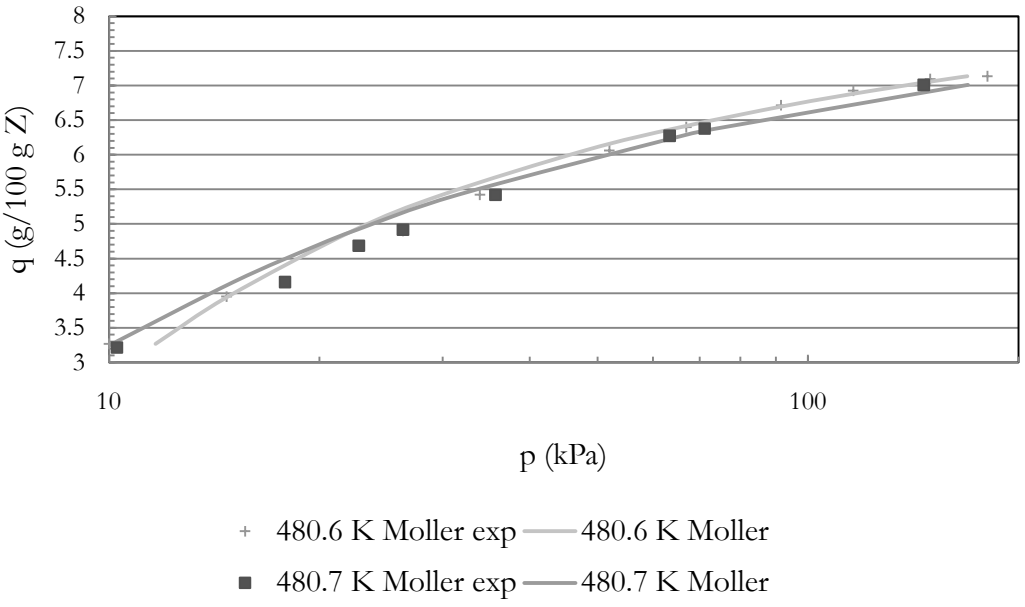

Figure 22: Fitting results for Moller isotherms for the adsorption of C_4 on zeolite 5A.

CHAPTER 4. KINETICS OF ADSORPTION OF WATER IN 5A ZEOLITE-ONE RESISTANCE MODELS

4.1 Introduction

With adsorption playing a critical role in many applications like gas processing and pollution reduction, the need to have accurate models describing this phenomenon is essential. The importance of developing accurate models will result in a better performance for adsorption units and hence an improved productivity. Knowledge of diffusion coefficients and heat transfer coefficient, if applicable, is critical for modeling adsorption systems. Adsorption kinetics can be studied either on crystals or pellets. Crystals are the pure form of zeolite with pore sizes in the order of angstroms., while zeolite pellets are composed of zeolite crystals bound with any sort of binder in order to gain mechanical strength needed for practical uses [3]. The pellet structure is shown Figure 23. In most cases, it is assumed that the adsorption on the binder material is negligible. The importance of knowing the kinetics of adsorption stems from the vital role of zeolites in many applications. For example, in gas processing, dehydration is an essential step of the process to avoid the formation of hydrates during liquefaction. To achieve the desired dehydration, zeolites are used to remove water down to 6-7 ppm. The rates of adsorption and desorption needs to be determined to meet desired specifications. These rates do not really depend on the intrinsic kinetics of sorption at the surface, but on the rate of diffusion through the pores. This is generally true for porous catalysts or adsorbents on which physical adsorption is generally high so that it is controlled by mass and heat transfer resistances [3].These resistances are not always clear from experimental data and this why there is a need to study the models of these resistances to be able to detect them and overcome them.

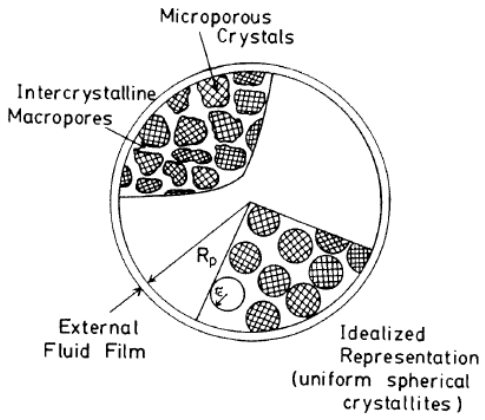

Figure 23: Pellet Structure.

Models describing these resistances are divided into two types: One Resistance Models and Dual Resistance Models. All one resistance models assume isothermality and their solution will give the concentration profile across the crystal or pellet. Dual resistance models can be isothermal or nonisothermal. For nonisothermal dual resistance models, the solution will give the concentration and temperature profiles across the crystal or pellet. In this chapter one resistance models will be introduced.

4.2 One Resistance Models

The following one resistance models will be derived assuming isothermality:

1. Film model
2. Pore mouth model
3. Micropore diffusion controlled model
4. Macropore diffusion controlled model
5. Shrinking core model

First, a differential mass balance for a spherical shell element, see Figure below, is derived from first principles:

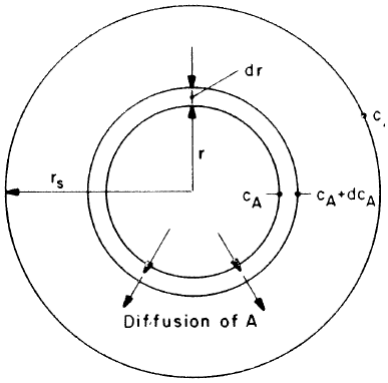

Figure 24: Spherical Shell Element.

$$Accumulation = Rate\ in - Rate\ out$$

$$Rate\ of\ mass\ in = 4\pi r^2 \epsilon N_r$$

$$Rate\ of\ mass\ out = 4\pi r^2 \epsilon N_{r+\Delta r}$$

where N is the flux and ϵ is the void volume.

$$Accumulation = (4\pi r^2 \Delta r \epsilon)\frac{\partial c}{\partial t} + (1-\epsilon)4\pi r^2 \Delta r \frac{\partial q}{\partial t}$$

Using Fick's law:

$$N = -D_p \frac{\partial c}{\partial r} \qquad 4.1$$

Substitute for the flux:

$$(\epsilon 4\pi r^2 \Delta r)\frac{\partial c}{\partial t} + (1-\epsilon)4\pi r^2 \Delta r \frac{\partial q}{\partial t} = \left(-\epsilon 4\pi r^2 D_p \frac{\partial c}{\partial r}\Big|_r\right) - \left(-\epsilon 4\pi r^2 D_p \frac{\partial c}{\partial r}\Big|_{r+\Delta r}\right)$$

Divide by $4\pi r^2$:

$$(\Delta r \epsilon)\frac{\partial c}{\partial t} + (1-\epsilon)\Delta r \frac{\partial q}{\partial t} = \epsilon D_p \frac{\partial c}{\partial r}\Big|_{r+\Delta r} - \epsilon D_p \frac{\partial c}{\partial r}\Big|_r$$

Divide by Δr:

$$\epsilon \frac{\partial c}{\partial t} + (1-\epsilon)\frac{\partial q}{\partial t} = \epsilon \left(D_p \frac{\frac{\partial c}{\partial r}\Big|_{r+\Delta r} - \frac{\partial c}{\partial r}\Big|_r}{\Delta r} \right)$$

Take the $\lim_{\Delta r \to 0}$ for both sides:

$$\epsilon \frac{\partial c}{\partial t} + (1-\epsilon)\frac{\partial q}{\partial t} = \epsilon \frac{1}{r^2}\frac{\partial}{\partial r}\left(D_p r^2 \frac{\partial c}{\partial r}\right) \quad 4.2$$

where ϵ is the external void fraction. This is the general mass balance equation for diffusion in a porous molecular sieve pellet.

4.2.1 Film model

If the diffusion within the particle is very rapid or the particle is nonporous so adsorption can occur only at the external surface, then the adsorption rate will be controlled by the diffusion through the laminar fluid film surrounding the particle. See Figure 24. For this case, $\frac{\partial c}{\partial t}$ is negligible due to negligible adsorption at the gas phase and $\frac{\partial c}{\partial r} \approx 0$ as there are no internal gradients. The mass balance reduces to:

$$Accumulation\ at\ the\ solid\ phase = flux\ at\ the\ surface\ x\ surface\ area$$

$$\frac{4}{3}\pi R_P^3 (1-\epsilon)\frac{dq}{dt} = k_f 4\pi R_P^2 (C - C^*)$$

$$(1-\epsilon)\frac{dq}{dt} = k_f a (C - C^*) \quad 4.3$$

Define:

$$\bar{q} = (1-\epsilon)q \quad 4.4$$

So the equation becomes:

$$\frac{d\bar{q}}{dt} = k_f a (C - C^*) \quad 4.5$$

where k_f is the film mass transfer coefficient and, for a spherical particle, the specific external area $a = \frac{3}{R_p}$, and R_P is the diameter of the particle.

Assuming a linear equilibrium relationship:

$$q^* = KC \tag{4.6}$$

where q^* is the final equilibrium adsorbed phase concentration. The assumption of the linearity of the equilibrium relation is generally true when the concentration change is sufficiently small, and the bulk fluid phase concentration C is maintained constant, then the rate becomes:

$$\frac{d\bar{q}}{dt} = \frac{3k_f}{KR_p}(q^* - \bar{q}) \tag{4.7}$$

For a step change in concentration at time zero:

$$< 0, \qquad C = q = 0 \tag{4.8a}$$

$$t \geq 0, \qquad C = C_\infty = \frac{q_\infty}{K} \tag{4.8b}$$

Integration of equation (4.7) and solving according to the given boundary condition, equation (4.8) becomes [38] :

$$\frac{\bar{q}}{q_\infty} = 1 - exp\left[-\frac{3k_f t}{KR_p}\right] \tag{4.9}$$

4.2.2 Pore mouth resistance model

The analogous situation of film resistance for porous particles is the skin resistance at the surface of the microparticle resulting from constriction of the pore mouth. This model often results when the size of sorbate molecule to much smaller than microparticles pores. The assumptions of linear equilibrium relation and isothermality are taken for this case as well. The equation is similar to the film resistance one except that the relevant radius is the crystal radius:

$$Accumulation\ at\ the\ solid\ phase = flux\ at\ the\ pore\ mouth$$

$$\frac{4}{3}\pi r_c^3(1-\epsilon)\frac{dq}{dt} = k_f 4\pi r_c^2(C - C^*)$$

$$\frac{d\bar{q}}{dt} = \frac{3k_s}{Kr_c}(q^* - \bar{q}) \tag{4.10}$$

As the boundary conditions will be same as the film resistance, the solution is:

$$\frac{\bar{q}}{q_\infty} = 1 - exp\left[-\frac{3k_s t}{Kr_c}\right] \tag{4.11}$$

where $k_s = \frac{D_s}{\delta}$ is the ratio of the effective diffusivity to the thickness of the solid surface film [38].

4.2.3 Micropore diffusion controlled model

To get the equation describing this model, $\frac{\partial c}{\partial t}$ and $\frac{\partial c}{\partial r}$ in Equation 4.2 are assumed negligible. Performing a differential mass balance on a microparticle will result:

$$\frac{\partial q}{\partial t} = \frac{1}{r^2}\frac{\partial}{\partial r}\left(r^2 D_c \frac{\partial q}{\partial r}\right) \quad 4.12$$

If the diffusivity is constant, equation (4.12) simplifies to:

$$\frac{\partial q}{\partial t} = D_c\left(\frac{\partial^2 q}{\partial r^2} + \frac{2}{r}\frac{\partial q}{\partial r}\right) \quad 4.13$$

where D_c is the intracrystalline diffusivity and $q(r,t)$ is the adsorbed phase concentration. The assumption of constant diffusivity is valid as long as the uptake curve is measured over a small differential change of the concentration of the adsorbed phase. For a step change of concentration at time zero: the relevant initial and boundary conditions are:

$$t < 0, \qquad C = C_0, \qquad q = q_0 \quad 4.14a$$

$$t \geq 0, \qquad C = C_\infty, \qquad q(r_c, t) \rightarrow q_\infty \quad 4.14b$$

$$\left.\frac{\partial q}{\partial t}\right|_{r=0} = 0 \quad for\ all\ t \quad 4.14c$$

The solution obtained by the separation of variables:

$$\frac{m_t}{m_\infty} = \frac{\overline{q}-q_0}{q_\infty - q_0} = 1 - \frac{6}{\pi^2}\sum_{n=1}^{\infty}\frac{1}{n^2} exp\left(-\frac{n^2\pi^2 D_c t}{r_c^2}\right) \quad 4.15$$

where m_t is the mass adsorbed at time t and m_∞ is the mass adsorbed at $t \rightarrow \infty$.

An equivalent form of the solution using Laplace transformations is:

$$\frac{m_t}{m_\infty} = \frac{\overline{q}-q_0}{q_\infty - q_0} = 6\left(\frac{D_c t}{r_c^2}\right)^{1/2}\left[\frac{1}{\sqrt{\pi}} + 2\sum_{n=1}^{\infty} ierfc\left(\frac{n r_c}{\sqrt{D_c t}}\right)\right] - 3\frac{D_c t}{r_c^2} \quad 4.16$$

Neglecting the higher order terms in Equation 4.16 will result in a simplified expression for the initial region of the uptake curve, which is more convenient for short times:

$$\frac{m_t}{m_\infty} \approx \frac{6}{\sqrt{\pi}}\sqrt{\frac{D_c t}{r_c^2}} \quad 4.17$$

For the long time region, all terms except the first in the series of exponential terms in Equation 4.15 become negligible so that the uptake curve approaches the asymptotic form:

$$\frac{m_t}{m_\infty} = 1 - \frac{6}{\pi^2} exp\left[-\frac{\pi^2 D_c t}{r_c^2}\right] \quad 4.18$$

Rearrange and taking the logarithms gives:

$$\ln\left(1-\frac{m_t}{m_\infty}\right)=\ln\frac{6}{\pi^2}-\frac{\pi^2 D_c t}{r_c^2}$$

By plotting $\ln\left(1-\frac{m_t}{m_\infty}\right)$ versus t, the slope is $-\frac{\pi^2 D_c}{r_c^2}$ and hence D_c can be calculated.

Assuming variable diffusivity using Darken relation for integral step changes:

$$D_c = D_o\left(1-\frac{q}{q_s}\right)^{-1} \qquad 4.19$$

Substituting in Equation 4.12 and assuming an integral step change in the adsorbed phase concentration:

$$\frac{\partial q}{\partial t}=\frac{D_o}{r^2}\frac{\partial}{\partial r}\left(\frac{r^2}{\left(1-q/q_s\right)}\frac{\partial q}{\partial r}\right) \qquad 4.20$$

The equation has to be solved numerically with the boundary conditions as before [3] [3]. The solution for a Langmuir system with a micropore diffusion control is shown in Figure 25 [3]:

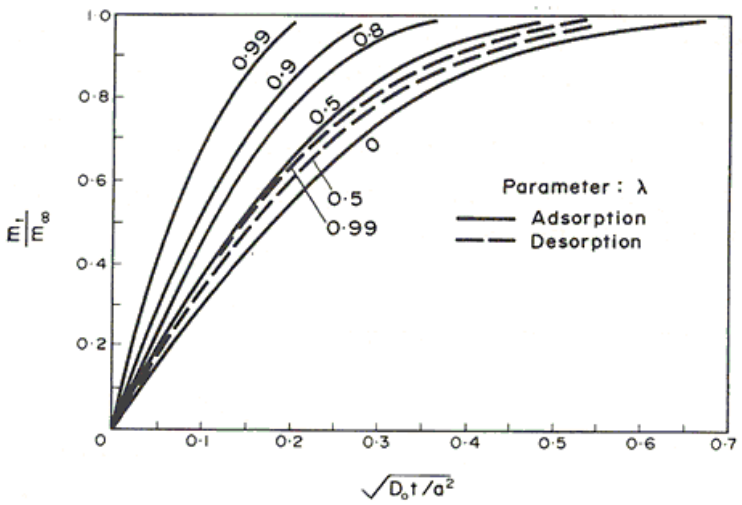

Figure 25: Theoretical uptake curve for a Langmuir system with micropore diffusion control.

The solution with the variation of effective diffusivity with sorbate concentration for a Langmuir system and Volmer system is shown in Figure 26 [3].

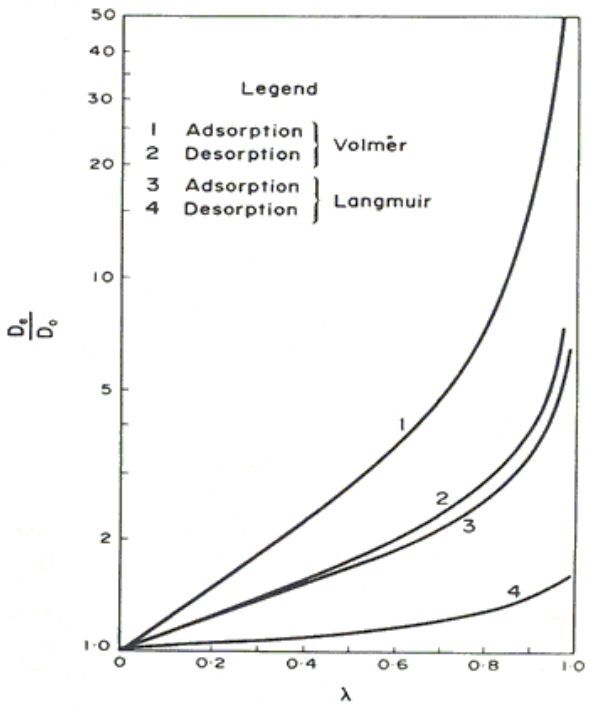

Figure 26: Variation of effective diffusivity with sorbate concentration for a Langmuir system and Volmer system

4.2.4 Macroparticle diffusion controlled model

Equation 4.2 with the assumption of constant diffusivity will result in the model of macropore diffusion controlled model:

$$\left(1-\epsilon_p\right)\frac{\partial q}{\partial t}+\epsilon_p\,\frac{\partial c}{\partial t}\;=\;\epsilon_p D_p\left(\frac{\partial^2 c}{\partial R^2}+\frac{2}{R}\,\frac{\partial c}{\partial R}\right) \qquad 4.21$$

Using the assumption of linear equilibrium relation, and substituting for q using Equation 4.6 gives:

$$\frac{\partial c}{\partial t}=\frac{\epsilon_p D_p}{\epsilon_p+\left(1-\epsilon_p\right)K}\left(\frac{\partial^2 c}{\partial R^2}+\frac{2}{R}\,\frac{\partial c}{\partial R}\right) \qquad 4.22$$

$$c(R,0)=c'_0\,,\quad q\,(R,t)=\,q'_0 \qquad 4.23a$$

$$c\left(R_p\,,0\right)=\,c_0\,,\quad q\left(R_p,t\right)=\,c_0 \qquad 4.23b$$

$$\left(\frac{\partial c}{\partial R}\right)_{R=o}=\left(\frac{\partial q}{\partial R}\right)_{R=0}=0 \qquad 4.23c$$

The solution for this model is identical to Equation 4.15 and Equation 4.16 with $\frac{D_c}{r_c^2}$ is replaced by $\left(\frac{D_p}{R_p^2}\right)/\left[\epsilon_p+\left(1-\epsilon_p\right)K\right]$. For the non-linear equilibrium relation using Langmuir isotherm:

$$\frac{q^*}{q_s}=\frac{bc}{1+bc}$$

$$\frac{dq^*}{dc} = \frac{bq_s}{(1+bc)^2} = bq_s\left(1 - \frac{q}{q_s}\right)^2 \quad 4.24$$

where q^* is the equilibrium value of q.

For the case of adsorption from the gas phase, $q \gg c$ and since $\frac{\partial c}{\partial R} = \left(\frac{\partial q}{\partial R}\right)\left(\frac{dc}{dq^*}\right)$, and a concentration dependent diffusivity, Equation 4.22 results which must be solved numerically in terms of λ [3] [3]:

$$\frac{\partial q}{\partial t} = \frac{\epsilon_p D_p}{(1-\epsilon_p) b q_s} \frac{1}{R_p^2} \frac{\partial}{\partial R}\left(\frac{R^2}{\left(1-q/q_s\right)^2} \frac{\partial q}{\partial R}\right) \quad 4.25$$

4.2.5 Shrinking core model

For a large concentration step a highly favorable type I isotherm (e.g., a Langmuir isotherm) approaches the rectangular or irreversible form

$$C = 0,\ q^* = 0,\ c > 0,\ q^* = q_s \quad 4.26$$

The rectangular model therefore provides a useful and mathematically tractable model for analysis of the sorption curves for strongly adsorbed species. The isotherm for water at 25 °C on 4A zeolite approaches this rectangularity when plotted on rectangular paper, and hence the analysis that follows taken from [38] is applicable.

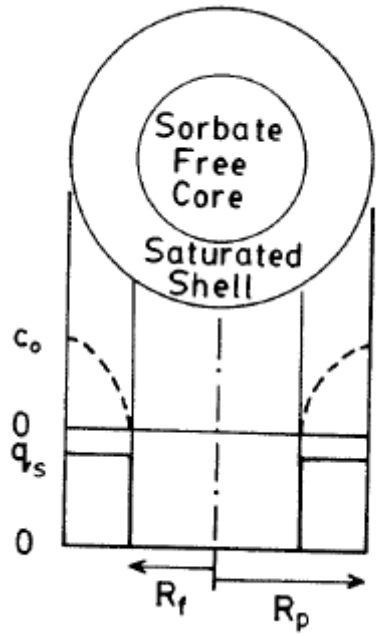

Figure 27: Concentration Profiles for Shrinking Core Model

Consider a composite macroporous pellet of the type sketched in Figure 23 where most of the sorption capacity lies in the microparticles (zeolite crystals) while the dominant resistance to mass transfer is diffusion through the channels or pores between the microparticles. Intracrystalline diffusion is assumed to be sufficiently rapid to maintain the sorbate concentration practically uniform through a microparticle and at equilibrium with the sorbate concentration in the micropore just outside the microparticle. Under these conditions the concentration profile in the adsorbed phase penetrates as a shock front separating the shrinking core region to which sorbate has not yet penetrated, from the saturated outer shell, as sketched in Figure 27. Adsorption occurs entirely at the shock front ($R = R_f$). Over the region $R_f < R < R_p$ the flow of sorbate through the pores is therefore constant:

$$4\pi R^2 \epsilon_p D_p \frac{\partial c}{\partial R} = k(t) \tag{4.27}$$

Integration at constant *t* yields

$$c = -\frac{k}{4\pi R \epsilon_P D_P} + const. \tag{4.28}$$

From which, using the boundary conditions at the particle surface and at $R = R_f$ (@ $R = R_p$, $c = c_0$; @ $R = R_f$, $c = 0$) we obtain

$$R^2 \frac{\partial c}{\partial R} = \frac{k}{4\pi \epsilon_p D_P} = \frac{c_0}{1/R_f - 1/R} \tag{4.29}$$

A mass balance at $R = R_f$ gives for the flow across the control surface:

$$4\pi \epsilon_p D_P \left(R^2 \frac{\partial c}{\partial R}\right) = \frac{4\pi \epsilon_p D_p c_0}{1/R_f - 1/R} = 4\pi R_f^2 q_s \frac{dR_f}{dt} \tag{4.30}$$

which may be integrated directly to obtain

$$\frac{\epsilon_p D_p C_0 t}{R^2 q_s} = -\frac{1}{2}\left(\frac{R_f}{R_p}\right)^2 + \frac{1}{3}\left(\frac{R_f}{R_p}\right)^3 + \frac{1}{6} \tag{4.31}$$

and since $1 - m_t/m_\infty = ((R_f/R_p)^3$, the uptake curve is given by:

$$6\tau = 1 + 2\left(1 - \frac{m_t}{m_\infty}\right) - 3\left(1 - \frac{m_t}{m_\infty}\right)^{\frac{2}{3}} \tag{4.32}$$

where

$$\tau = \frac{\epsilon_p D_p}{R_p^2} \frac{C_0}{q_s} t \tag{4.33}$$

The stoichiometric time is given by $\tau = 1/6$. The latter Equation may also be written in explicit form as:

$$1 - \frac{m_t}{m_\infty} = \left\{\frac{1}{2} + \cos\left[\frac{\pi}{3} + \frac{1}{3}\cos^{-1}(1 - 12\tau\right]\right\}^3 \quad [0 < \tau < 1/6] \qquad 4.34$$

These expressions appear to have been first obtained by Weisz and Goodwin in relation to the burn-off of carbon from coked catalysts and first applied in the context of adsorption by Dedrick and Beekman [18] and Timofeev [18] [38].

4.3 Results and Discussion

The system under study is a set of adsorption data collected from an Intelligent Gravimetric Analyzer (IGA). The data is for adsorption of water on zeolite 5A pellets. The objective is to identify the diffusion limitations and find the appropriate model to describe the system. The models presented in the previous section will be used to extract the isothermal diffusivity for the system under study. The primary analysis for the system showed a rise in temperature during adsorption, which makes the system nonisothermal. This means that the above models won't be able to fully describe the experimental data since they are all derived isothermally. Furthermore, the previous models, except for the film model, will yield a straight line with a zero intercept when adsorbate loading, q (g H_2O/100 g ads), is plotted against the square root of time, t (min). The change in the value of the intercept from zero indicates the presence of at least two resistances [3]. Plotting q vs. $\sqrt{t}$ for the experimental data will be the first check for the existence of more than one resistance. Figure 28 shows the plot of q vs. $\sqrt{t}$ with q increasing linearly with the square root of time before it reaches to saturation at around 20 (g H_2O/100 g ads). The linear part of the curve is fitted through a straight line with a coefficient of determination, R^2, equals to 0.9956 and an intercept equals to -1.2753. The non zero intercept indicates the presence of another resistance. This conclusion is later supported when temperature measurements were carried out to show a clear rise in temperature during the adsorption process. The concentration and temperature profiles are shown in Figure 29 and Figure 30 respectively. Figure 29 shows a rapid concentration increase initially and followed by an increase at a slower rate which continues until reaching saturation limit at around 20 (g H_2O/ 100 g ads). Figure 30 shows the change of the sample temperature during the course of adsorption. There is a clear rise in temperature up to 308K and then slowly decreasing to 293K, which is the system original temperature. This rise confirmed the conclusion of the presence of another resistance,

which shows to be heat resistance. This shows the need for a heat equation in order to model this system correctly. The introduction of a second resistance is discussed in the following chapter accompanied with the solution of the dual resistance model.

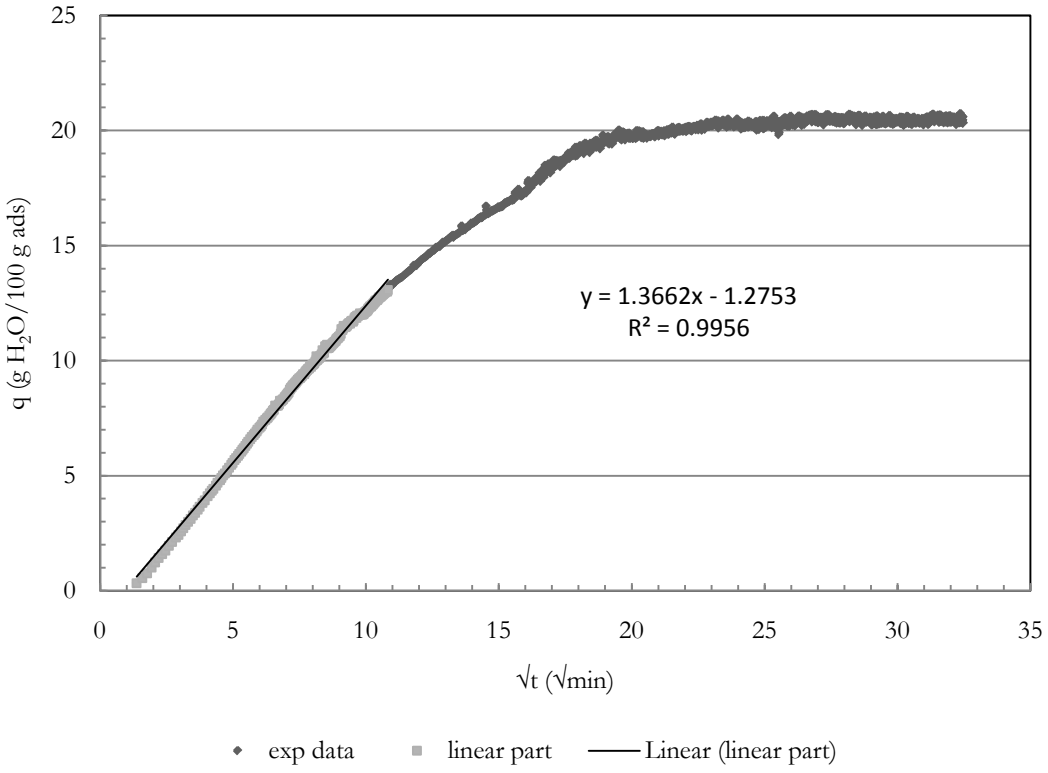

Figure 28: The dependence of the adsorption loading of water on zeolite 5A on the square root of time, showing a non zero intercept.

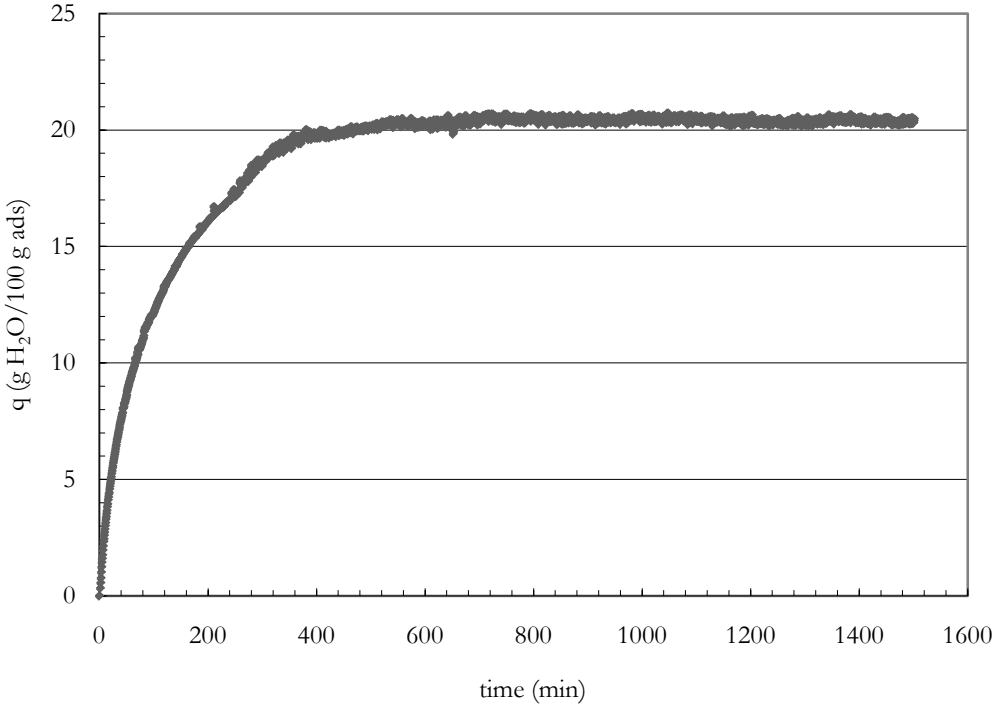

Figure 29: Concentration profile for the adsorption of water on zeolite 5A.

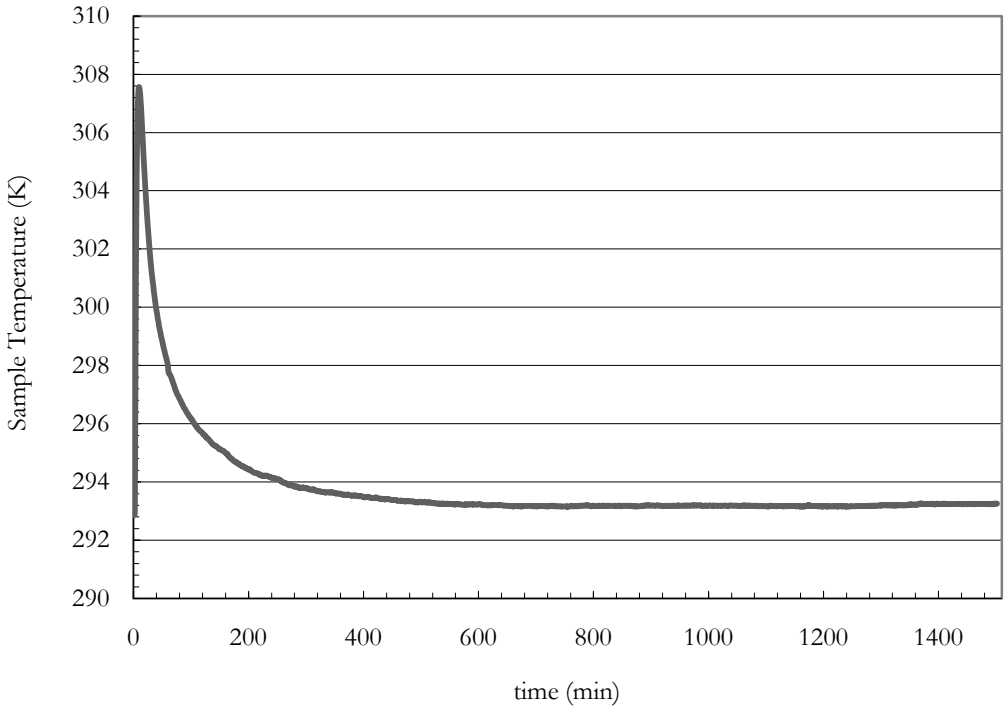

Figure 30: Temperature profile of the adsorption of water on zeolite 5A.

CHAPTER 5. DIFFUSION OF WATER IN 5A CRYSTALS AND PELLETS-TWO RESISTANCE MODELS

5.1 Introduction

From the analysis in the previous chapter it was clear the presence of another resistance exists, which was later found to be a heat resistance. In this chapter the two resistance models are presented for the sake of modeling the nonisothermal adsorption of water on zeolite 5A. The objective of in this chapter is model the data, report diffusion and heat transfer coefficients and study the effects of parameters on the system. Previous studies by Ruthven [3], Do [39], Eagan et al. [40], Abdallah et al.[41], Moller et al.[42], and Do and Wang [43] were reviewed. The work of Eagan et al. studied the kinetics of adsorption of nitrogen on 4A and propane on 5A [40]. Abdallah et al.'s work investigated nonisothermal adsorption of water by 13X zeolite [41]. The work by Do and Wang presented a new model for describing adsorption kinetics in heterogeneous activated carbon. Moller et al. studied the adsorption of n-alkanes on zeolite 5A [42].

5.2 Experimental

The experiment was carried out on an IGA unit using fresh beads of zeolite 5A with water as adsorbate. Table 17 summarizes the system properties.

Table 17: A summary of system properties

Property	Value
Bulk gas pressure, P_b	1 mbar
Bulk gas concentration, c_b	$4.277*10^{-8}$ mol/cm^3
Reference gas concentration, c_0	$4.277*10^{-8}$ mol/cm^3
Water density at reference temperature, ρ_{H_2O}	0.998 g/cm^3
Specific heat at at reference temperature, C_P	4.182 J/g.K
Water thermal conductivity at reference temperature	0.597 W/m.K
Mass adsorbed initially, m_0	0 µg
Mass adsorbed finally, m_∞	1610.071 µg
Pellet porosity, ε_p	0.38
Pellet density, ρ_p	1.1544 g/cm^3
Pellet Radius, R	0.3175 cm
Bulk Temperature, T_B	293 K
Reference Temperature, T_0	293 K
Maximum temperature observed	308 K
Adsorption affinity at reference temperature, b_0	$1*10^6$ cm^3/mol
Reference adsorbed phase concentration, q_0	$8.203*10^{-3}$ mol/cm^3
Heat of adsorption, ΔH_{ads}	72 kJ/mol
Surface diffusion activation energy, E_q	30 kJ/mol
Initial time, t_0	0 min
Final time t_∞	1501 min

5.3 Analysis

In most cases, the film resistance can be eliminated by controlling the experimental conditions such that the mass transfer coefficient is large enough to overcome any film resistance and in the case of a pure component system there is no film resistance. This leaves the possibility of micropore resistance, macropore resistance or both along with the heat resistance. Literature on adsorption discusses various methods to identify the type of resistance [3], [38], [39]. While the common case for zeolite particles is the existence of both micropore and macropore diffusion limits, this is not the case for the system under investigation [3]. The relative importance of micropore and macropore resistances depends on the ratio of diffusion time constant ($D*t/R^2$) for

both types. The diffusion time constant depend on the square of the particle radius and thus a variation of the particle size will provide a straightforward way to check the type of diffusional resistance. This is done by calculating the ratio of both diffusional constants, but this can't be done due to the difficulty in obtaining some parameters. So another way is needed. One way is by checking the dependence of adsorption loading on the pellet size. If adsorption loading changes with pellet size, then macropore diffusion is limiting. On the other hand, if adsorption changes with crystal size, then micropore diffusion is limiting. Figure 31 shows clearly the change of fractional uptake with the change of the pellet size confirming the presence of macropore diffusion and the absence of micropore diffusion limitation. In addition to that, the large pellet size (R=0.3175 cm) and the small bulk concentration (1 mbar which is equivalent to $4.277*10^{-8}$ mol/cm^3 using ideal gas law) are additional proofs for the presence of macropore diffusion [39]. Micropore diffusion controls uptake when the pellet size is small, the bulk concentration is high, and the adsorbate molecule size is close to the size of micropores [39]. The dimension of a water molecule is 2.78 Å, which is much smaller than the zeolite 5A effective pore size of 8 Å [3]. So, the two main resistances present are macropore diffusion limitation and heat resistance. Because of the high thermal conductivity for zeolite pellets and that the pellet is treated as a lumped parameter system for temperature. it is safe to assume that all heat resistance is present in the film around the particle [3], [39]. The equations describing the two resistances are presented, normalized and solved using orthogonal collocation.

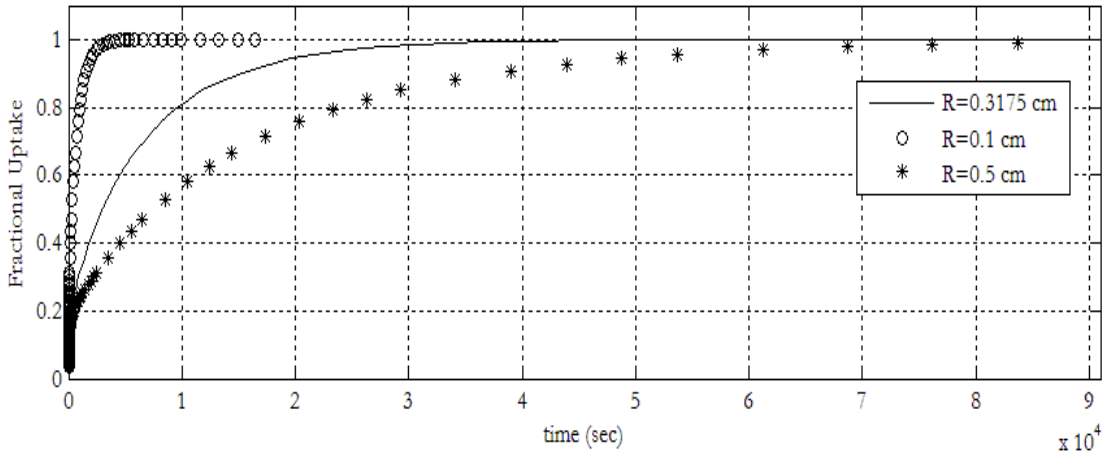

Figure 31: Fractional uptake of water on zeolite 5A for different pellet sizes.

The macropore diffusion model is derived assuming that the adsorbed phase, q, is in equilibrium with the bulk gas phase, C. This equilibrium relation is governed by the Langmuir isotherm, which is accurate enough for this case. Another assumption is the

presence of both diffusion mechanisms: pore diffusion and surface diffusion. Pore diffusion refers to diffusion in voids between micropores, while surface diffusion refers to the diffusion of adsorbate on the surface of adsorbents from one adsorption site to another [42]. The mass balance equation over a thin shell of a particle in which the dual diffusion mechanisms are operative is:

$$\left(1-\varepsilon_p\right)\frac{\partial q}{\partial t}+\varepsilon_p\frac{\partial c}{\partial t}=-\frac{1}{r^2}\frac{\partial}{\partial r}\left\{r^2\left[\varepsilon_p N_p+(1-\varepsilon_p)N_q\right]\right\} \quad 5.1$$

where c is the concentration in the void space, q is the concentration of the adsorbed phase, ε_p is the pellet porosity, N_p is the flux of adsorbate through the void volume and N_q is the flux of adsorbate in the adsorbed phase. Next, N_p and N_q need to be calculated.

The flux in the pore volume:

$$N_p=-D_p(T)\frac{\partial c}{\partial r} \quad 5.2$$

$$D_p(T)=D_{p0}\left(\frac{T}{T_0}\right)^{\alpha} \quad 5.3$$

where D_{p0} is the pore diffusivity at reference temperature. The exponent α is 0.5 if Knudsen diffusion is the controlling mechanism within the void space and 1.75 if molecular diffusion is the controlling mechanism. For the system being studied, the value of 0.5 is chosen due to the very low pressure and Knudsen diffusivity is dominant at low pressures. Also, the macropore size is a consideration.

The flux in the adsorbed phase:

$$N_q=-Lq\frac{\partial \mu}{\partial r} \quad 5.4$$

where L is the mobility constant, which is assumed to independent of concentration and is dependent on temperature only, and μ is the chemical potential of the adsorbed phase. The assumption of local equilibrium between the gas and the adsorbed phase leads to equality of the chemical potential of the two phases:

$$\mu=\mu_G=\mu^0+R_gT\ln c \quad 5.5$$

Substituting equation 5.5 in equation 5.4 and perform the differentiation results in:

$$N_q=-D_s\frac{q}{c}\frac{\partial c}{\partial r} \quad 5.6$$

where D_s has the following form:

$$D_s=LR_gT \quad 5.7$$

D_s follows an Arrhenius form and evaluating it at a reference temperature gives:

$$D_s(T)=D_{s0}exp\left[\frac{-E_q}{R_gT_0}\left(1-\frac{T}{T_0}\right)\right] \quad 5.8$$

where D_{s0} is the surface diffusivity at a reference temperature T_0 and E_q is the activation energy for surface diffusion.

Substitute equations 5.2 and 5.6 in 5.1 to get:

$$(1-\varepsilon_p)\frac{\partial q}{\partial t} + \varepsilon_p \frac{\partial c}{\partial t} = \frac{1}{r^2}\frac{\partial}{\partial r}\left\{r^2\left[\varepsilon_p D_p(T) + (1-\varepsilon_p)D_s(T)\frac{q}{c}\right]\frac{\partial c}{\partial r}\right\} \quad 5.9$$

The equilibrium relation between the two phases is described by Langmuir isotherm:

$$q = f(c,T) = \frac{q_{max} b c}{1+bc} \quad 5.10$$

where q_{max} is the adsorbed phase saturation concentration in (mol/cm^3), b is the adsorption affinity in (cm^3/mol), c is the gas concentration in (mol/cm^3), and T is the temperature in (K). The term $\frac{\partial q}{\partial t}$ in equation 5.9 complicates the solution of the equation, so it is a good idea to use the relation in equation 5.10 with the application of the chain rule differentiation to eliminate $\frac{\partial q}{\partial t}$ by:

$$\frac{\partial q}{\partial t} = \left.\frac{\partial q}{\partial c}\right|_T \frac{\partial c}{\partial t} + \left.\frac{\partial q}{\partial T}\right|_c \frac{\partial T}{\partial t}$$

The expression of $\frac{\partial q}{\partial c}$ and $\frac{\partial q}{\partial T}$ is obtained using equation 5.10:

$$\left.\frac{\partial q}{\partial c}\right|_T = \left.\frac{\partial f(c,T)}{\partial c}\right|_T = \frac{q_{max} b}{(1+bc)^2}; \quad \left.\frac{\partial q}{\partial T}\right|_c = \left.\frac{\partial f(c,T)}{\partial T}\right|_c = \frac{q_{max} b_0 c \left(\frac{\Delta H_{ads}}{RT^2}\right) exp\left(\frac{-\Delta H_{ads}}{RT}\right)}{\left(1 + b_0 exp\left(\frac{-\Delta H_{ads}}{RT}\right)c\right)^2}$$

So equation 5.9 becomes:

$$\left[(1-\varepsilon_p)\frac{\partial f(c,T)}{\partial c} + \varepsilon_p\right]\frac{\partial c}{\partial t} + (1-\varepsilon_p)\frac{\partial f(c,T)}{\partial T}\frac{\partial T}{\partial t} = \frac{1}{r^2}\frac{\partial}{\partial r}\left\{r^2\left[\varepsilon_p D_p(T) + (1-\varepsilon_p)D_s(T)\frac{q}{c}\right]\frac{\partial c}{\partial r}\right\} \quad 5.11$$

The second term in the above equation refers to the temperature variation with the variation of mass transfer. This means that the two effects are coupled and hence their equations have to be solved simultaneously. The temperature variation can be described by a simple energy balance around the particle:

$$\langle \rho C_p \rangle \frac{dT}{dt} = (1-\varepsilon_p)(-\Delta H_{ads})\frac{d\langle q \rangle}{dt} - ha(T - T_b) \quad 5.12$$

where $-\Delta H_{ads}$ (J/mol) is the molar heat of adsorption, $\frac{d\langle q \rangle}{dt}$ is the adsorption rate per unit volume (mol/cm^3.s), h is the heat transfer coefficient per unit surface area (W/cm^2.K), a is the heat transfer surface area per unit volume (cm^2/cm^3). The left term refers to the accumulation term per unit volume, while the terms on the left hand side refers to the generation of heat per unit of volume while adsorption is taking place and the rate of heat transfer to the surroundings respectively. It is noted that equation 5.12 is

derived assuming that heat resistance inside the particle is negligible compared to the heat resistance in the film surrounding the particle. The term $\langle q \rangle$ is the volumetric average concentration of the adsorbed species:

$$\langle q \rangle = \frac{3}{R^3} \int_0^R r^2 q \, dr \qquad 5.13$$

The term $\frac{d\langle q \rangle}{dt}$ in heat balance, equation 5.12, is troublesome when it comes to numerical solution To eliminate this problem the volume average of the mass balance is taken to get:

$$\left(1 - \varepsilon_p\right) \frac{\partial \langle q \rangle}{\partial t} + \varepsilon_p \frac{\partial \langle c \rangle}{\partial t} = \frac{3}{R} \left[\varepsilon_p D_p(T) + (1 - \varepsilon_p) D_s(T) \frac{q}{c} \right] \frac{\partial c}{\partial r} \Big|_{r=R} \qquad 5.14$$

Now, it is assumed that the concentration in the void space is much smaller than the concentration of the adsorbed phase:

$$\varepsilon_p \frac{\partial \langle c \rangle}{\partial t} \ll \left(1 - \varepsilon_p\right) \frac{\partial \langle q \rangle}{\partial t} \qquad 5.15$$

This will give an expression for $\frac{d\langle q \rangle}{dt}$:

$$\left(1 - \varepsilon_p\right) \frac{\partial \langle q \rangle}{\partial t} \cong \frac{3}{R} \left[\varepsilon_p D_p(T) + (1 - \varepsilon_p) D_s(T) \frac{q}{c} \right] \frac{\partial c}{\partial r} \Big|_{r=R} \qquad 5.16$$

Equation 5.16 is substituted back in the heat balance to get:

$$\langle \rho C_p \rangle \frac{dT}{dt} = \frac{3(-\Delta H_{ads})}{R} \left[\varepsilon_p D_p(T) + (1 - \varepsilon_p) D_s(T) \frac{q}{c} \right] \frac{\partial c}{\partial r} \Big|_{r=R} - ha(T - T_b) \qquad 5.17$$

Now, the boundary conditions for the system are defined as follows:

$$r = 0; \quad \frac{\partial c}{\partial r} \qquad 5.18a$$

$$r = R; \quad - \left[\varepsilon_p D_p(T) + (1 - \varepsilon_p) D_s(T) \frac{q}{c} \right] \frac{\partial c}{\partial r} \Big|_{r=R} = k_m (c|_R - c_b) \qquad 5.18b$$

where c_b is the bulk concentration in (mol/cm^3). Equation 5.18a refers the symmetry condition at the center of the pellet, while equation 5.18b refers to the equality of the flux of concentration at the surface and the flux through the stagnant film surrounding the pellet. Next, initial conditions are defined:

$$t = 0; \quad c = c_i; \quad q_i = f(c_i, T_i) = \frac{q_{max} b_i c_i}{1 + b_i c_i}; \quad T = T_i \qquad 5.19$$

Equations 5.11, 17, 18, 19 describe the system completely and are in convenient form to be solved using orthogonal collocation after performing dimensionless analysis, a must step for applying orthogonal collocation.

5.4 Normalization/Dimensionless Analysis

In order to solve the system using orthogonal collocation, equations 5.11, 17, 18, 19 have to be rewritten in dimensionless form. To do this, a reference concentration is defined as follows:

$$q_0 = f(c_0, T_0) = \frac{q_{max}\, b_0 c_0}{1 + b_0 c_0} \quad 5.20$$

where q_0 the reference adsorbed phase concentration (mol/cm^3), c_0 is the reference gas phase concentration (mol/cm^3) and T_0 is the reference temperature (K). Now define the dimensionless time and spatial variable:

$$\tau = \frac{\varepsilon D_{p0} t}{R^2}; \quad \eta = \frac{r}{R} \quad 5.21a$$

The dimensionless gas concentration, adsorbed concentration and temperature are:

$$y = \frac{c}{c_0}; \quad x = \frac{q}{q_0}; \quad \theta = \frac{T - T_0}{T_0} \quad 5.21b$$

The dimensionless bulk concentration, initial concentration and temperature are:

$$y_b = \frac{c}{c_b}; \quad y_i = \frac{c}{c_i}; \quad \theta_b = \frac{T - T_b}{T_b}; \quad \theta_i = \frac{T - T_i}{T_i} \quad 5.21c$$

Subsequently, the dimensionless groups are introduced. The ratio of surface diffusion to pore diffusion at reference temperature and the Biot number are:

$$\delta_0 = \frac{(1-\varepsilon_p) D_{s0} q_0}{\varepsilon_p D_{p0} c_0}; \quad Bi = \frac{k_m R}{\varepsilon_p D_{p0}} \quad 5.21d$$

where k_m is the mass transfer coefficient (cm/s), and Bi is the Biot number. Biot number is a measure of the mass transfer resistance in the film surrounding the particle. For the case of adsorption of multiple components, setting Bi to a large number, ≈ 1000, guarantees elimination of film resistance. The activation energy for surface diffusion number, heat of adsorption number and heat capacity number are as follows:

$$\gamma_q = \frac{E_q}{R_g T_0}; \quad \gamma_H = \frac{(-\Delta H_{ads})}{R_g T_0}; \quad \beta = \frac{(-\Delta H_{ads}) q_0}{\langle \rho C_p \rangle T_0} \quad 5.21e$$

Transforming the Arrhenius expressions into dimensionless form will result in the following groups:

$$\varphi(\theta) = exp\left[\gamma_q \left(\frac{\theta}{1+\theta}\right)\right]; \quad \phi(\theta) = exp\left[\gamma_H \left(\frac{\theta}{1+\theta}\right)\right] \quad 5.21f$$

$$b = b_0 \phi(\theta) \quad 5.21g$$

Another group that will result is the LeBi number defined as follows:

$$LeBi = \frac{haR^2}{\langle \rho C_p \rangle \varepsilon_p D_{p0}} \quad 5.21h$$

As a result of normalization the mass balance and heat balance become like this:

$$G_1(y,\theta)\frac{\partial y}{\partial \tau} + G_2(y,\theta)\frac{\partial \theta}{\partial \tau} = \frac{1}{\eta^2}\frac{\partial}{\partial \eta}\left[\eta^2 \cdot H(y,\theta)\frac{\partial y}{\partial \eta}\right] \quad 5.22$$

$$\frac{d\theta}{d\tau} = 2\beta\left(\frac{c_0}{q_0}\right) H(y,\theta)\frac{\partial y}{\partial \eta}\bigg|_{\eta=1} - LeBi(\theta - \theta_b) \quad 5.23$$

where:

$$G_1(y,\theta) = \left[\varepsilon_p + (1-\varepsilon_p)\frac{\partial f(c_0 y, T_0(1+\theta))}{\partial c}\right] \quad 5.24a$$

$$G_1(y,\theta) = \left[\varepsilon_p + (1-\varepsilon_p)\frac{q_{max} b_0 \phi(\theta) y}{[1+b_0 c_0 \phi(\theta) y]^2}\right] \quad 5.24b$$

$$G_2(y,\theta) = (1-\varepsilon_p)\frac{T_0}{c_0}\frac{\partial f(c_0 y, T_0(1+\theta))}{\partial T} \quad 5.25a$$

$$G_2(y,\theta) = -(1-\varepsilon_p)\gamma_H \frac{q_{max} b_0 \phi(\theta) y}{[1+b_0 \phi(\theta) y \phi(\theta)]^2 (1+\theta)^2} \quad 5.25b$$

$$H(y,\theta) = \left[(1+\theta)^\alpha + \delta_0 \varphi(\theta)\frac{f(c_0 y, T_0(1+\theta))}{q_0 y}\right] \quad 5.26a$$

$$H(y,\theta) = (1+\theta)^\alpha + \delta_0 \varphi(\theta)\phi(\theta)\frac{(1+b_0 c_0)}{[1+b_0 \phi(\theta) y \phi(\theta)]^2} \quad 5.26b$$

The dimensionless boundary conditions are:

$$\eta = 0; \quad \frac{\partial y}{\partial \eta} \quad 5.27a$$

$$\eta = 1; \quad H(y,\theta)\frac{\partial y}{\partial \eta} = Bi(y_b - y) \quad 5.27b$$

Initial conditions after transformation are:

$$\tau = 0; \quad y = y_i; \quad \theta = \theta_i \quad 5.28$$

To facilitate the solution by orthogonal collocation, the left hand side of equation 5.22 has to be expanded:

$$\frac{1}{\eta^2}\frac{\partial}{\partial \eta}\left[\eta^2 \cdot H(y,\theta)\frac{\partial y}{\partial \eta}\right] = H(y,\theta)\left[\frac{1}{\eta^2}\frac{\partial}{\partial \eta}\left(\eta^2 \frac{\partial y}{\partial \eta}\right)\right] + \frac{\partial H(y,\theta)}{\partial x}\frac{\partial y}{\partial \eta}$$

$$G_1(y,\theta)\frac{\partial y}{\partial \tau} + G_2(y,\theta)\frac{\partial \theta}{\partial \tau} = H(y,\theta)\left[\frac{1}{\eta^2}\frac{\partial}{\partial \eta}\left(\eta^2 \frac{\partial y}{\partial \eta}\right)\right] + \frac{\partial H(y,\theta)}{\partial x}\frac{\partial y}{\partial \eta} \quad 5.29$$

Another technique applied to make the solution easier is to use the following transformation:

$$u = \eta^2 \quad 5.30$$

Now the system's equations are rewritten in terms of the new variable u:

$$G_1(y,\theta)\frac{\partial y}{\partial \tau} + G_2(y,\theta)\frac{\partial \theta}{\partial \tau} = H(y,\theta)\left[4u\frac{\partial^2 y}{\partial u^2} + 4\frac{\partial y}{\partial u}\right] + 4u\frac{\partial H(y,\theta)}{\partial u}\frac{\partial y}{\partial u} \quad 5.31a$$

$$\frac{d\theta}{d\tau} = 4\beta\left(\frac{c_0}{q_0}\right)H(y,\theta)\frac{\partial y}{\partial u}\Big|_{u=1} - LeBi(\theta - \theta_b) \quad 5.31b$$

$$u = 1; \quad H(y,\theta)\frac{\partial y}{\partial u} = \frac{Bi}{2}(y_b - y) \quad 5.31c$$

5.5 Orthogonal Collocation

When it comes to coupled partial differential equations (PDEs), orthogonal collocation is one of the best methods available. The concept of the method is simple. The method turns a set of coupled ordinary differential equations (ODEs) into set of algebraic equations and similarly a set of coupled PDEs into a set of ODEs which can be solved by numerous techniques developed to solve coupled ODEs numerically, namely

Runge Kutta method (RK). In this section only the application of orthogonal collocation will be shown. For detailed discussion on the method, the reader is referred to texts by Finlayson (Chapter 4 and 6) [43] and Villadsen and Michelsen (Chapter 3) [44]. The general method is applied by discretizing the domain into intervals and solving the equation at these intervals by using the following relations:

$$\frac{\partial y}{\partial x} = \sum_{i=1}^{N+1} A_{ji} y_i \; ; \quad \frac{\partial^2 y}{\partial x^2} = \sum_{i=1}^{N+1} B_{ji} y_i$$

where A and B are matrices with the dimension of (N+1, N+1), j is the index to denote the dependent variable at the collocation points, and N refers to the number of collocation points and consequently the number of intervals and divisions of the spatial domain. To apply orthogonal collocation, N interior collocation points is chosen in the spatial domain u, $0< u_1, u_2,...., u_N < 1$. These points with the point at the boundary u=1 form N+1 interpolation points. Now applying the method to the mass balance to get the j-th interior collocation point:

$$G_1(y_j, \theta)\frac{\partial y_j}{\partial \tau} + G_2(y_j, \theta)\frac{\partial \theta}{\partial \tau} =$$

$$H(y_j, \theta)\left[4u_j \sum_{k=1}^{N+1} B_{jk} y_k + 4\sum_{k=1}^{N+1} A_{jk}\, y_k\right] + 4u_j\left[\sum_{k=1}^{N+1} A_{jk}\, H(y_k, \theta)\right]\left[\sum_{k=1}^{N+1} A_{jk}\, y_k\right] \quad 5.32$$

The boundary condition expressed in orthogonal collocation notation:

$$H(y_{N+1}, \theta)\sum_{k=1}^{N+1} A_{N+1,k} y_k = \frac{Bi}{2}(y_b - y_{N+1}) \quad 5.33$$

From equation 5.33, the surface concentration can be solved using Newton-Raphson method and the initial guess for that method is [42]:

$$y_{N+1} = \frac{y_b - \left(\frac{2}{Bi}\right) H(y_b,\theta) \sum_{k=1}^{N} A_{N+1,k} y_k}{1 + \left(\frac{2}{Bi}\right) A_{N+1,N+1}} \quad 5.34$$

The temperature change in orthogonal collocation notation:

$$\frac{d\theta}{d\tau} = 4\beta\left(\frac{c_0}{q_0}\right) H\left(y_{N+1}, \theta \sum_{j=1}^{N+1} A_{N+1,j}\, y_j\right) - LeBi(\theta - \theta_b) \quad 5.35$$

Equations 5.32-35 are solved using Matlab. The code used to generate the solution can be found in the accompanying appendix.

5.6 Results and Discussion

In this section, the solution for the system's equations will be provided in addition to the effect of various parameters on the behavior on the fractional uptake and the temperature profile. It should be noted that the author has developed the code for the definition of equations, but the solution code was adopted from [42] with some modifications to suit the author's case. The reason for this adoption is the generality of

the program, as the number of collocation points can be set in the same file. Getting the solution for this model was cumbersome. The solution was obtained by optimizing the different parameters and trying to compromise their opposing effects. The parameters used to get the solution for the isothermal case were: adsorbed saturation concentration, q_{max}, pore diffusivity, D_p, and surface diffusivity, D_s. The parameters used to get the solution for the nonisothermal case were: LeBi number, adsorbed saturation concentration, q_{max}, pore diffusivity at reference temperature, D_{p0}, and surface diffusivity at reference temperature, D_{s0}. The list of parameters' values is summarized in Table 18.

Table 18: Summary of optimized parameters' values and dimensionless groups' values

Parameter	Value
LeBi number	0.129
Adsorbed saturation concentration, q_{max}	$2*10^{-1}$ mol/cm^3
Pore diffusivity at reference temperature, D_{p0}	0.0024 cm^2/s
Pore diffusivity for isothermal case, D_p	0.0024 cm^2/s
Surface diffusivity at reference temperature, D_{s0}	$2.9*10^{-5}$ cm^2/s
Surface diffusivity for isothermal case, D_s	$2.9*10^{-5}$ cm^2
Affinity constant at reference temperature, b_0	$1*10^6$ cm^3/mol
Affinity constant for isothermal case, b	$1*10^6$ cm^3/mol
Final Dimensionless time, τ	817
δ_0	3781
β	0.483
Heat of adsorption number, γ_H	29.557
Activation energy number, γ_q	12.315
Heat transfer coefficient, h	$5.155*10^{-3}$ W/cm^2.K
Biot number, Bi	1000
Mass transfer coefficient, k_m	2.872 cm/s

The fractional uptake for the isothermal case is obtained by using the values quoted in Table 18. It can be seen in Figure 32 that the isothermal diffusivity values fit the experimental data perfectly.

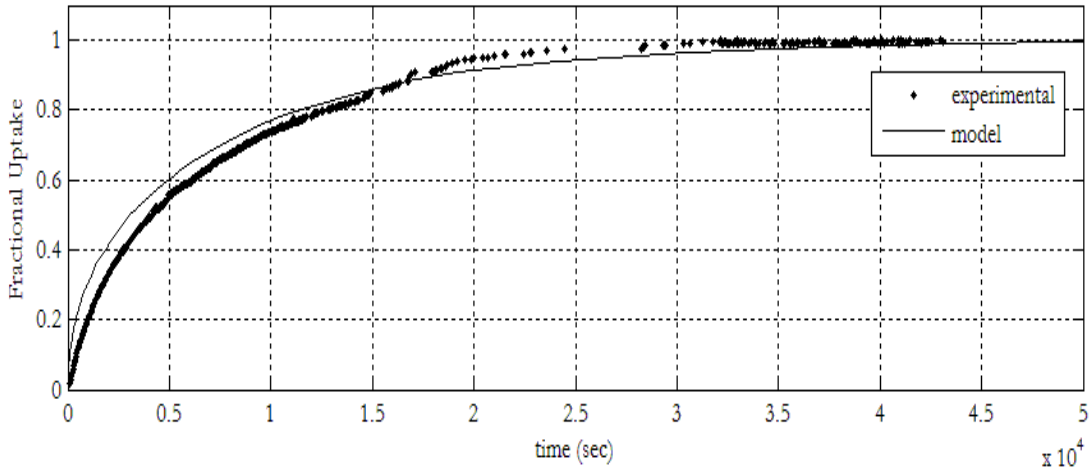

Figure 32: Fractional uptake of water on zeolite 5A (isothermal).

For comparison purposes, the fractional uptake for isothermal and nonisothermal cases is plotted in Figure 33. From Figure 32, it is clear that the experimental points deviate

from the isothermal model after 20000 s. After this time the experimental data are close to the nonisothermal model line.

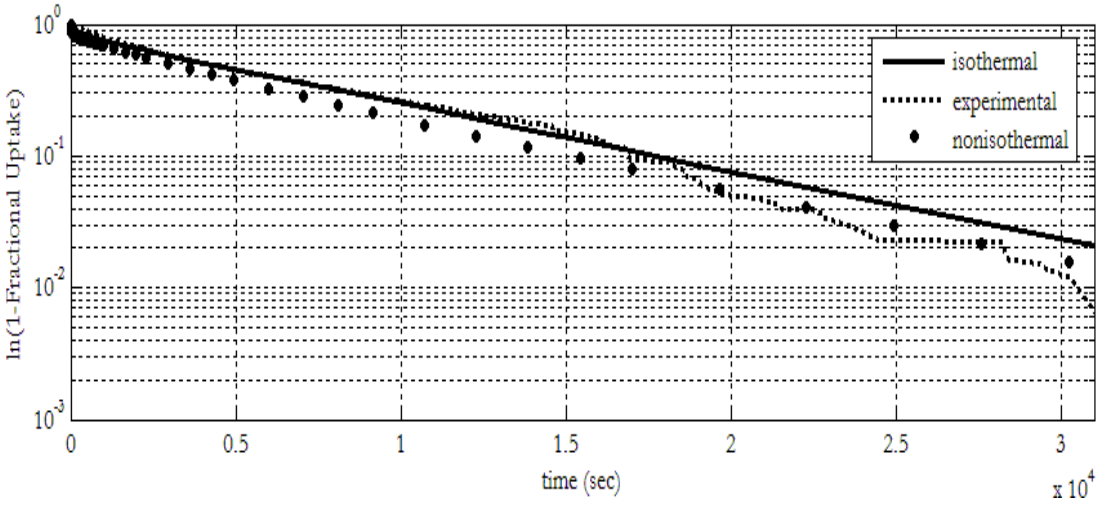

Figure 33: Fractional uptake of water on zeolite 5A, experimental, isothermal, and nonisothermal.

The solution of the nonisothermal model gives a number of concentration profiles equal to the number of collocation points plus the concentration profile at the surface. The dimensionless concentration profiles are shown in Figure 34. For the sake of clarity, only five collocation points were used to produce this figure. Using five collocation points will result in six curves (N+1) for the dimensionless concentration, y.

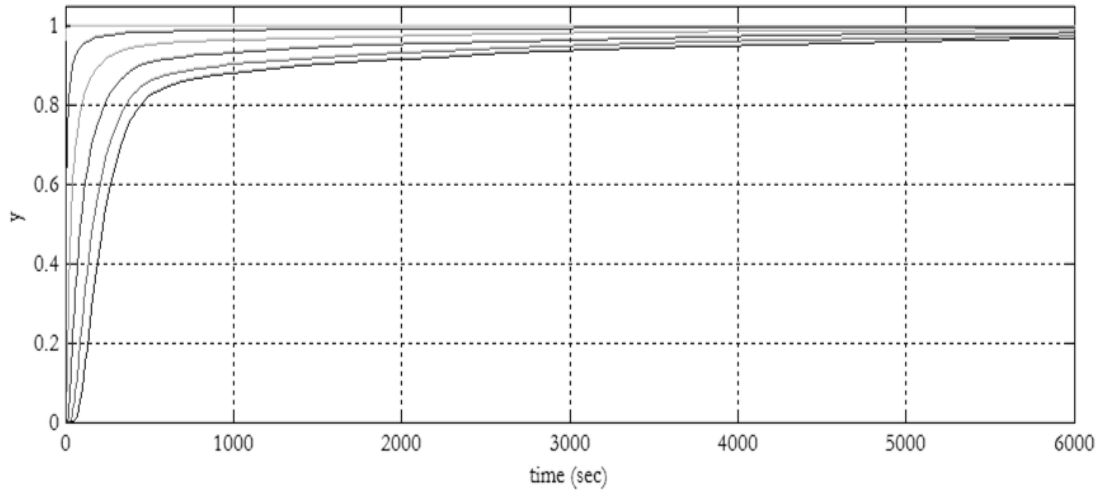

Figure 34: Dimensionless concentration profiles of water on zeolite 5A.

The first five curves refer to solution for the first term in equation 5.32, while the last curve refers to the surface concentration. Next, the experimental uptake is calculated:

$$F = \frac{m_t}{m_\infty} = \frac{m(t) - m_i}{m_\infty - m_i} \qquad 5.36$$

where $\frac{m_t}{m_\infty}$ is the fractional uptake, $m(t)$ is the mass adsorbed at time t (μg), m_i is the initial mass adsorbed at time zero (μg), and m_∞ is the mass adsorbed at time infinity (μg). The experimental uptake, on the other hand, was calculated after getting the concentration profile:

$$F = \frac{[\varepsilon\langle c\rangle+(1-\varepsilon)\langle q\rangle]-[\varepsilon c_i+(1-\varepsilon)q_i]}{[\varepsilon c_b+(1-\varepsilon)q_b]-[\varepsilon c_i+(1-\varepsilon)q_i]} \qquad 5.37$$

where c_i is the initial gas concentration (mol/cm^3), q_i is the initial adsorbed phase concentration (mol/cm^3) calculated using Langmuir isotherm, equation 5.20, evaluated at c_i, c_b is the gas bulk concentration (mol/cm^3), q_b is the adsorbed phase bulk concentration (mol/cm^3) calculated using Langmuir isotherm, equation 5.20, evaluated at c_b, and $\langle c\rangle$ and $\langle q\rangle$ are the volumetric averages over the particle which can now be calculated because of the knowledge of the gas and adsorbed phase concentration across the pellet. The integration of the two averages was performed numerically using the quadrature method using the dot product command in Matlab.

$$\langle c\rangle = 3\int_0^1 \eta^2 c\, d\eta = \sum_{j=1}^{N+1} W_j\, c_j; \quad \langle q\rangle = 3\int_0^1 \eta^2 q\, d\eta = \sum_{j=1}^{N+1} W_j\, q_j \qquad 5.38$$

where $W_j$is the matrix that contains the weights of the quadrature formula with a dimension of (N+1), N is the number of collocation points, and j is the index for the collocation points. After evaluating equation 5.36 and equation 5.37, the two equations are plotted to in Figure 35:

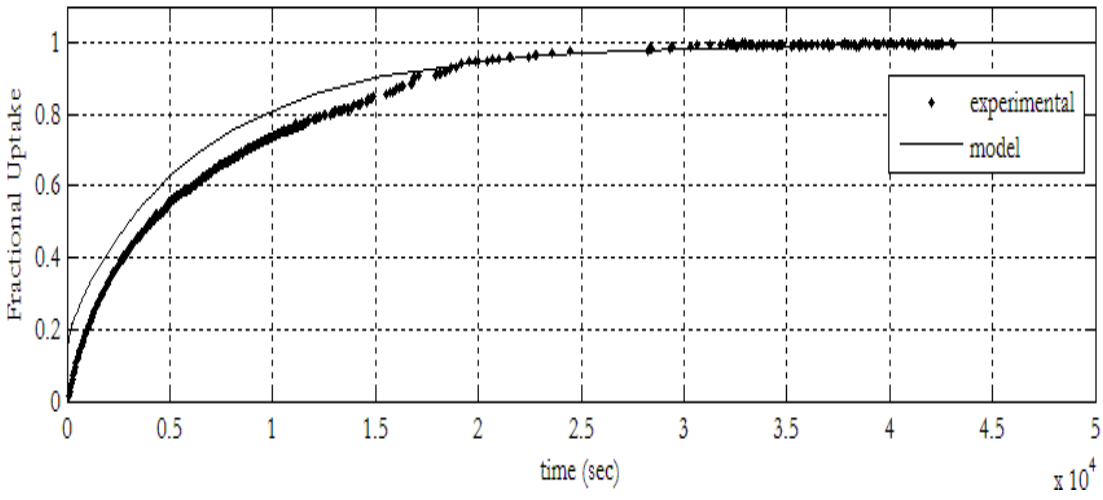

Figure 35: Fractional uptake of water on zeolite 5A (nonisothermal).

In Figure 35 the solution to the mass uptake is plotted in blue and the experimental uptake is plotted in red. The model solution is very close to the experimental curve, which shows the applicability of the model proposed. The solution curve seems to seem to start faster than the experimental curve. This fast pick up is due

to the relative high surface diffusivity value. Another observation about the solution is it deviates from the experimental curve more between the time of 5,000 s and 20,000 s. This is can be attributed to the fact that experimental data at the abovementioned time range had a lot of fluctuations which forced to the author to try to eliminate some outliers while preserving the shape of the curve. This might resulted in increasing the deviation between the two curves at that particular time range. The two curves, however, reach to the same saturation point. Another important thing to look at is how the concentration inside the pellet is evolving with time. To do this, the time interval is divided into ten intervals and the concentration at each interval is plotted on the same plot. To get accurate profiles and smooth curves, twenty collocation points were used.

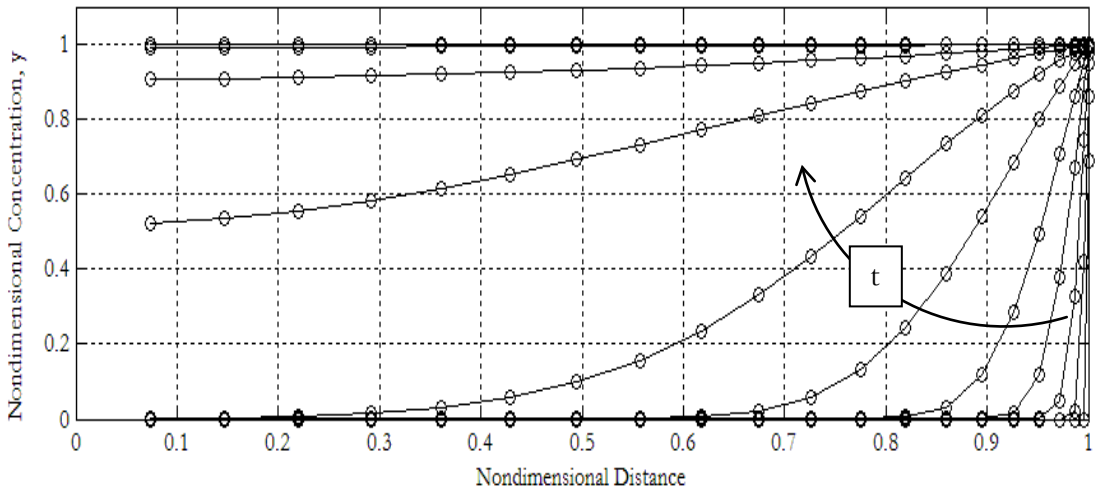

Figure 36: Concentration profiles of water across the zeolite 5A pellet for different time intervals.

It can be seen in Figure 36, at the first time intervals the concentration is zero at the center of the pellet. Then, the concentration starts to grow more with each time interval until reaching the surface with the tenth time interval where the dimensionless concentration is one. This figure shows the satisfaction of the boundary conditions introduced earlier. Finally, the temperature profile across the pellet is solved and compared to the experimental data in Figure 37. In this figure, it can be seen that the model solution for the heat balance equation gave a very close solution to the experimental curve. The two curves show the sharp rise in temperature inside the pellet reaching the peak at 310 K and then the pellet starts to cool down to reach to the bulk temperature, 293 K. For the model, the pellet seems to cool at a slower rate than the experimental case. The reason for this can be attributed to the fact that in zeolite 5A, the two cages has two distinct heats of adsorption, which is something not accounted for the

in the model. Another reason might be the interference and interdependence of system parameters. This is going to be discussed in details in the next section.

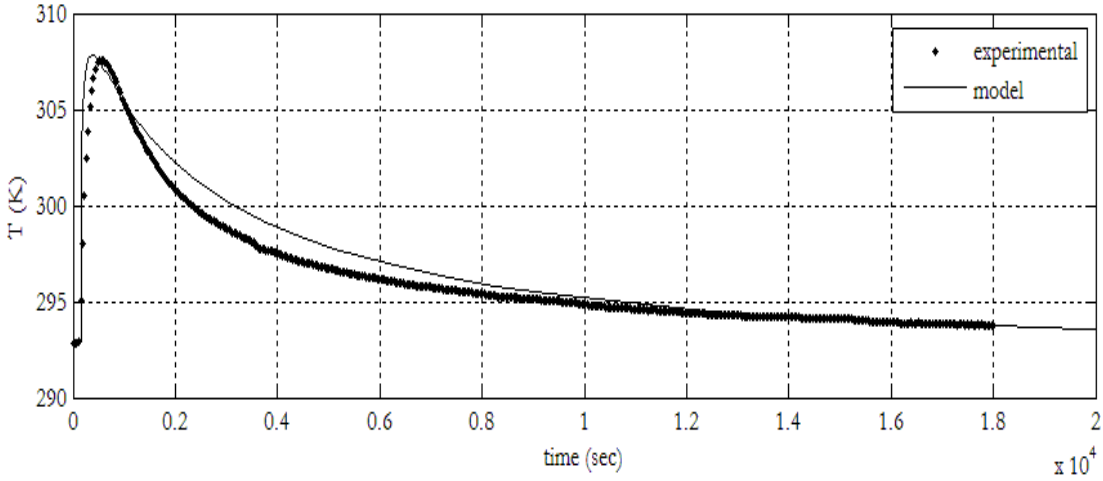

Figure 37: Temperature profile of the adsorption of water on zeolite 5A, Model in red and Experimental in blue.

5.7 Effect of parameters

The effect of the different parameters on the solution gives a good insight about the physics of the system being studied. In this section, the effect of different parameters on the uptake curve and the temperature profile will be studied. This study will give valuable information about parameters that affect the system most and how to compromise between these parameters to get an acceptable solution. It should be noted that the uptake curve and the temperature profile were obtained after tiresome trials of different combinations of diffusivities and other parameters values. The effect of change of the pellet radius on the fractional uptake is already discussed in section 5.3, so only the effect of temperature will be studied. For the effect of each parameter, the model is solved at the true value, a lower value and a higher value. In all cases, the correct value of the parameter will be plotted using a solid line, —, the smaller value will be plotted using an empty circle, o, and the higher value will be plotted using an asterisk, *. Also for the sake of clarity, the temperature profile will be plotted twice. One plot will show the profile over the whole time and the second will over a short period of time to enable reading the temperature peaks.

5.7.1 Pellet Radius, R

The effect of the pellet radius on temperature is shown in Figure 38. From the figure it is clear that changing the pellet size do not affect the value of temperature, as it is the same for the three curves. The three curves reach around 308 K. The main

difference between the three curves is the rate of cooling of the pellet, or in terms of the figure the width of the peak. The rate of cooling for the smaller pellet is obviously faster as surface area is less, while the rate of cooling for bigger pellets is slower because of the larger surface area.

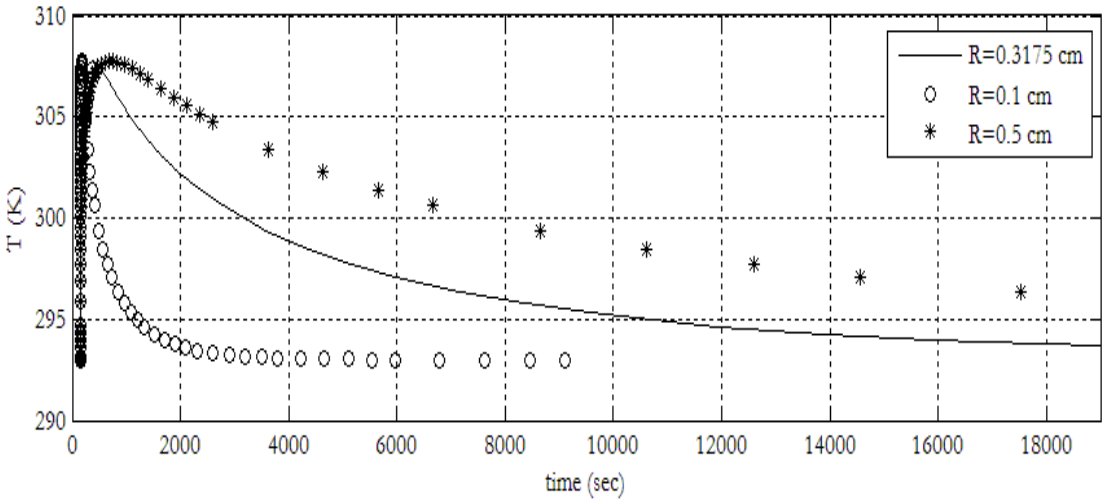

Figure 38: Temperature profile of the adsorption of water on zeolite 5A for different pellet sizes.

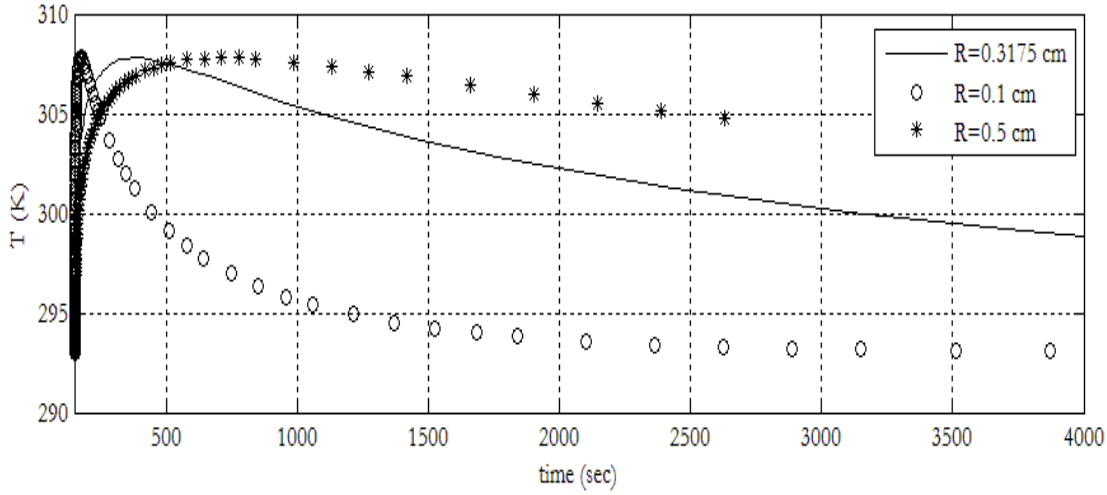

Figure 39: Temperature profile of the adsorption of water on zeolite 5A for different pellet sizes-short time region.

5.7.2 Bulk Concentration, c_b

This parameter is one of the most crucial parameters. Although for the system under examination it is fixed by the conditions of the experiment, it is useful to study the effect of the change of bulk temperature on the mass uptake curve and the temperature profile. The effect of changing the bulk concentration on the fractional uptake curve is shown in Figure 40. In the figure it can be seen that higher bulk concentration makes the mass uptake much faster, i.e. it reaches equilibrium or saturation in a shorter time, while lower bulk concentrations makes the mass uptake much slower. It should be noted though, the change in bulk concentrations only affects how fast the system reaches equilibrium but it does not change the equilibrium concentration.

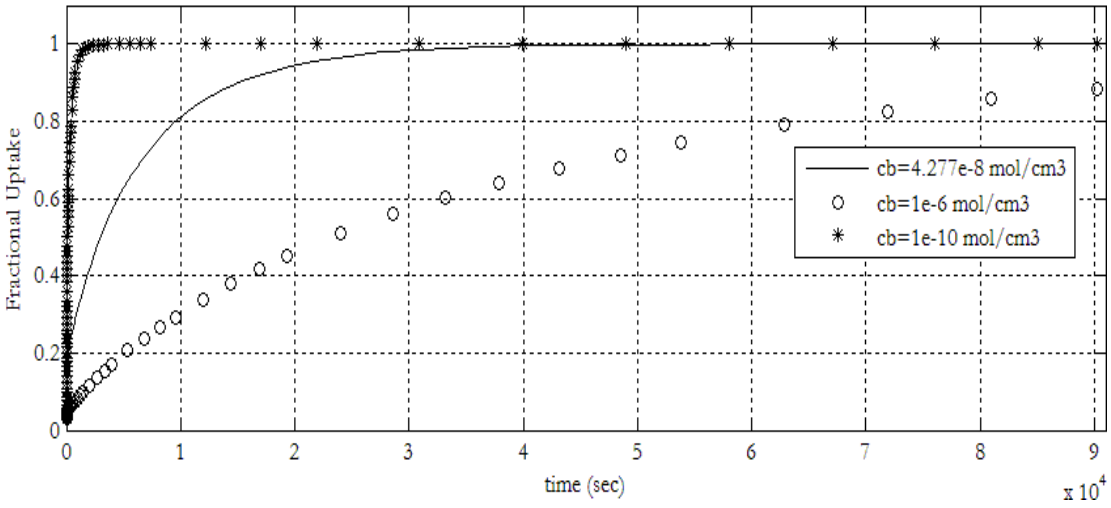

Figure 40: Fractional uptake of water on zeolite 5A for different bulk concentrations, c_b.

Now, the effect of changing the bulk concentration on the temperature profile will be examined. Figure 41 shows the effect of bulk concentration on temperature.

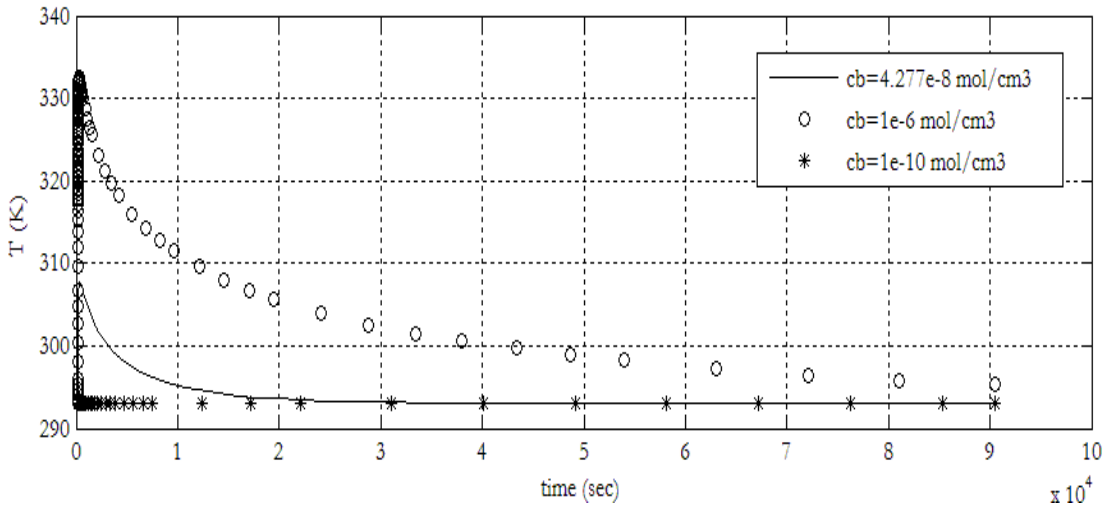

Figure 41: Temperature profile of the adsorption of water on zeolite 5A for different bulk concentrations, c_b.

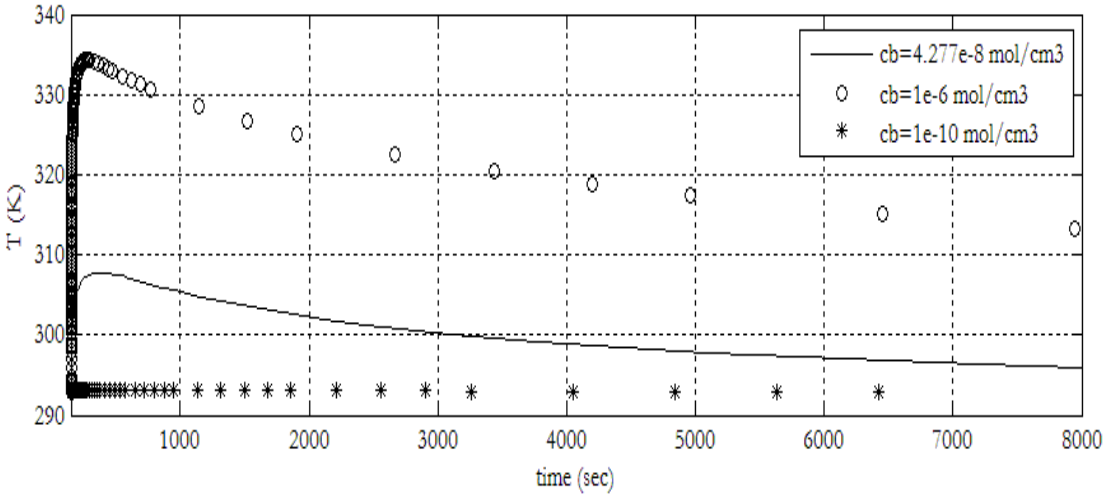

Figure 42: Temperature profile of the adsorption of water on zeolite 5A for different bulk concentrations- short time region.

Temperature increases with the increase in bulk concentration, while a decrease in bulk concentration makes the system almost isothermal. For a bulk concentration of $1*10^{-6}$ (mol/cm^3), the temperature reached to 332 K approximately, while for $1*10^{-10}$(mol/cm^3) the change in temperature is minimal. The reason for the temperature rise is that high bulk concentration will lead to more molecules reaching the pores. The increase in the number of molecules with the contribution of the heat of adsorption leads to the increase in temperature. Similarly, at low bulk concentration, the number of molecules adsorbing to the surface is less which will make the heat transfer rate to the surrounding fast enough to keep the pellet at approximately the same temperature.

5.7.3 LeBi number

In simple terms LeBi number measures the effect of heat transfer on mass transfer. LeBi number is a very important parameter, as it represents a ratio of the diffusion time to the time of dissipation of heat to the surroundings. The definition of LeBi number is recalled:

$$LeBi = \frac{haR^2}{\langle \rho C_p \rangle \varepsilon_p D_{p0}} = \frac{\frac{R^2}{\varepsilon_p D_{p0}}}{\frac{\langle \rho C_p \rangle}{ha}} \qquad 5.21h$$

The effect of LeBi number on the mass uptake and the temperature profile is significant.

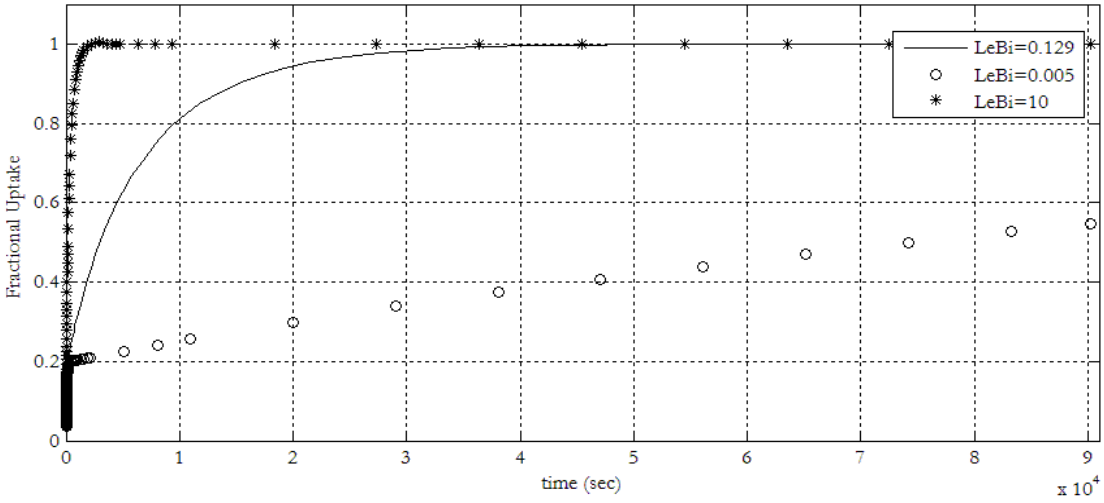

Figure 43: Fractional uptake of water on zeolite 5A for different LeBi number.

In Figure 43, the effect of LeBi number on the fractional uptake. At high LeBi number, the mass uptake is much faster, while low LeBi number results in a very slow mass uptake. Again, the LeBi number only affects how fast or slow does the system reach equilibrium. The effect of LeBi number on the temperature is shown in Figure 44. Lower LeBi number indicates more heat resistance in the film surrounding the pellet and hence results in a rise in temperature, though not much, while significantly slows the rate of cooling the pellet. Higher LeBi number indicates less heat resistance in the film surrounding the pellet which results in lower temperature for the pellet and a faster rate of cooling.

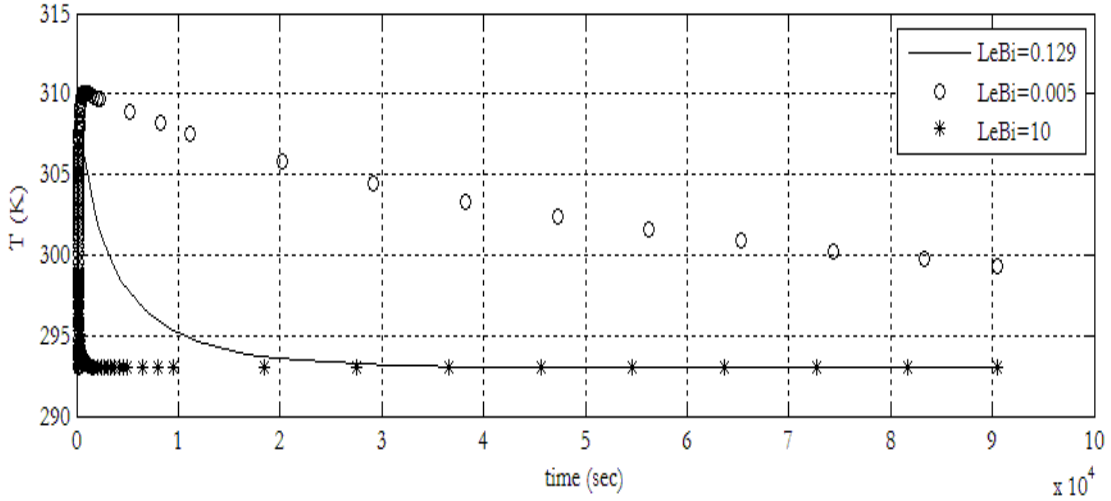

Figure 44: Temperature profile of the adsorption of water on zeolite 5A for different LeBi number.

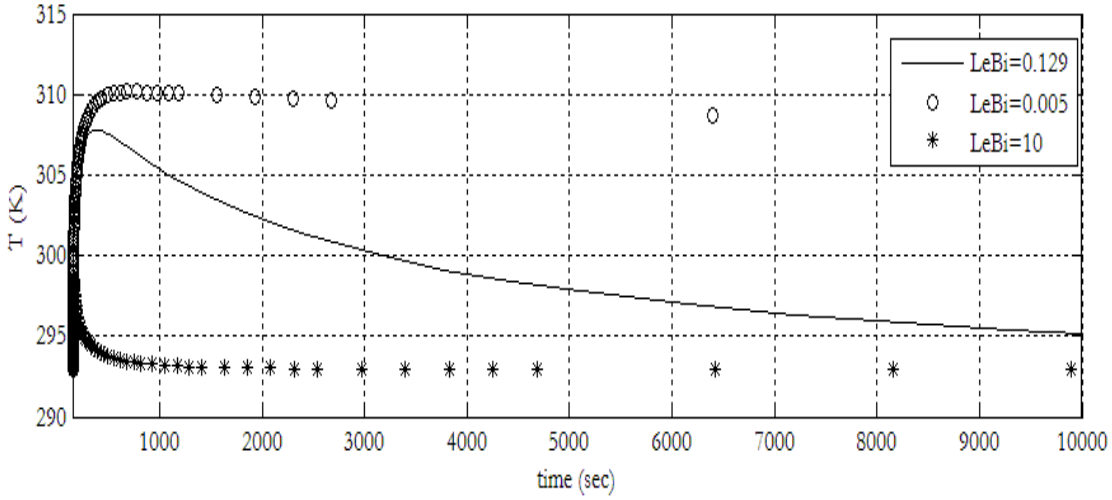

Figure 45: Temperature profile of the adsorption of water on zeolite 5A for different LeBi number-short time region.

5.7.4 Saturation Concentration, q_{max}

The saturation concentration is also one of the crucial parameters in any adsorption system. The fact that this parameter is decided from experimental data makes hard to identify the appropriate value. Previous work by Loughlin [45] was used to get an idea about the range this parameter should fall in. The effect of q_{max} on the fractional uptake is shown next:

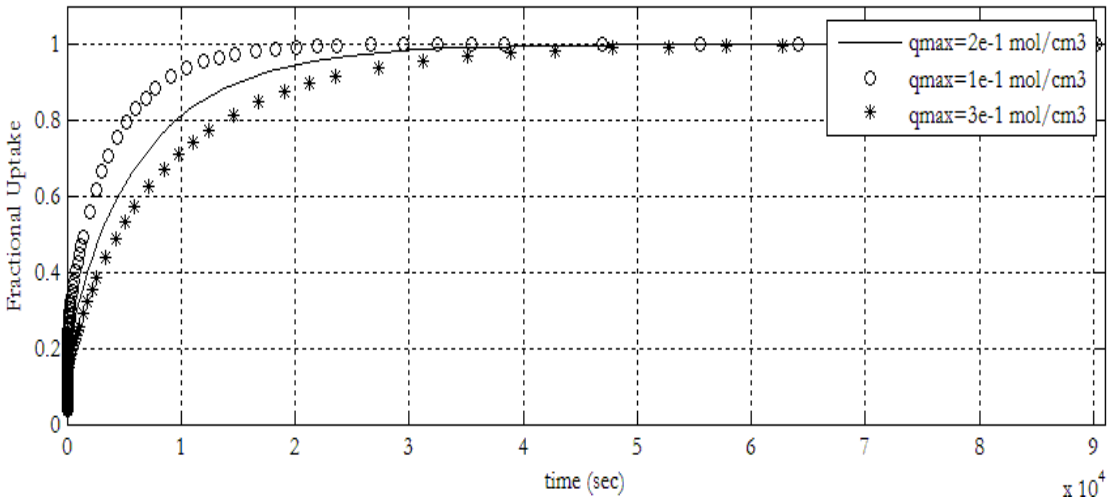

Figure 46: Fractional uptake of water on zeolite 5A for different q_{max} values.

In Figure 46, the lower value of the saturation concentration results in a slower mass uptake while higher values make the mass uptake reaches equilibrium much faster. The effect of temperature is shown in Figure 47:

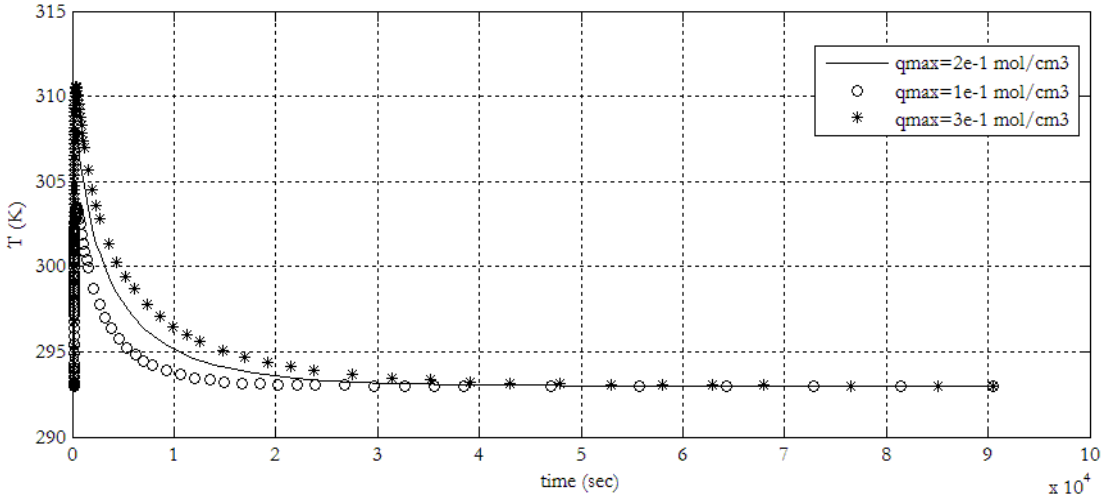

Figure 47: Temperature profile of the adsorption of water on zeolite 5A for different q_{max} values.

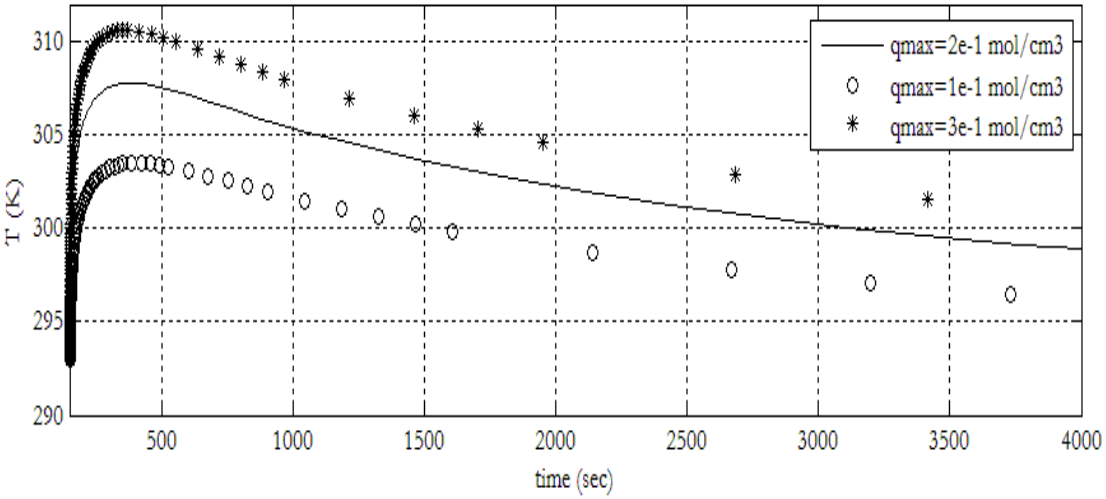

Figure 48: Temperature profile of the adsorption of water on zeolite 5A for different q_{max} values-short time region.

The saturation concentration, q_{max}, only affects the temperature of the system, but has no effect on the rate of cooling of the pellet. The curves for q_{max} =1*10^{-1} mol/cm^3 and q_{max} =3*10^{-1} mol/cm^3 possess the same shape as the curve for 2*10^{-1} mol/cm^3. The lower value curve, q_{max} =1*10^{-1} mol/cm^3, goes up to around 303 K while the higher value curve reaches above 310 K.

5.7.5 Pore Diffusivity at T_0, D_{p0}

Pore diffusivity is one of the most important parameters in adsorption studies and in particular in kinetic studies. Determining the value of this parameter is one of the

objectives of this chapter. Again, the effect of this parameter on both fractional uptake and temperature profile is going to be explored.

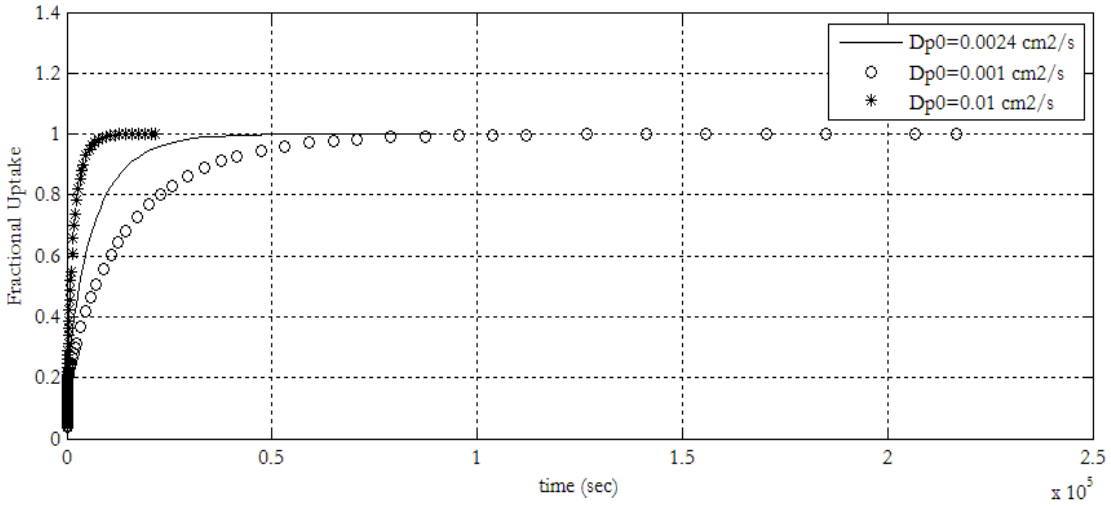

Figure 49: Fractional uptake of water on zeolite 5A for different pore diffusivity values.

Figure 49 show the effect of pore diffusivity on the fractional uptake. The first observation is higher value of pore diffusivity, D_{p0}=0.01 cm^2/s, results in a faster uptake. Another observation is that for the higher value the uptake curve is shorter than the other two curves. This can be easily explained by looking at equation 5.21a:

$$\tau = \frac{\varepsilon D_{p0} t}{R^2} \qquad 5.21a$$

It can be seen from equation 5.21a that time is inversely proportional to pore diffusivity. So a high value of pore diffusivity will result in molecules reaching the interior of the pellet in a shorter time and consequently a shorter curve. For the lower value, D_{p0}=0.001 cm^2/s, the opposite is observed. The fractional uptake is slower and the curve is longer than the other two curves. The effect of pore diffusivity on temperature is shown in Figure 50. The effect of D_{p0} on the temperature is clear on two aspects. The first aspect is the temperature, the lower the diffusivity value the higher the temperature, as for D_{p0}=0.001 cm^2/s, the temperature is around 309 K. To explain, the lower value of diffusivity means that it takes more time for the heat to be dissipated to the surrounding which would result in raising the temperature of the pellet. The second aspect is the rate of cooling of the pellet, as for lower diffusivity value the rate of cooling is slower, i.e. the temperature peak is wider. On the other hand, the increase of the diffusivity value will result in a lower temperature and a faster cooling rate, i.e. a narrower temperature peak.

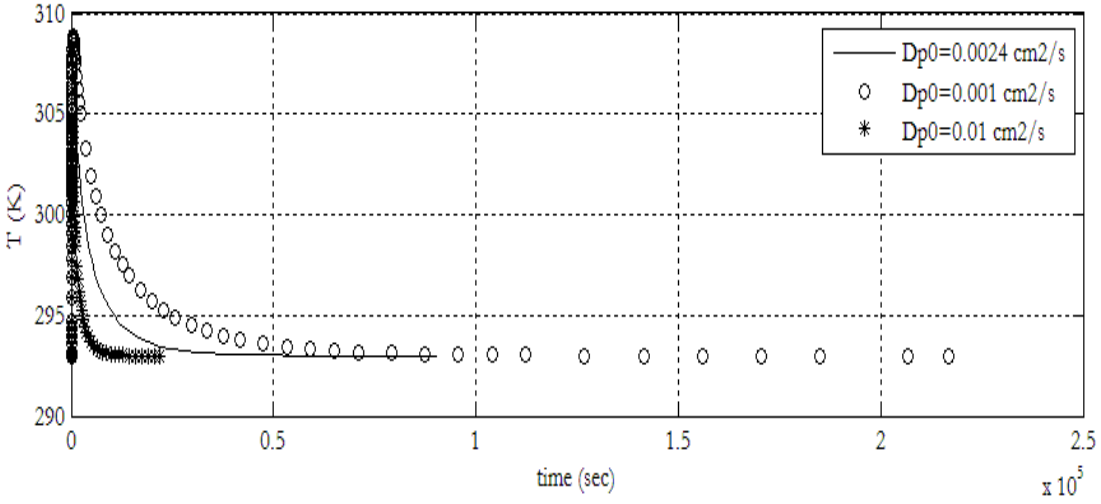

Figure 50: Temperature profile of the adsorption of water on zeolite 5A for different pore diffusivity values.

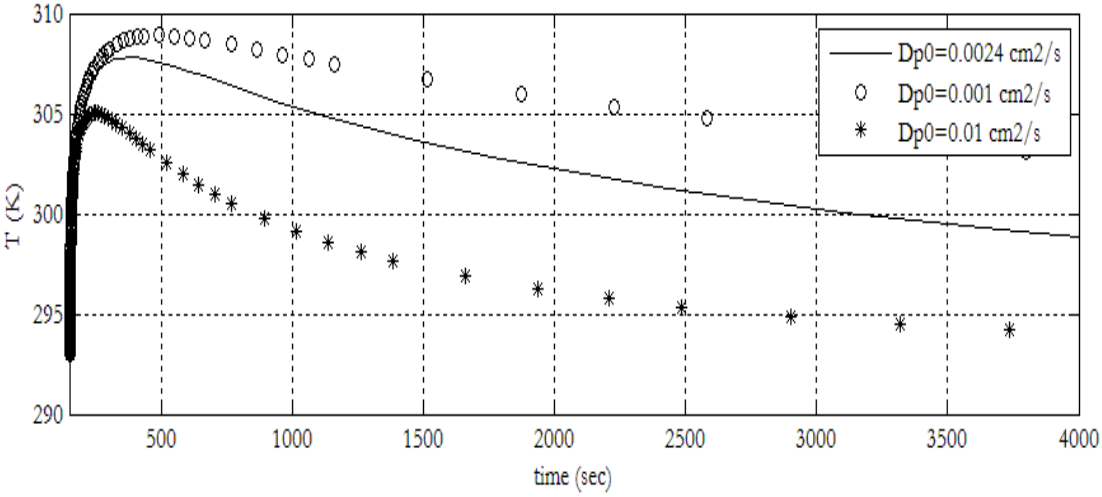

Figure 51: Temperature profile of the adsorption of water on zeolite 5A for different pore diffusivity values-short time region.

Obtaining the solution for the temperature profile enables the calculation of pore diffusivity, D_p, as a function of temperature. This is done using the definition of pore diffusivity in equation 5.3. Figure 52 shows that pore diffusivity is a linear function of temperature when α takes the value of 0.5. Pore diffusivity increases linearly from 0.0024 cm^2/s at 293 K to 0.00246 cm^2/s at 308 K.

$$D_p(T) = D_{p0}\left(\frac{T}{T_0}\right)^{\alpha} \qquad 5.3$$

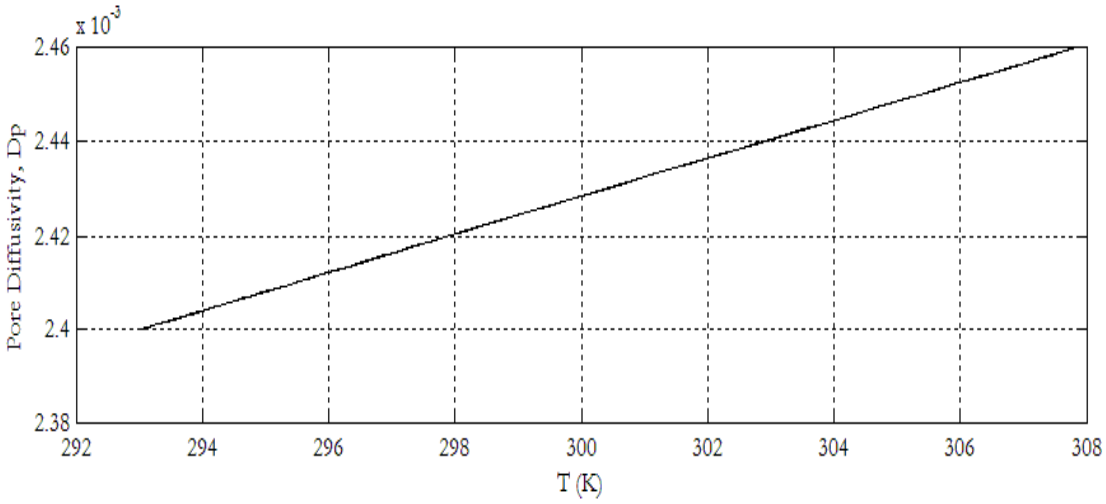

Figure 52: Pore Diffusivity, D_p, as a function of temperature.

5.7.6 Surface Diffusivity at T_0, D_{s0}

Surface diffusivity is the diffusivity that accounts for the diffusion of molecules on the adsorbent surface and it occurs at the pore mouth. In many studies, [3], [38], [39], [40], and [41], this parameter is neglected due to its small value compared to the pore diffusivity. The water molecule is so small that the only restriction facing mass transfer, besides macropore diffusion, is pore mouth. So, this gives an indication that surface diffusivity can't be neglected here.

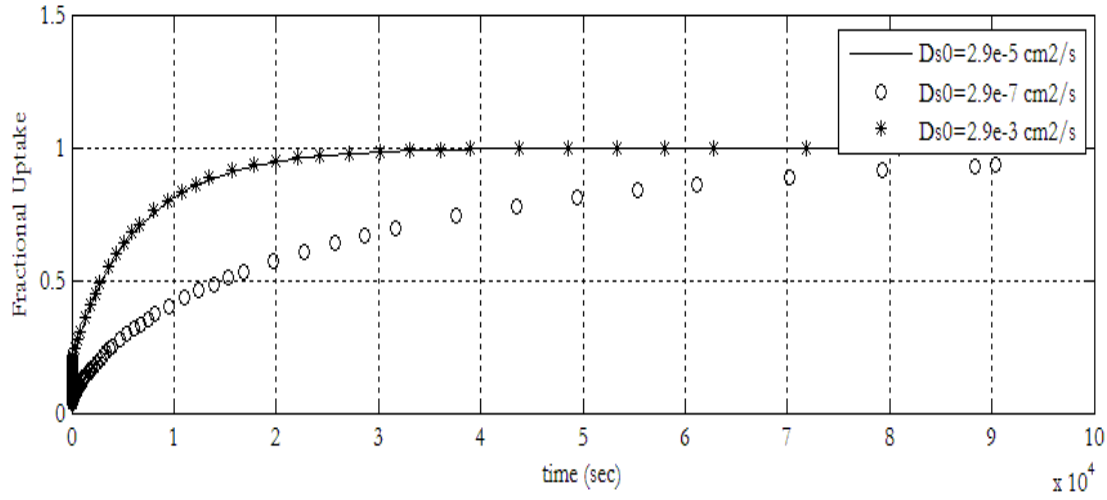

Figure 53: Fractional uptake of water on zeolite 5A for different surface diffusivity values.

Increasing the surface diffusivity will result in a faster fractional uptake but up to a point. As it can be seen in Figure 53, increasing the value beyond the mark of 10^{-5} cm^2/s does not affect the fractional uptake. This is because beyond this mark the surface diffusivity is much smaller than the pore diffusivity and so its affect on the fractional uptake will be insignificant. On the contrary, the effect of surface diffusivity on temperature is more

obvious. In Figure 54, the observation is that lower surface diffusivity values results in higher temperature because a lower value means a slower dissipation of heat, while a higher value means a faster dissipation of heat and approaching the limiting case of isothermality.

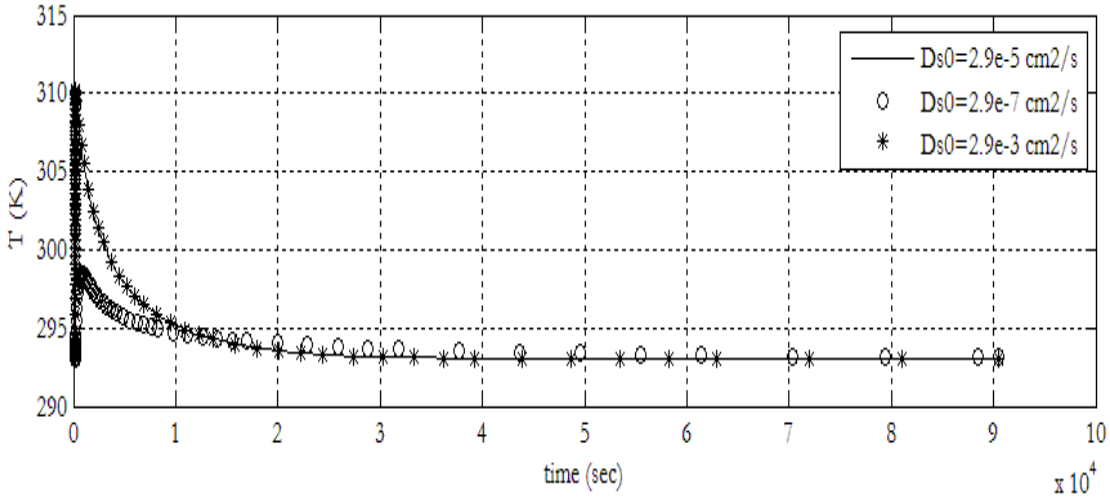

Figure 54: Temperature profile of the adsorption of water on zeolite 5A for different surface diffusivity values.

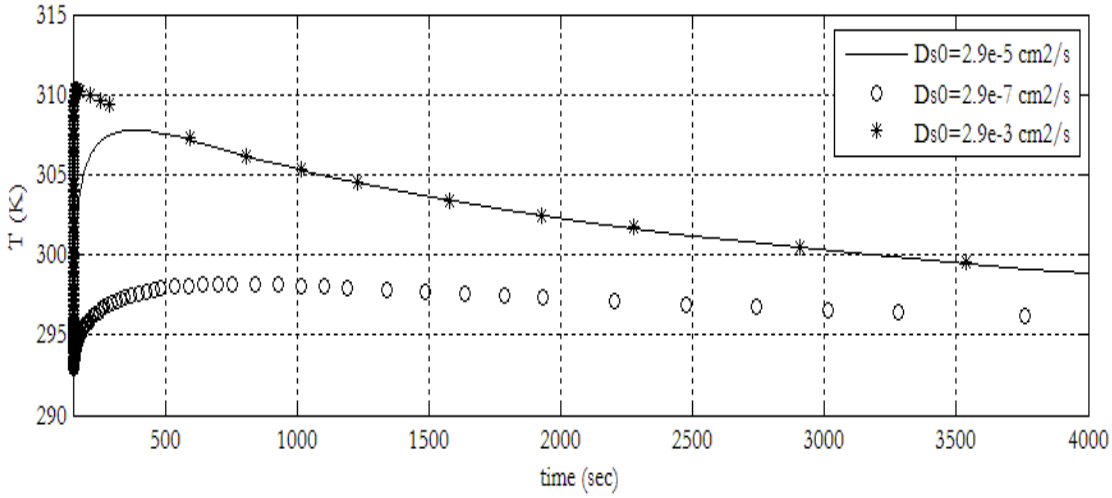

Figure 55: Temperature profile of the adsorption of water on zeolite 5A for different surface diffusivity values-short time region.

Similar to pore diffusivity, surface diffusivity can be shown as a function of temperature because of the knowledge of the temperature profile and the activation energy. Equation 5.8 shows the Arrhenius form of surface diffusivity.

$$D_s(T) = D_{s0} exp\left[\frac{-E_q}{R_g T_0}\left(1 - \frac{T}{T_0}\right)\right] \quad 5.8$$

Surface diffusivity increases from $2.9*10^{-5}$ cm^2/s at 293 K to about $5.3*10^{-5}$ cm^2/s at 308 K.

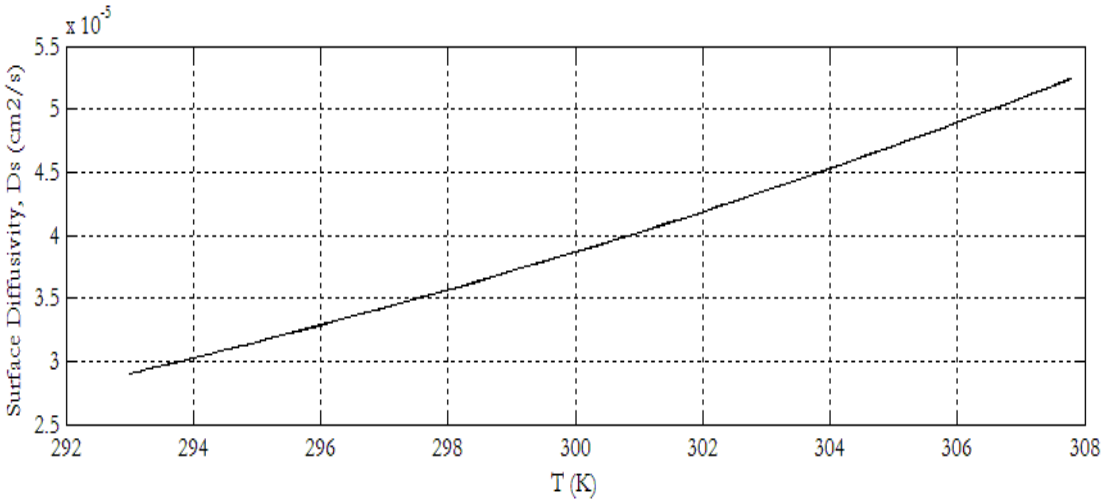

Figure 56: Surface Diffusivity, D_s, as a function of temperature.

5.7.7 Heat of Adsorption, $-\Delta H_{ads}$

The heat of adsorption is the last parameter to be studied. The heat of adsorption is a measure of the heat released due to the bonding of the adsorbate on the adsorbent. It is also serves as a measure for the strength of adsorption. The higher the heat of adsorption, the stronger the bond is between the adsorbate and the adsorbent. For zeolite 5A in particular, the two cages, β and α cage, have two different heat of adsorption. For the small β cage, the heat of adsorption is 60 kJ/mol, while the heat of adsorption for the large α cage is 120 kJ/mol. To overcome this problem, the average of the two values is taken in the solution of the model equations. It is useful to study the heat of adsorption on both fractional uptake and temperature profile. See Figure 58 and Figure 59 respectively. At 60 kJ/mol, the fractional uptake is a bit faster than the 72 kJ/mol case, while at 120 kJ/mol the fractional uptake is much slower. Similar to the case of surface diffusivity, beyond the mark of 100 kJ/mol the effect of increasing the heat of adsorption on the fractional uptake is negligible. The reason for this behavior is not very direct. The effect of the heat of adsorption on the fractional uptake comes from the dependence of the adsorption affinity parameter, or as sometimes called the Langmuir constant, b, on the heat of adsorption. Recall equations 5.21e-g.

$$\gamma_H = \frac{(-\Delta H_{ads})}{R_g T_0} \qquad 5.21f$$

$$\phi(\theta) = exp\left[\gamma_H \left(\frac{\theta}{1+\theta}\right)\right] \qquad 5.21g$$

$$b = b_0 \phi(\theta) \qquad 5.21e$$

The dependence of b on temperature is plotted in Figure 57.

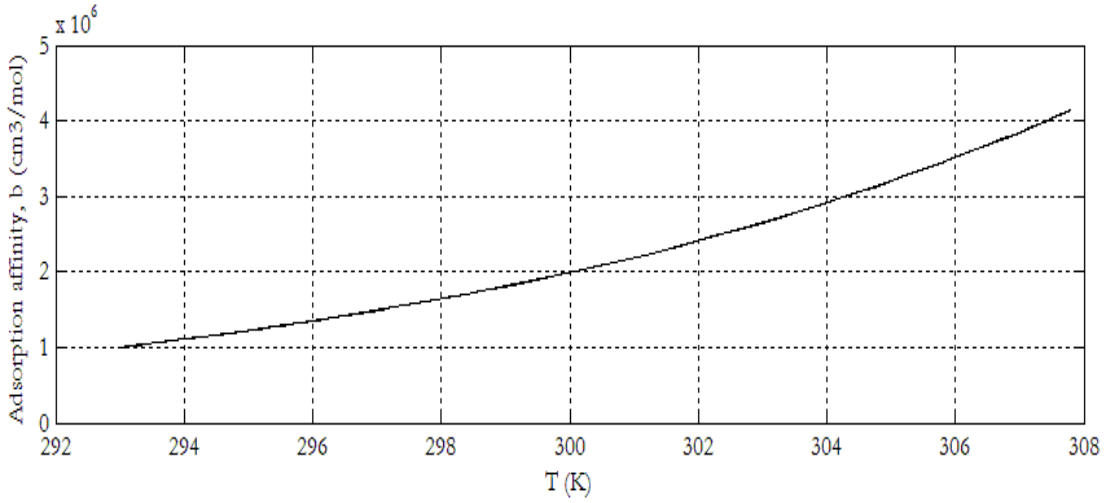

Figure 57: Affinity constant, b, as a function of temperature.

Similar to surface diffusivity, the affinity constant, b, follows an Arrhenius form as it increases from $1*10^6$ cm^3/mol at 293 K to around $4*10^6$ cm^3/mol. The parameter b affects the amount adsorbed, q, and hence a higher value of b will result in a faster mass uptake but up to a point because of the Langmuir isotherm definition. At high values of b the denominator of the Langmuir isotherm becomes $\gg 1$ and the Langmuir isotherm simplifies to 1. So, the continuous increase of the heat of adsorption and consequently b will not affect the adsorbed amount, q, and accordingly it will not affect the fractional uptake.

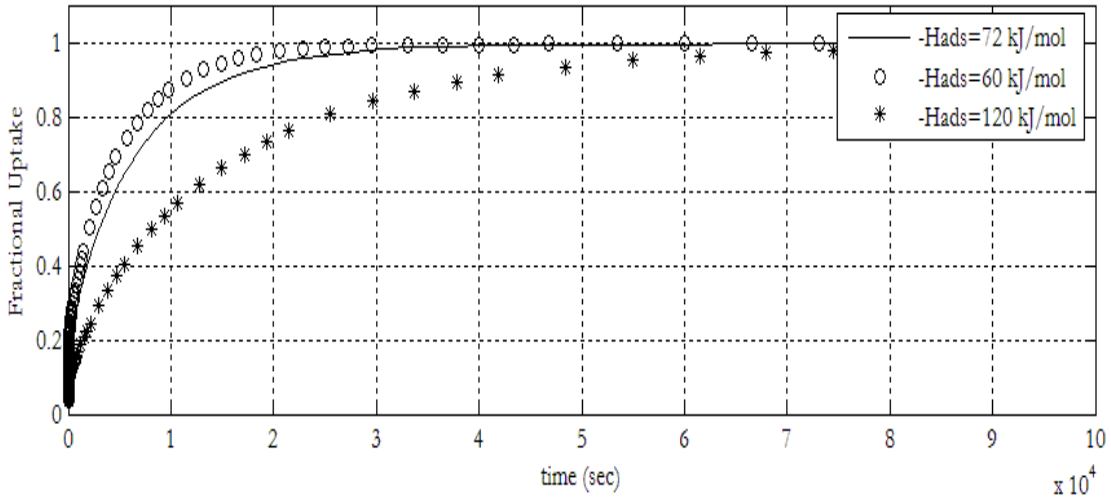

Figure 58: Fractional uptake of water on zeolite 5A for different heat of adsorption values.

The effect of the heat of adsorption on temperature is very direct as the heat generation term depends on the heat of adsorption. The effect is also related to the effect on the fractional uptake. Figure 59 shows the effect of the heat of adsorption on temperature. The 60 kJ/mol curve has the highest peak as temperature approaches 308 K. From the

effect on the fractional uptake, it is already known that at 60 kJ/mol the fractional uptake is faster which results in more molecules inside the pores and hence more generation of heat. The increase in the generation term leads to a slower rate of cooling and hence the peak is wider for the 60 kJ/mol curve. On the contrary, at 120 kJ/mol there are less molecules reaching to the interior of the pellet and therefore the generation term is smaller. So, the temperature for this case is a bit lower, around 305 K, and the rate of cooling is faster which translates to a narrower peak in Figure 59.

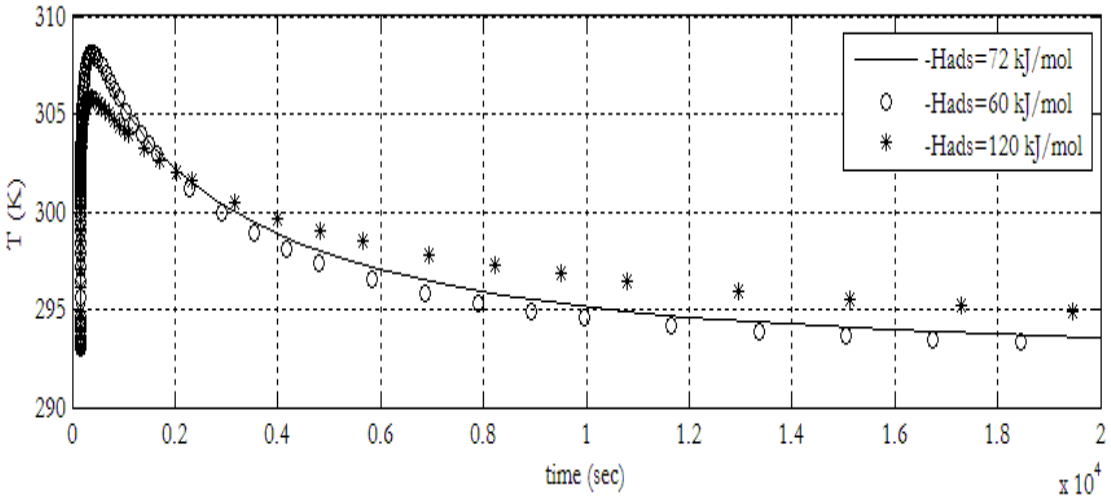

Figure 59: Temperature profile of the adsorption of water on zeolite 5A for different heat of adsorption values.

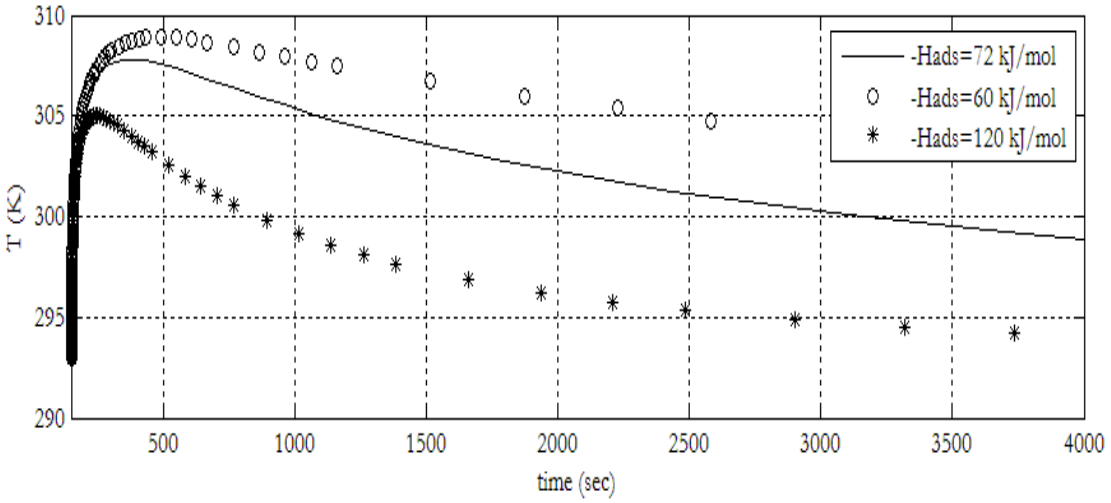

Figure 60: Temperature profile of the adsorption of water on zeolite 5A for different heat of adsorption values-short time region.

CHAPTER 6. CONCLUSIONS AND RECOMMENDATIONS

- A full intrinsic analysis is carried out for the adsorption of CO_2 on 5A and 13X zeolite in Chapter 2.
- The importance of such study is evident nowadays with environmental concern becoming a global issue.
- Most of literature found regarding this topic either lacked some equilibrium analysis or high pressure data.
- The knowledge of the saturation concentration of CO_2 on zeolite 5A and 13X is still not conclusive.
- A full equilibrium analysis is provided along with unpublished data to test findings.
- The model proposed for calculating the saturation concentration is good enough up to the critical point.
- Henry's constants cannot be obtained from isotherms as these values interact with the saturation concentration reducing the level of confidence in both parameters.
- The importance of determining the MSL model parameters stems from the use of the MSL model in the design of adsorption columns.
- A new technique to start the optimization is presented.
- Three optimization techniques are discussed with the application of the first technique on the adsorption of C_2 and C_4 on zeolite 5A.
- Results of these two compounds were satisfactory, though some studies did not fit the MSL model.
- Future work should include the application of the two remaining optimization techniques.
- One resistance models and two resistance models are discussed with ways to identify types of resistances from the uptake data in Chapter 4 and Chapter 5.
- Solution of these models are quoted from literature and reported. Derivations are also provided.
- The solution of the nonisothermal adsorption of water on zeolite 5A is presented.
- Verification of type of resistances is shown along with the derivation of the nonisothermal macropore diffusion model.

- Orthogonal collocation is the method used to solve the model.
- The solution is provided and compared to the experimental data.
- Effect of parameters is studied.
- In the future, some assumptions can be relaxed to give more detail about the system. It is well known that the heat of adsorption of the large cage in 5A zeolite differs from the heat of adsorption of the small cage. Including this in future solutions to this model will provide useful information.

REFERENCES

[1] Internation Adsorption Society. What is Adsorption. [Online]. http://ias.vub.ac.be/What%20is%20adsorption.html#adsorbents

[2] Xinyuan Molecular Sieve. Zeolite Molecular Sieve. [Online]. http://www.molecularsieve.org/Zeolite_Molecular_Sieve.htm

[3] D. M. Ruthven, *Principles of Adsorption and Adsorption Processes*.: John Wiley & Sons, Inc., 1984.

[4] M. Llano-Restrepo, "Accurate Correlation Sturctural Imnterpretation, and Thermochmistry of Equilibrium Adsortption Isotherms of Carbon Dioxide in Zeolite NaX by means of the GSTA Model," *Fluid Phase Equilibria*, vol. 293, pp. 225-236, 2009.

[5] A. L. Pulin, A. A. Fomkin, V. A. Sinitsyn, and A. A. Pribylov, "Adsorption and adsorption-induced deformation of NaX zeolite under high pressures of carbon dioxide," *Russ. Chem. Bull*, vol. 50, pp. 60-62, 2001.

[6] D. W. Breck, *Zeolite Molecular Sieves*. New York: Wiley & Sons, Inc., 1974.

[7] M.M. Dubinin and V. A. Astakhov, *Russ. Chem. Bull.*, vol. 20, pp. 8-12, 1971.

[8] R. M. Barrer, *Zeolites and Clay Materials as Sorbents and Molecular Sieves*. London, United Kingdom: Academic Press, 1978.

[9] D. Shen and M. Bulow, "Isosteric Study of Sorption Thermodynamics of Single Gases and Multi-Component Mixtures on Microporous Materials.," *Microporous and Mesoporous Materials*, vol. 21, pp. 237-249, 1998.

[10] H. B. Abdul Rahman, M. A. Hasanian, and K. F. Loughlin, "Quaternary, Ternary, Binary, and Pure Component Sorption on Zeolite. 1. Light Alkanes on Linde S-115 Silicalite at Moderate to High Pressures.," *Ind. Eng. Chem. Res.*, vol. 29, pp. 1525-1535, 1990.

[11] Y. D. Chen, J. A. Ritter, and R. T. Yang, "Nonideal Adsorption from Mulicomponent Gas Mixtures at Elevated Pressures on a 5A Molecular Sieve.,"

Chem. Eng. Sci. , vol. 45, pp. 2877-2894, 1990.

[12] S. Pakseresht, M. Kazemeini, and M. M. Akbarnejad, "Equilibrium isotherms for CO, CO2, CH4 and C2H4 on the 5A Molecular Sieve by a Simple Volumetric Apparatus. ," *Separation/Purification Technology*, vol. 28, pp. 53-60, 2002.

[13] L. M. Mulloth and J. E. Finn, "Carbon Dioxide Adsorption on a 5A Zeolite Designed for CO2 Removal in Spacecraft Cabins.," *NASA/TM*, vol. 208752, 1998.

[14] Z. M. Wang, T. Arai, and M. Kumagai, "Adsorption Separation of Low Concentrations of CO2 and NO2 by Synthetic Zeolites.," *Energy & Fuels*, vol. 12, pp. 1055-1060, 1998.

[15] F. Brandani, R. Ruthven, and C. G. Coe, "Measurement of Adsorption Equilibrium by the Zero Length Column (ZLC) Technique Part 1: Single-Component Systems," *Ind. Eng. Chem. Res.*, vol. 42, pp. 1451-1461, 2003.

[16] J. Merel, M. Clausse, and F. Meunier, "Experimental Investigation on CO2 Post-Combustion Capture by Indirect Thermal Swing Adsorption using 13X and 5A Zeolites.," *Ind. Eng. Chem. Res.*, vol. 47, pp. 209-215, 2008.

[17] Y. Wang and Y. D. LeVan, "Adsorption Equilibrium of Carbon Dioxide3 and Water Vapor on Zeolites 5A and 13X and Silica Gel: Pure Components," *J. Chem. Eng. Data*, vol. 3, pp. 2839-2844, 2009.

[18] N. Tlili, G. Grevillot, and C. Ballieres, "Carbon Dioxide Capture and Recovery by means of TSA and/or VSA ," *International Journal of Greenhouse Gas Control*, vol. 3, pp. 519-527, 2009.

[19] D. Saha, Z. Bao, F. Jia, and S. Deng, "Adsorption of CO2, CH4, N2O and N2 on MOF-4, MOF-177, and Zeolite 5A," *Environ. Sci. Technol.* , vol. 44, pp. 1820-1826, 2010.

[20] N. N. Avgul, B. G. Aristov, A. V. Kiselev, and L. Ya. Kurdyukova, "Heat of Adsorption of Carbon Dioxide by NaX and NaA zeolites and dependence of the adsorption on gas pressure and temperature," *Russ. J. Phys. Chem.* , vol. 42, pp. 1424-1426, 1968.

[21] S. H. Hyun and R. P. Danner, "Equilibrium Adsorption of Ethane, Ethylene, Isobutane, Carbon Dioxice, and Their Binary Mixtures on 13X Molecular Sieves," *J. Chem. Eng. Data*, vol. 27, pp. 196-200, 1982.

[22] A. Burgess, "Computer Modeling of Equilibrium Adsorption Isotherms: CO2 on 13X Zeolite.," King Fahd University of Petroleum and Minerals, Dhahran, Senior Design Project 1989.

[23] K. Kyaw, T. Shibata, F. Watanabe, H. Matsuda, and M. Hasatani, "Applicability of Zeolite for CO2 Storage in a CaO-CO2 High Temperature Energy Storage System," *Energy Convers. Mgmt*, vol. 38, pp. 1025-1033, 1997.

[24] R. V. Siriwardane, M. S. Shen, E. P. Fisher, and J. A. Patron, "Adsorption of CO2 on Molecular Sieves and Activated Carbon," *Energy & Fuels*, vol. 15, pp. 279-284, 2001.

[25] S. Cavenati, C. A. Grande, and A. E. Rodrigues, "Adsorption Equilibrium of Methane, Carbon Dioxide, and Nitrogen on Zeolite 13X at High Pressures.," *J. Chem. Eng. Data*, vol. 49, pp. 1095-1101, 2009.

[26] G. Li, P. Xiao, P. A. Webley, J. Zhang, and R. Singh, "Competition of CO2/H2O in Adsorption Based CO2 Capture," *Energy Procedia*, vol. 2009, pp. 1123-1130, 2009.

[27] X. Huang, C. J. Margulis, Y. Li, and B. J. Brene, "Why is the Partial Molar Volume of CO2 So Small When Dissolved in a Room Temperatrue Ionic Liquid? Structure and Dynamics of CO2 Dissolved in [Bmim+][PF6]," *J. Am. Chem. Soc.*, vol. 127, pp. 17842-17851, 2005.

[28] R. M. Barrer and R. M. Gibbons, "Zeolite Carbon Dioxide: Energetic and Equilibria in Relation to Exchangeable Cations in Faujasite," */j. Chem. Soc. Farad. Trans.*, vol. 61, pp. 941-961, 1965.

[29] K.F. Loughlin and D.M. Abouelnasr, "Sorbate Densities on 5A Zeolite above and below the Critical Conditions: n alkane Data Evaluation and Modeling," *Adsorption*, vol. 15, pp. 521-533, 2009.

[30] A. Al Mousa, American Univeristy of Sharjah, Sharjah, M.S. Thesis 2011.

[31] J. A. Dunne, M. Rao, S. Sircar, R. J. Gorte, and A. L. Myers, "Calorimetric Heats of Adsorption and Adsorption Isotherms. 2. O2, N2, Ar, CO2, CH4, C2H6 and SF6 on NaX, H-ZSM-5, and Na-ZSM-5 Zeolites," *Langmuir*, vol. 12, pp. 5896-5904, 1996.

[32] D. Shen, M. Bulow, F. Siperstein, M. Engelhard, and A. L. Myers, "Comparison of Experimental Techniques for Measuring Isosteric Heat of Adsorption ," *Adsorption*, vol. 6, pp. 275-286, 2000.

[33] J.A.C. Silva and A.E. Rodrigues, "Multisite Langmuir Model Applied to the Interpretation of Sorption of n-paraffins in 5A Zeolite," *Ind. Eng. Chem. Res.*, vol. 38, pp. 2434-2438, 1999.

[34] F. Roma, J.L Riccardo, and A.J. Ramierz-Pastor, "Statistical Thermodynamics Models for Polyatomic Adsorbates: Application to Adsorption of n-Paraffins in 5A Zeolite," *Langmuir*, vol. 21, pp. 2454-2459, 2005.

[35] C. T. Spencer and R. P. Danner, "Improved Equation for Prediction of Saturated Liquid Density," *Journal of Chemical Engineering and Data*, vol. 17, no. 2, pp. 236-240, 1972.

[36] Academy of Sciences of the DDR, *Adsorption of Hydrocarbons in Zeolites*. Berlin, GDR, 1979, vol. 1 & 2.

[37] K. F. Loughlin, "Sorption in 5A Zeolite," University of New Brunswick, Frederictoin, PhD Thesis 1970.

[38] D. M. Ruthven and J. Karger, *Diffusion in Zeolites*.: John Wiley & Sons, Inc., 1991.

[39] James D. Eagan, Bruno Kindl, and Robert B. Anderson, "Kinetics of Adsorption on A Zeolites. Temperature Effects," in *Molecular Sieve Zeolites-II*.

[40] K. Abdallah, Ph Grenier, L. M. Sun, and F. Meunier, "Nonisothermal Adsorption of Water by Synthetic NaX Zeolite Pellets," *Chemical Engineering Science* , vol. 43, no. 10, pp. 2633-2643, 1988.

[41] Andreas Moller, A. Pessoa Guimaraes, Roger Glaser, and Reiner Staudt, "Uptake-

curves for the determination of diffusion coefficients and sorption equilibria for n-alkanes on zeolites," *Microporous and Mesoporous Materials*, vol. 125, pp. 23-29, 2009.

[42] Doung D. Do, *Adsorption Analysis: Equilibria and Kinetics*. London, United Kingdon: Imperial College Press, 1998.

[43] Bruce A. Finlayson, *Nonlinear Analysis in Chemical Engineering*. United States of America: McGraw-Hill Inc., 1980.

[44] John Villadsen and Michael L. Michelsen, *Solution of Differential Equation Models using Polynomial Approximation*. Englewood Cliffs, New Jersey, United States of America: Prentice-Hall, Inc., 1978.

[45] K.F Loughlin, "Water isotherm models for 4A (NaA) zeolite," *Adsorption*, vol. 15, pp. 337-353, 2009.

[46] J.S. Lee, J. T. Kim, J. K Suh, J. M Lee, and C. H. Lee, "Adsorption Equilibria of CO2 on Zeolite 13X and Zeolite X/Activated Carbon Composite," *J. Chem. Eng. Data* , vol. 47, pp. 1237-1242, 2002.

[47] Y. Wang and M. D. Revan, "Adsorption Equilibrium of Carbon Dioxide and Water vapor on zeolites 5A and 13X and Silica Gel: Pure Components," *J. Chem. Eng. Data*, vol. 54, pp. 2839-2844, 2009.

[48] K.F. Loughlin and R. Amer, "Water Isotherm Models 3A, 4A, 5A and 13X Zeolite," in *5th Pacific Basic conference on Adsorption Science and Technology*, Singapore, 2008.

[49] D.P. Valenzula and A.L. Myers, *Adsorption Equilibrium Data Handbook*. New York: Prentice-Hall, 1989.

APPENDIX: MATLAB CODE

A.1 File for roots of Jacobi Polynomial

```
%+++++++++++++++++++++++++++++++++++++++++++++++++++++++++++++++
%   FUNCTION JCRoot.m
%   THIS FUNCTION CALCULATES ROOTS OF N-TH ORDER JACOBI
POLYNOMIAL.  THE EVALUATION
%   OF THE DERIVATIVES OF THE POLYNOMIALS p IS TAKEN FROM J.
VILLADSEN & M. MICHELSEN
%   "SOLUTION OF DIFFERENTIAL EQUATION MODELS BY
POLYNOMIAL APPROXIMATION", PRENTICE
%   HALL, NEW JERSEY, 1978.
%
%   Written by  D.D. Do
%               Department of Chemical Engineering
%               University of Queensland, St.Lucia, Qld 4072, Australia
%
%               Date written:   3 January 1998
%---------------------------------------------------------------------------

function [d, u] = JCRoot(n,n0,n1,al,be)

 %CONSTRAINT ON SOME PARAMETERS
   if n>20;    disp(' The parameter "n" must be smaller than 20'); return; end
   if al<=-1;  disp('The parameter "al" must be greater than -1'); return; end
   if be<=-1;  disp('The parameter "be" must be greater than -1'); return; end

% CALCULATION OF ZEROS
  g = ones(1,n+1);
  for i=2:n+1
   g(i) = - (n-i+2)*(n+i-1+al+be)*g(i-1)/(i-1)/(i-1+be);
   end

   p = fliplr(g);

   u = roots(p);                        % Calling built-in "roots" to evaluate zeroes
   if n0==1;   u = [0 ; u];    end
   if n1==1;   u = [u ; 1];    end
  u = sort(u);                      % Sort the roots in ascending order

% CALCULATION OF DERIVATIVES OF POLYNOMIALS
%   Ref: Villadsen & Michelsen, eqs. (51)-(53) of Chapter 3
   nt = n+n0+n1;
   for i=1:nt
      d(1,i) = 1; d(2,i) = 0; d(3,i) = 0;
      for j=1:nt;
         if j~=i;
            z          = u(i) - u(j);
            d(3,i)  = z*d(3,i)+3*d(2,i);
            d(2,i)  = z*d(2,i)+2*d(1,i);
```

```
            d(1,i)  = z*d(1,i);
         end
      end
   end
```

A.2 Generating A and B matrices

```
%+++++++++++++++++++++++++++++++++++++++++++++++++++
%   FUNCTION AB.M (MatLab Version 5.1)
%   THIS FUNCTION CALCULATES THE FIRST & SECOND DERIVATIVE
MATRICES FOR
%   THE ORTHOGONAL COLLOCATION METHOD
%               The algorithm is taken from Villadsen & Michelsen (1978)
(V&M)
%               "Solution of Differential Equation Models by Polynomial
Approximation"
%               Prentice Hall, New Jersey, 1978, eqs. (40) to (43) pgs 120, 121.
%+++++++++++++++++++++++++++++++++++++++++++++++++++++++++++++++++++
++++++++++++
% Nomenclature:
%   d         :   dif matrix from jcob function program
%   id        :   index on the nature of output
%               =1 for calculation of the first derivative matrix
%               =2 for calculation of the second derivative matrix
%   n         :   number of interior collocation points
%   n0        :   =1 if x=0 is included, otherwise =0
%   n1        :   =1 if x=1 is included, otherwise =1
%   u         :   interpolation points of length (n+n0+n1)
%
%+++++++++++++++++++++++++++++++++++++++++++++++++++++++++++++++++++
++++++++++++
% USAGE:
%   v   = AB(n,n0,n1,id,d,u)
%+++++++++++++++++++++++++++++++++++++++++++++++++++++++++++++++++++
++++++++++++

function v = AB(n,n0,n1,id,d,u)
   nt      = n+n0+n1;

% DIMENSIONALIZE THE OUTPUT VECTOR
   v       = zeros(nt);

% START THE CALCULATION
   for i=1:nt;
      for j=1:nt;
         if j==i;
            if id==1;
               v(i,i)  = d(2,i)/d(1,i)/2;                    % Eq.(40),Chapter 3,
V&M
            else;
```

```
            v(i,i)  = d(3,i)/d(1,i)/3;                    % Eq.(41),Chapter 3,
V&M
          end;
        else
          v(i,j)     = d(1,i)/d(1,j)/( u(i)-u(j) );        % Eq.(42),Chapter 3, V&M
          if id==2;
            v(i,j) = v(i,j)*( d(2,i)/d(1,i)-2/(u(i)-u(j)) );   % Eq.(43),Chapter 3,
V&M
          end;
        end
      end
  end;
```

A.3 Generating quadrature weights, W's

```
%++++++++++++++++++++++++++++++++++++++++++++++++++++++++++++++++++++
++% Function RDW MatLab version 5.1
% THIS FUNCTION CALCULATES THE NORMALISED RADAU WEIGHTS
% Ref: J. Villadsen & M. Michelsen, "Solution of Differential Equation Models
%         by Polynomial Approximation", Prentice Hall, New Jersey, 1978
%         Chapter 3, eqs. (83)-(85)
%
% Written by    D. D. Do
%               Department of Chemical Engineering
%               University of Queensland
%               St. Lucia, Qld 4072, Australia
%++++++++++++++++++++++++++++++++++++++++++++++++++++++++++++++++++++
+++
%   Nomenclature:
%   al        :   exponent of the integrand factor (1-x)
%   be        :   exponent of the integrand factor x
%   d         :   dif matrix from JCRoot function routine
%   n         :   number of interior collocation point
%   n0        :   =1 if x=0 is included, otherwise =0
%   n1        :   =1 if x=1 is included, otherwise =0
%   u         :   interpolation points, having length (n+n0+n1)
%
%++++++++++++++++++++++++++++++++++++++++++++++++++++++++++++++++++++
+++
% USAGE:
%   w = RDW(n,n0,n1,al,be,u,d)
%++++++++++++++++++++++++++++++++++++++++++++++++++++++++++++++++++++
+++
function w = RDW(n,n0,n1,al,be,u,d)
  nt      = n+n0+n1;
   w      = zeros(1,nt);
%
   if n0==0 & n1==1;
     w     = 1./u./d(1,:)'.^2;
     w(nt) = w(nt)/(1+al);
  end
```

```
   if n0==1 & n1==0;
     w     = 1./(1-u)./d(1,:)'.^2;
     w(1)  = w(1)/(1+be);
   end
   if n0==1 & n1==1;
     w     = 1./d(1,:)'.^2;
     w(1)  = w(1)/(1+be);
     w(nt) = w(nt)/(1+al);
   end
%
   w   = w./sum(w);
```

A.4 Functions File

```
%-------------------------------------------------------------------------
% Kinetics of Nonisothermal Macropore Diffusion
%-------------------------------------------------------------------------
%
%This file contains the governing differential equations and functions
% included in them
%
%Written by: Qassim Hassan
%
% This code is developed using the following reference:
%
%D.D.Do, "Adsorption Analysis: Equilibria and Kinetics"
%
%Chapter 9, eqs. (9.3-13), Appendix 9.4
%-------------------------------------------------------------------------
function dy = me2(t,pot)

% SET GLOBAL STATEMENT
   global n u A B C
   global porosity R s
   global b0 qmax
   global c0 cb ci
   global q0 qb qi
   global alpha beta gammaq gammaH LeBi
   global Dp0 Ds0
   global biot delta0
   global thetab thetai

   %We will use pot as a vector that contains concentration and
   %temperature

   y          = pot(1:n); % Assigning the dimensionless concentration
   theta      = pot(n+1);   % Assinging the dimensionless temperature

%-------------------------------------------------------------------
% Definition of surface concentration
%-------------------------------------------------------------------
```

```
    yb      = cb/c0; %Normalized bulk concentration

    ys      = ( yb - 2*sum(A(n+1,1:n).*y(1:n)')/biot )/( 1 + 2*A(n+1,n+1)/biot);

%-------------------------------------------------------------------------
%Definition of temperature equation, which will be the
%last row in the matrix dy
%-------------------------------------------------------------------------

    dy(n+1) = 2.*beta.*c0./q0.*(1+s).*h(ys,theta).*(A(n+1,n+1).*ys + ...
                  sum( A(n+1,1:n).*y(1:n)')) - LeBi.*(theta - thetab);

% Calculation for rows between 1 to n

    for i=1:n
        sum1 = C(i,n+1)*ys + sum(C(i,1:n).*y(1:n)');
        sum2 = A(i,n+1)*ys + sum(A(i,1:n).*y(1:n)');
        sum3 = A(i,n+1)*h(ys,theta) + sum(A(i,1:n).*h(y(1:n),theta)');
        dy(i)= ( h(y(i),theta)*sum1 + 4*u(i)*sum2*sum3 - ...
                      g2(y(i),theta).*dy(n+1) )/g1(y(i),theta) ;
    end

dy=dy';

%We need to define functions inside the differential equations

%-------------------------------------------------------------------------
%Definition of G1(y,theta)
%-------------------------------------------------------------------------
function l = g1(y,theta)
% SET GLOBAL STATEMENT
    global porosity R s
    global b0 qmax
    global c0 cb ci
    global alpha gammaq gammaH LeBi
termQ   = exp( - gammaH*theta/(1+theta) );
l          = porosity +(1-porosity).*b0*termQ.*qmax./(1 + b0.*c0.*termQ.*y).^2;
%differentiation of Langmuir isotherm w.r.t. concentration

%-------------------------------------------------------------------------
%Definition of G2(y,theta)
%-------------------------------------------------------------------------
function l = g2(y,theta)
% SET GLOBAL STATEMENT
    global porosity R s
    global b0 qmax
    global c0 cb ci
    global alpha gammaq gammaH LeBi
termQ   = exp( - gammaH*theta/(1+theta) );
```

```
l          = -(1-porosity).*gammaH.*b0*termQ.*qmax.*y./...
             (1+theta).^2./(1 + b0.*c0.*termQ.*y).^2; %differentiation of Langmuir
isotherm w.r.t. Temperature

%-------------------------------------------------------------------------
%Definition of H(y,theta)
%-------------------------------------------------------------------------
function l = h(y,theta)
% SET GLOBAL STATEMENT
   global b0 qmax
   global c0 cb ci
   global alpha gammaq gammaH LeBi
   global biot delta0
termQ   = exp( - gammaH*theta/(1+theta) );
termE   = exp( gammaq*theta/(1+theta) );
l          = (1+theta).^alpha + delta0.*termE.*termQ.*(1 + b0*c0)./...
             (1 + b0.*c0.*termQ.*y).^2;
```

A.5 Solution File

```
%+++++++++++++++++++++++++++++++++++++++++++++++++++++++++++++++++++++++++
%   SINGLE COMPONENT ADSORPTION KINETICS IN A SINGLE
%PARTICLE
%   WITH LANGMUIR ISOTHERM: NONISOTHERMAL SYSTEM
%   Written by  D. D. Do
%   Editted by Qassim Hassan
%
%+++++++++++++++++++++++++++++++++++++++++++++++++++++++++++++++++++++++++
%               This is the basic problem of solving the problem of adsorption
%               kinetics in a single particle with LANGMUIR isotherm
%               under nonisothermal conditions.
%
%               Ref: D.D.Do, "Adsorption Analysis: Equilibria and Kinetics"
%                                Chapters 9, eqs. (9.3-19), Appendix 9.3
%
%+++++++++++++++++++++++++++++++++++++++++++++++++++++++++++++++++++++++++
% NOMENCLATURE:
%
%   Variable          Units         Description
%   --------          -----         -----------
%   A                 :             : First derivative collocation matrix
%   al                :               : Parameter alpha for Jacobi polynomial
%   alpha             : (-)           : Exponent for pore diffusivity
%   amount            : mole/cc   : Adsorbate amount per unit particle volume
%   amounti     : mole/cc   : Adsorbate amount per unit particle volume at t = 0
%   amountb  : mole/cc   : Adsorbate amount per unit particle volume at %t =
%infinity
%   b0 : cc/mole   : Affinity constant in the isotherm equation at %reference T0
%   B                 :             : Second derivative collocation matrix
%   be                :             : Parameter beta for Jacobi polynomial
```

```
%   beta          : (-)          : Nondimensional heat number (=H*q0/rhoCp*T0)
%   biot                :              : Biot number for mass transfer through film
%   C                   :              : Matrix defined as: 4*root(i)*b(i,j)+2*(s+1)*a(i,j)
%   c                  : mole/cc   : Concentration of the free species
%   c0                  : mole/cc   : Reference concentration
%   cb                  : mole/cc   : Bulk concentration
%   ci                 : mole/cc   : Initial concentration
%   q                : mole/cc   : Concentration of the adsorbed species
%   q0                 : mole/cc   : Reference concentration of the adsorbed
%species evaluated at c0 and T0
%   qi         : mole/cc   : Initial adsorbed concentration evaluated at ci and Ti
%   qb     : mole/cc   : Final adsorbed concentration evaluated at cb and Tb
%   qmax                : mole/cc   : Saturation adsorbed concentration
%   delta0  (-)     : Ratio of surface diffusion to pore diffusion at %reference T0
%   Dp0          : cm^2/sec  : Pore diffusivity at reference temperature T0
%   Ds0          : cm^2/sec  : Surface diffusivity at reference temperature %T0
%   fractional_uptake   : (-)          : Fractional uptake
%   gammaq             : (-)          : Nondimensional parameter = Eq/Rg/T0
%   gammaH             : (-)          : Nondimensional parameter = H/Rg/T0
%   LeBi       : (-)       : LewisBiot number for heat transfer to the %surrounding
%   n                  :              : Number of interior collocation points
%   n0                  :              : = 1 if the point x=0 is counted; otherwise =0
%   n1                  :              : = 1 if the point x=1 is counted; otherwise =0
%   nt                 :              : n + n0 + n1
%   porosity              : (-)          : particle porosity
%   rhoCp                 : J/cc/K       : particle volumetric heat capacity
%   R       : cm    Particle radius for cylinder and sphere, half %length for slab
%   Rg             :       : J/mole/K  : Gas constant
%   s                : Particle shape factor (0 for slab, 1 for cylinder, 2 for sphere)
%   t, tout           :              : nondimensional time
%   time                : sec          : time
%   T                  : Kelvin       : Temperature
%   T0                  : Kelvin       : reference temperature
%   Tb                  : Kelvin       : Bulk temperature
%   Ti                 : Kelvin       : Initial temperature
%   theta                : (-)          : Nondimensional temperature
%   thetab            : (-)          : Nondimensional bulk temperature
%   thetai            : (-)          : Nondimensional initial temperature
%   u                  : (-)          : Interpolation points = x^2
%   y                  :              : Nondimensional concentration
%   ys                :             : Nondimensional concentration at surface (x=1)
%   yout                :              : Integration vector for ODE15s
%   y0                  :              : Initial condition for the integration vector
%   w                   :              : Radau quadrature weight
%++++++++++++++++++++++++++++++++++++++++++++++++++++++++++++++++++++++++
    clear all
    clc
% DECLARE SOME GLOBAL VARIABLES

    global n u A B C                    % Collocation vectors and matrices
```

```
    global porosity R s                 % Particle characteristics
    global b0 qmax                      % Isotherm characteristics
    global c0 cb ci                     % Concentrations of free species
    global q0 qb qi                     % Concentrations of adsorbed species
    global T0 Tb Ti                     % Temperature
    global thetab thetai
    global alpha beta gammaq gammaH LeBi
    global Dp0 Ds0
    global biot delta0

%-----------------------------------------------------------------
% System Properties
%-----------------------------------------------------------------

    s             = 2;                  % particle shape factor
    R             = 0.5;                % particle radius (cm)
    porosity      = 0.38;               % particle porosity (-)
    ci            = 0;                  % initial gas concentration (mole/cc)
    cb            = 4.277e-8;           % bulk gas concentration (mole/cc)
    c0            = 4.277e-8;           % reference concentration (mole/cc)
    Ti            = 293;                % initial temperature (K)
    Tb            = 293;                % bulk temperature (K)
    T0            = 293;                % reference temperature (K)
    alpha         = 0.5;            % exponent for pore diffusivity ( 0.5 < alpha < 1.75 )
    LeBi          = 0.129;              % LeBi number
    b0            = 1e6;                % adsorption affinity at reference T0 (cc/mole)
    qmax          =20e-2;               % maximum adsorption capacity (mole/cc)
    biot          = 1000;               % biot number
    Dp0           = 0.0024;             % pore diffusivity at reference T0 (cm^2/sec)
    Ds0           = 2.9e-5;             % surface diffusivity at reference T0 (cm^2/sec)
    H             = 72000;              % heat of adsorption (Joule/mole)
    Eq            = 30000;          % surface diffusivity activation energy (Joule/mole)
    rhoCp         = 4.17;               % volumetric heat capacity (Joule/cc/K)
    t_initial     = 0;                  % initial time for integration
%-------------------------------------------------------------------------------

% COLLOCATION SECTION

    n             = 20; %number of interior points
    n0            = 0;
    n1            = 1;
    al            = 1;
    be            = (s-1)/2;
    nt            = n + n0 + n1;
    A             = zeros(nt);
    B             = zeros(nt);
    C             = zeros(nt);
    [dif,u]       = JCRoot(n,n0,n1,al,be); %JCRoot is a file attached to this file, it
%is the file where the roots of the orthogonal polynomial are calculated
    A             = AB(n,n0,n1,1,dif,u); %AB is the file contains A and B
    B             = AB(n,n0,n1,2,dif,u);
```

```
    w              = RDW(n,n0,n1,al-1,be,u,dif); %Here we are calculating the
%quadrature constants according to the number of collocation points
    for i=1:nt;
        C(i,:)  =4.*u(i).*B(i,:)+2.*(s+1).*A(i,:);
    end

% Calculation of constants and dimensionless numbers

    Rg             = 8.3142;
    gammaH      = H/Rg/T0;
    gammaq      = Eq/Rg/T0;

    theta0      = 0;
    thetab      = (Tb - T0)/T0;
    thetai      = (Ti - T0)/T0;

    factori        = exp( - gammaH*thetai/(1+thetai) );
    factorb        = exp( - gammaH*thetab/(1+thetab) );
    q0             = qmax*b0*c0/(1+b0*c0);
    qi             = qmax*b0*factori*ci/(1+b0*factori*ci);
    qb             = qmax*b0*factorb*cb/(1+b0*factorb*cb);

    beta           = H.*q0./rhoCp./T0;
    delta0         = (1 - porosity)*Ds0*q0/porosity/Dp0/c0;
    amounti        = porosity*ci + (1 - porosity)*qi;
    amountb        = porosity*cb + (1 - porosity)*qb;

% Solving the system of ODEs numerically using ode15s

    omega0         = (ci/c0)*ones(1,n);
    omega0         = [omega0 thetai]';
    t_final        =817;       % final dimensionless time
    options        = odeset('Reltol',1e-2,'Abstol',1e-5,'bdf','off');
    [tout,pot]     = ode15s('me2',[t_initial t_final], omega0,options);

%-----------------------------------------------------------------
% SOLUTIONS: CONCENTRATION PROFILES, FRACTIONAL UPTAKE,
TEMPERATURE
%-----------------------------------------------------------------
    time    = tout.*R.^2./porosity/Dp0;

    for i=1:length(tout)
        y(i,1:n)    = pot(i,1:n);
        theta(i)    = pot(i,n+1);
    end

    for i=1:length(tout)
        ys(i)       = (cb/c0 -
2*sum(A(n+1,1:n).*y(i,1:n))/biot)/(1+2*A(n+1,n+1)/biot);
    end

    y               = [y ys'];
```

```
    for i=1:length(tout)
        c(i,:)                = c0.*y(i,:);
        term                  = exp( - gammaH*theta(i)/(1+theta(i)) );
        q(i,:)                = qmax.*b0.*term.*c(i,:)./(1 + b0.*term.*c(i,:) );
        amount(i)             = porosity*dot( w, c(i,:) ) + (1 - porosity)*dot( w, q(i,:) );
        fractional_uptake(i)  = (amount(i) - amounti) ./ (amountb - amounti);
    end

    T                         = T0*(1 + theta);

%-----------------------------------------------------------------------
% PLOTTING
%-----------------------------------------------------------------------
    figure(1)
    subplot(2,2,1)
    plot(time,y,'r-');
    xlabel('time (sec)');
    ylabel('y');
    title('Nondimensional conc. vs. time');
    grid;

    subplot(2,2,2)
    plot(time,T,'r-');
    xlabel('time (sec)');
    ylabel('T (Kelvin)');
    title('Temperature vs. time');
    grid;

    subplot(2,2,3)
    plot(time,fractional_uptake,'r-');
    xlabel('time (sec)');
    ylabel('uptake');
    title('Fractional uptake vs. time');
    grid;

    subplot(2,2,4)
    plot(time,1000*amount,'r-');
    xlabel('time (sec)');
    ylabel('Adsorbed conc. (mmole/cc)');
    title('Amount adsorbed vs. time');
    grid;

    figure(2)
    dt = floor( length(tout)/10 );
    for i=1:dt:length(tout)
        plot(sqrt(u),y(i,:),'k-',sqrt(u),y(i,:),'bo');
        hold on
    end
    xlabel('Nondimensional distance');
    ylabel('Nondimensional conc. (-)');
```

```
    title('Concentration profiles');
    grid;

%-------------------------------------------------------------------------
% Experimental Data, Fractional Uptake and Temperature
%-------------------------------------------------------------------------
%
% 'mine' refers to fractional uptake and 'ppp' refers to time
%
mine=[0.0160,        0.2955,        0.4375,
0.0272,              0.2991,        0.4401,
0.0370,              0.3026,        0.4419,
0.0494,              0.3074,        0.4450,
0.0603,              0.3126,        0.4480,
0.0700,              0.3163         0.4507,
0.0780,              0.3218,        0.4515,
0.0854,              0.3265,        0.4543,
0.0954,              0.3308,        0.4564,
0.1040,              0.3342,        0.4600,
0.1135,              0.3381,        0.4596,
0.1189,              0.3420,        0.4640,
0.1264,              0.3464,        0.4667,
0.1328,              0.3492,        0.4683,
0.1394,              0.3533,        0.4714,
0.1466,              0.3588,        0.4719,
0.1529,              0.3623,        0.4766,
0.1600,              0.3660,        0.4754,
0.1657,              0.3680,        0.4794,
0.1725,              0.3718,        0.4805,
0.1787,              0.3756,        0.4832,
0.1865,              0.3781,        0.4871,
0.1921,              0.3823,        0.4980,
0.2008,              0.3842,        0.4897,
0.2067,              0.3932,        0.4922,
0.2127,              0.3925,        0.4937,
0.2162,              0.3934,        0.4962,
0.2235,              0.3961,        0.4985,
0.2291,              0.4034,        0.5021,
0.2350,              0.4019,        0.5105,
0.2399,              0.4049,        0.5042,
0.2451,              0.4070,        0.5060,
0.2493,              0.4106,        0.5189,
0.2561,              0.4127,        0.5199,
0.2614,              0.4155,        0.5221,
0.2674,              0.4181,        0.5150,
0.2716,              0.4210,        0.5153,
0.2779,              0.4269,        0.5170,
0.2819,              0.4307,        0.5189,
0.2864,              0.4324,        0.5209,
0.2907,              0.4358,        0.5228,
```

0.5247,	0.6137,	0.6811,
0.5264,	0.6160,	0.6818,
0.5280,	0.6164,	0.6847,
0.5305,	0.6173,	0.6850,
0.5341,	0.6200,	0.6909,
0.5359,	0.6222,	0.6893,
0.5363,	0.6235,	0.6895,
0.5390,	0.6242,	0.6917,
0.5407,	0.6260,	0.6907,
0.5451,	0.6269,	0.6905,
0.5552,	0.6288,	0.6952,
0.5538,	0.6302,	0.6946,
0.5572,	0.6314,	0.6976,
0.5626,	0.6328,	0.6983,
0.5601,	0.6347,	0.6992,
0.5599,	0.6356,	0.7012,
0.5615,	0.6354,	0.7032,
0.5639,	0.6381,	0.7034,
0.5665,	0.6396,	0.7046,
0.5681,	0.6423,	0.7058,
0.5674,	0.6479,	0.7069,
0.5717,	0.6505,	0.7071,
0.5731,	0.6473,	0.7089,
0.5710,	0.6468,	0.7093,
0.5736,	0.6488,	0.7107,
0.5789,	0.6513,	0.7111,
0.5811,	0.6540,	0.7141,
0.5794,	0.6538,	0.7158,
0.5839,	0.6566,	0.7176,
0.5834,	0.6581,	0.7188,
0.5856,	0.6597,	0.7193,
0.5889,	0.6594,	0.7217,
0.5864,	0.6603,	0.7234,
0.5880,	0.6623,	0.7236,
0.5858,	0.6626,	0.7242,
0.5877,	0.6642,	0.7289,
0.5883,	0.6645,	0.7292,
0.5911,	0.6652,	0.7293,
0.5922,	0.6665,	0.7304,
0.5937,	0.6677,	0.7314,
0.5952,	0.6695,	0.7325,
0.5979,	0.6708,	0.7337,
0.5998,	0.6716,	0.7338,
0.6015,	0.6729,	0.7381,
0.6039,	0.6749,	0.7388,
0.6041,	0.6748,	0.7392,
0.6067,	0.6766,	0.7399,
0.6082,	0.6790,	0.7423,
0.6098,	0.6787,	0.7433,
0.6120,	0.6806,	0.7449,

0.7468,	0.8005,	0.9120,
0.7467,	0.8016,	0.9129,
0.7467,	0.8039,	0.9172,
0.7501,	0.8027,	0.9193,
0.7496,	0.8049,	0.9221,
0.7519,	0.8069,	0.9291,
0.7513,	0.8065,	0.9326,
0.7547,	0.8067,	0.9415,
0.7525,	0.8082,	0.9449,
0.7502,	0.8083,	0.9472,
0.7531,	0.8096,	0.9501,
0.7542,	0.8107,	0.9502,
0.7547,	0.8116,	0.9519,
0.7552,	0.8126,	0.9534,
0.7562,	0.8148,	0.9576,
0.7567,	0.8150,	0.9601,
0.7582,	0.8169,	0.9610,
0.7594,	0.8170,	0.9639,
0.7594,	0.8204,	0.9668,
0.7598,	0.8226,	0.9703,
0.7614,	0.8238,	0.9768,
0.7633,	0.8248,	0.9775,
0.7743,	0.8261,	0.9808,
0.7653,	0.8279,	0.9828,
0.7645,	0.8300,	0.9837,
0.7652,	0.8302,	0.9847,
0.7657,	0.8303,	0.9850,
0.7674,	0.8451,	0.9857,
0.7684,	0.8429,	0.9882,
0.7665,	0.8440,	0.9913,
0.7697,	0.8449,	0.9946,
0.7712,	0.8471,	0.9949,
0.7709,	0.8532,	0.9951,
0.7725,	0.8610,	0.9991,
0.7733,	0.8611,	0.9930,
0.7747,	0.8637,	0.9922,
0.7747,	0.8639,	0.9935,
0.7747,	0.8691,	0.9939,
0.7784,	0.8707,	0.9976,
0.7795,	0.8718,	0.9910,
0.7799,	0.8758,	0.9902,
0.7837,	0.8794,	0.9891,
0.7852,	0.8835,	0.9916,
0.7869,	0.8843,	0.9970,
0.7899,	0.8986,	0.9939,
0.7912,	0.9018,	0.9991,
0.7920,	0.9065,	0.9918,
0.7937,	0.9098,	0.9921,
0.7958,	0.9106,	0.9937,
0.7967,	0.9108,	0.9920,

0.9958,
0.9944,
0.9901,
0.9958,
0.9902,
0.9936,
0.9914,
0.9920,
0.9923,
0.9915,
0.9935,
0.9901,
0.9916,
0.9909,
0.9950,
0.9954,
0.9915,
0.9903,
0.9927,
0.9932,
0.9907,
0.9881,
0.9971,
0.9909,
0.9949,
0.9902,
0.9906,
0.9912,
0.9962,
0.9945,
0.9951,
0.9984,
0.9904,
0.9911,
0.9930,
0.9911,
0.9934,
0.9920,
0.9979,
0.9955,
0.9929,
0.9919,
0.9913,
0.9911,
0.9935,
0.9924,
0.9903,
0.9904,
0.9946,
0.9976,
0.9985,
0.9995,
0.9910,
0.9965,
0.9907,
0.9920,
0.9914,
0.9947,
0.9919,
0.9987,
0.9925,
0.9915,
0.9973,
0.9982,
0.9917,
0.9939,
0.9965,
0.9974,
0.9984,
0.9982,
0.9906,
0.9910,
0.9986,
0.9918,
0.9956,
0.9901,
0.9939,
0.9933,
0.9998,
0.9951,
0.9969,
0.9931,
0.9915,
0.9954,
0.9955,
0.9962,
0.9960,
0.9959,
0.9962,
0.9981,
0.9986,
0.9952,
1.0000];

ppp=[1.897,
2.536,
3.133,
3.74,
4.312,
4.862,
5.482,
6.035,
6.689,
7.34,
8.158,
8.678,
9.257,
9.782,
10.36,
10.985,
11.596,
12.188,
12.791,
13.454,
14.022,
14.8,
15.457,
16.341,
17.008,
17.614,
18.19,
18.985,
19.575,
20.332,
20.856,
21.427,
22,
22.859,
23.572,
24.312,
24.879,
25.618,
26.149,
26.894,
27.447,
28.156,
28.682,
29.22,
29.824,
30.529,
31.13,
31.906,
32.543,
33.363,
34.026,
34.613,
35.142,
35.954,
36.557,
37.123,

37.734,
38.556,
39.32,
39.838,
40.495,
41.113,
41.692,
42.209,
42.805,
43.453,
44.202,
44.754,
45.285,
45.821,
46.335,
46.87,
47.424,
48.189,
48.72,
49.274,
49.807,
50.365,
50.921,
51.473,
52.025,
52.582,
53.115,
53.648,
54.182,
54.696,
55.438,
56.084,
56.619,
57.175,
57.707,
58.239,
59.027,
59.581,
60.117,
60.725,
61.28,
61.839,
62.396,
62.951,
63.722,
64.347,
64.903,
65.67,
66.199,
66.734,
67.267,
67.819,
68.375,
68.956,
69.513,
70.046,
70.602,
71.136,
71.69,
72.228,
72.779,
73.335,
73.868,
74.4,
74.957,
75.49,
76.024,
76.581,
77.113,
77.672,
78.46,
79.017,
79.549,
80.102,
80.751,
81.282,
81.907,
82.46,
82.991,
83.523,
84.055,
84.571,
85.34,
85.876,
86.432,
86.964,
87.754,
88.542,
89.072,
89.862,
90.393,
90.946,
91.669,
92.411,
92.966,
93.499,
94.266,
95.03,
95.587,
96.353,
96.906,
97.438,
97.993,
98.554,
99.157,
99.757,
100.359,
100.962,
101.563,
102.162,
102.763,
103.366,
103.966,
104.567,
105.169,
105.772,
106.374,
106.975,
107.576,
108.176,
108.777,
109.379,
109.977,
110.578,
111.18,
111.782,
112.384,
112.985,
113.585,
114.185,
114.786,
115.385,
115.984,
116.585,
117.182,
117.783,
118.384,
118.984,
119.585,
120.183,
120.782,
121.384,
121.983,
122.585,
123.187,
123.789,
124.389,
124.989,
125.593,
126.193,

126.796,
127.398,
127.998,
128.599,
129.199,
129.801,
130.401,
131.004,
131.605,
132.204,
132.804,
133.405,
134.005,
134.605,
135.203,
135.804,
136.404,
137.005,
137.607,
138.209,
138.811,
139.411,
140.012,
140.612,
141.212,
141.813,
142.413,
143.016,
143.618,
144.221,
144.823,
145.423,
146.022,
146.623,
147.225,
147.826,
148.428,
149.028,
149.628,
150.227,
150.829,
151.43,
152.032,
152.633,
153.835,
155.04,
155.64,
156.241,
156.841,
157.442,
158.643,
159.245,
159.844,
161.049,
161.653,
162.255,
162.857,
163.457,
164.658,
165.259,
167.061,
167.663,
168.265,
168.868,
169.468,
170.068,
171.271,
171.872,
172.473,
173.075,
173.677,
174.278,
174.88,
175.481,
176.082,
176.682,
177.281,
177.882,
178.482,
179.083,
179.681,
180.281,
180.882,
181.483,
182.086,
182.688,
183.29,
183.89,
184.492,
185.091,
185.691,
186.293,
186.896,
187.492,
188.094,
188.696,
189.298,
189.896,
190.497,
191.098,
191.7,
192.301,
192.9,
193.501,
194.099,
194.702,
195.304,
195.902,
200.104,
201.307,
201.907,
202.508,
203.71,
204.91,
205.511,
208.516,
209.118,
213.926,
214.527,
215.129,
215.729,
216.329,
216.932,
217.532,
218.132,
219.966,
220.63,
221.294,
221.957,
223.279,
223.943,
224.604,
227.258,
227.919,
229.909,
231.236,
231.891,
232.562,
235.877,
236.539,
237.862,
239.184,
242.496,
243.159,
243.821,
244.485,
246.471,
247.135,
248.46,
258.397,

261.709,
262.371,
263.696,
265.685,
266.346,
267.008,
268.995,
270.98,
272.303,
278.262,
279.588,
280.914,
281.576,
284.887,
298.8,
299.461,
301.446,
302.109,
302.77,
305.423,
307.413,
310.065,
310.73,
315.365,
320.003,
325.961,
331.259,
333.246,
340.526,
345.168,
350.468,
358.417,
359.079,
374.311,
379.617,
380.279,
393.526,
407.444,
471.024,
471.687,
472.351,
474.341,
488.929,
489.664,
491.132,
505.083,
510.954,
521.238,
529.313,
535.19,
535.924,
536.659,
537.393,
538.861,
539.595,
540.33,
541.065,
542.533,
543.268,
546.208,
547.677,
548.412,
549.146,
549.881,
550.615,
552.817,
553.552,
555.02,
555.755,
558.691,
560.893,
563.834,
564.568,
565.302,
567.509,
571.181,
571.916,
572.65,
575.586,
576.32,
577.055,
577.789,
578.523,
579.989,
587.329,
588.063,
588.797,
592.468,
593.203,
594.67,
596.136,
598.34,
599.075,
602.747,
604.217,
608.622,
612.293,
613.762,
616.701,
617.434,
618.168,
619.637,
620.371,
621.106,
627.716,
629.918,
630.652,
632.123,
632.858,
633.592,
635.06,
637.262,
638.73,
640.2,
641.669,
643.136,
644.605,
645.339,
646.808,
649.746,
654.152,
655.622,
656.356,
657.089,
657.824,
658.559,
661.498,
664.434,
665.168,
666.636,
668.104,
670.307,
672.509,
676.178,
676.912,
677.646,
681.316,
682.05,
682.784,
683.518,
684.984,
685.718,
686.452,
687.92,
690.124,
691.594,
696,
696.736,
698.203,
700.407,

701.144,
703.348,
704.815,
705.549,
707.017,
708.486,
709.221,
715.83,
718.033,
1501.909];

temp=[0.013 19.865
0.612 19.865
1.216 19.8595
1.897 19.9405
2.536 22.0742
3.133 25.0053
3.74 27.5323
4.312 29.4319
4.862 30.8856
5.482 32.1192
6.035 32.9299
6.689 33.6291
7.34 34.0821
8.158 34.4234
8.678 34.5311
9.257 34.5662
9.782 34.5375
10.36 34.4625
10.985 34.3556
11.596 34.2288
12.188 34.0334
12.791 33.8676
13.454 33.6196
14.022 33.3923
14.8 33.0861
15.457 32.8462
16.341 32.5074
17.008 32.2404
17.614 32.0061
18.19 31.8068
18.985 31.5127
19.575 31.3055
20.332 31.0474
20.856 30.8769
21.427 30.6944
22 30.5239
22.859 30.2531
23.572 30.0476
24.312 29.8261
24.879 29.686
25.618 29.4932
26.149 29.3539
26.894 29.1611
27.447 29.0178
28.156 28.8426
28.682 28.728
29.22 28.6046
29.824 28.4748
30.529 28.3315
31.13 28.1993
31.906 28.0751
32.543 27.9589
33.363 27.8268
34.026 27.7313
34.613 27.6206
35.142 27.5299
35.954 27.4065
36.557 27.3054
37.123 27.2171
37.734 27.1375
38.556 27.0173
39.32 26.921
39.838 26.8613
40.495 26.7889
41.113 26.7046
41.692 26.6218
42.209 26.5629
42.805 26.5136
43.453 26.4333
44.202 26.3218
44.754 26.2868
45.285 26.2319
45.821 26.1842
46.335 26.1325
46.87 26.0808
47.424 26.002
48.189 25.9479
48.72 25.9089
49.274 25.8532
49.807 25.8214
50.365 25.7618
50.921 25.7124
51.473 25.6615
52.025 25.6058
52.582 25.5565
53.115 25.5343
53.648 25.4825
54.182 25.438
54.696 25.3871
55.438 25.3243
56.084 25.2916
56.619 25.2638
57.175 25.2105
57.707 25.1612
58.239 25.1175
59.027 25.061
59.581 24.9576
60.117 24.8399
60.725 24.75
61.28 24.723
61.839 24.7182
62.396 24.7031
62.951 24.684
63.722 24.6546
64.347 24.6307
64.903 24.6061
65.67 24.5687
66.199 24.5281
66.734 24.5067
67.267 24.4804
67.819 24.4335
68.375 24.4009
68.956 24.3858
69.513 24.3452
70.046 24.3134
70.602 24.2808
71.136 24.249
71.69 24.2069
72.228 24.1703
72.779 24.1512
73.335 24.1162
73.868 24.1019
74.4 24.0725
74.957 24.0415
75.49 24.0153
76.024 23.993
76.581 23.9803
77.113 23.962
77.672 23.9469
78.46 23.9135
79.017 23.8777
79.549 23.8563
80.102 23.8364
80.751 23.8236
81.282 23.795
81.907 23.7823
82.46 23.7473
82.991 23.7195
83.523 23.6972

84.055 23.6758
84.571 23.6726
85.34 23.6328
85.876 23.6082
86.432 23.5883
86.964 23.5629
87.754 23.5311
88.542 23.5144
89.072 23.5057
89.862 23.4778
90.393 23.45
90.946 23.4325
91.669 23.4055
92.411 23.3784
92.966 23.3626
93.499 23.3554
94.266 23.3395
95.03 23.2997
95.587 23.2775
96.353 23.2528
96.906 23.2465
97.438 23.233
97.993 23.2155
98.554 23.2131
99.157 23.1845
99.757 23.1622
100.359 23.1622
100.962 23.1344
101.563 23.1288
102.162 23.1082
102.763 23.0915
103.366 23.0581
103.966 23.0398
104.567 23.0295
105.169 23.0001
105.772 22.9929
106.374 22.977
106.975 22.9651
107.576 22.9333
108.176 22.923
108.777 22.9134
109.379 22.8896
109.977 22.8888
110.578 22.8578
111.18 22.8467
111.782 22.8196
112.384 22.8117
112.985 22.7974
113.585 22.7807
114.185 22.7743
114.786 22.7608
115.385 22.7481
115.984 22.7433
116.585 22.741
117.182 22.7227
117.783 22.7116
118.384 22.7076
118.984 22.6941
119.585 22.6734
120.183 22.6575
120.782 22.6281
121.384 22.6233
121.983 22.6201
122.585 22.6098
123.187 22.5947
123.789 22.5971
124.389 22.5836
124.989 22.5566
125.593 22.5319
126.193 22.5288
126.796 22.5009
127.398 22.5033
127.998 22.5025
128.599 22.4946
129.199 22.4842
129.801 22.4739
130.401 22.4517
131.004 22.4397
131.605 22.4254
132.204 22.4207
132.804 22.3992
133.405 22.3865
134.005 22.3706
134.605 22.3555
135.203 22.342
135.804 22.3285
136.404 22.3166
137.005 22.3142
137.607 22.2896
138.209 22.2752
138.811 22.2729
139.411 22.2625
140.012 22.253
140.612 22.2427
141.212 22.2435
141.813 22.2411
142.413 22.2355
143.016 22.2371
143.618 22.2204
144.221 22.218
144.823 22.2006
145.423 22.1846
146.022 22.1767
146.623 22.1703
147.225 22.1544
147.826 22.137
148.428 22.1282
149.028 22.1346
149.628 22.1211
150.227 22.1227
150.829 22.1171
151.43 22.1123
152.032 22.1028
152.633 22.0885
153.234 22.0845
153.835 22.0837
154.438 22.071
155.04 22.0607
155.64 22.0631
156.241 22.0567
156.841 22.0496
157.442 22.0472
158.042 22.0241
158.643 22.0114
159.245 21.9987
159.844 21.9892
160.445 21.9804
161.049 21.9685
161.653 21.9606
162.255 21.9749
162.857 21.9455
163.457 21.9367
164.058 21.924
164.658 21.8891
165.259 21.8882
165.86 21.8636
166.461 21.8485
167.061 21.8445
167.663 21.8294
168.265 21.812
168.868 21.8048
169.468 21.8104
170.068 21.7945
170.666 21.7842
171.271 21.7826
171.872 21.7714
172.473 21.7555
173.075 21.7357
173.677 21.7222
174.278 21.7142

174.88 21.7063
175.481 21.7055
176.082 21.6952
176.682 21.684
177.281 21.6856
177.882 21.669
178.482 21.6761
179.083 21.6698
179.681 21.661
180.281 21.6379
180.882 21.6316
181.483 21.6332
182.086 21.6205
182.688 21.6253
183.29 21.607
183.89 21.6046
184.492 21.5863
185.091 21.5776
185.691 21.5768
186.293 21.5688
186.896 21.5593
187.492 21.5362
188.094 21.5522
188.696 21.5474
189.298 21.5371
189.896 21.5386
190.497 21.5259
191.098 21.5235
191.7 21.5156
192.301 21.5124
192.9 21.487
193.501 21.4949
194.099 21.4775
194.702 21.4846
195.304 21.4791
195.902 21.4616
196.502 21.4608
197.103 21.4497
197.701 21.4473
198.301 21.4393
198.902 21.4226
199.503 21.4282
200.104 21.4322
200.705 21.4345
201.307 21.4338
201.907 21.4298
202.508 21.4091
203.11 21.4099
203.71 21.3924
204.31 21.375
204.91 21.371
205.511 21.367
206.112 21.3527
206.71 21.348
207.313 21.3384
207.913 21.3305
208.516 21.3202
209.118 21.3178
209.718 21.3082
210.319 21.3122
210.921 21.3122
211.522 21.3051
212.123 21.3043
212.724 21.3035
213.326 21.2995
213.926 21.3059
214.527 21.3003
215.129 21.2932
215.729 21.2892
216.329 21.2868
216.932 21.2614
217.532 21.2693
218.132 21.2511
218.732 21.2511
219.303 21.2407
219.966 21.2526
220.63 21.2376
221.294 21.2312
221.957 21.2328
222.618 21.2153
223.279 21.2002
223.943 21.2042
224.604 21.2058
225.267 21.1954
225.931 21.2185
226.595 21.2121
227.258 21.2121
227.919 21.2073
228.583 21.2089
229.247 21.2113
229.909 21.2121
230.573 21.2185
231.236 21.2073
231.899 21.1994
232.562 21.2113
233.224 21.197
233.889 21.1907
234.554 21.1787
235.216 21.174
235.877 21.1724
236.539 21.1716
237.202 21.1589
237.862 21.1637
238.524 21.1605
239.184 21.1493
239.848 21.1382
240.51 21.1454
241.171 21.1279
241.834 21.1398
242.496 21.1295
243.159 21.1343
243.821 21.1247
244.485 21.1239
245.147 21.1223
245.808 21.1255
246.471 21.1263
247.135 21.1152
247.796 21.1072
248.46 21.1041
249.126 21.1001
249.788 21.0906
250.45 21.0858
251.112 21.0834
251.776 21.0818
252.438 21.0914
253.1 21.081
253.762 21.0763
254.423 21.0699
255.086 21.0461
255.747 21.0262
256.41 21.0302
257.072 21.004
257.736 21.0024
258.397 20.9936
259.058 20.9921
259.721 20.9809
260.383 20.9762
261.047 20.9809
261.709 20.9722
262.371 20.9651
263.033 20.9706
263.696 20.9532
264.36 20.9547
265.025 20.9452
265.685 20.9381
266.346 20.9253
267.008 20.9222
267.671 20.9166
268.333 20.9007
268.995 20.8936

269.656 20.8864
270.318 20.8817
270.98 20.88
271.642 20.884
272.303 20.8848
272.964 20.8904
273.625 20.8888
274.289 20.888
274.951 20.8832
275.614 20.8912
276.276 20.8705
276.938 20.8689
277.6   20.8554
278.262 20.8594
278.925 20.834
279.588 20.8411
280.252 20.8387
280.914 20.8348
281.576 20.8419
282.237 20.8459
282.898 20.8364
283.561 20.826
284.225 20.8419
284.887 20.8292
285.55 20.8117
286.212 20.8117
286.875 20.7974
287.538 20.8038
288.199 20.7879
288.862 20.7998
289.525 20.7998
290.187 20.8046
290.851 20.7911
291.514 20.8038
292.178 20.7951
292.84 20.7998
293.502 20.7951
294.163 20.7959
294.826 20.8125
295.488 20.7871
296.15 20.8038
296.812 20.7784
297.474 20.7935
298.137 20.7847
298.8   20.7935
299.461 20.7752
300.125 20.7831];

```
figure(4)
hold on
plot(ppp*60,mine)
plot(time,fractional_uptake,'r-');
    xlabel('time (sec)');
    ylabel('uptake');
    title('Fractional uptake vs. time');
    grid;
figure(5)
plot(temp(:,1)*60,temp(:,2)+273)
hold on
plot((time+2.536*60),T,'k*')  %the 2.536 is the time lag of the experimental
curve so it is added here for better comparison
xlabel('time (sec)','FontName','Garamond');
ylabel('T (K)','FontName','Garamond');
 axis([150 4000 290 310]);
legend('R=0.3175 cm', 'R=0.1 cm', 'R=0.5 cm');
title('Temperature vs. time');
grid;
```

VITA

Qassim Hassan was born on April 22, 1986, in Omdruman, Sudan. He spent his early childhood in Sudan before moving to UAE in1996. He was educated at Al Khaleej Al Arabi High School. He received the award of Academic Distinction from the ruler of Sharjah two times while at school. He graduated from the American University of Sharjah with a Bachelor of Science in Chemical Engineering in January, 2009. He joined the Master of Science program in the same month. Qassim did an internship at Saipem Sharjah Engineering in the summer of 2008. He served as a teaching assistant for the course: Computer Methods in Chemical Engineering for the period between 2009 and 2011.